

Review Article

Advancements in CO₂ capture by absorption and adsorption: A comprehensive review



Xiang Yun Debbie Soo ^{a,1}, Johnathan Joo Cheng Lee ^{a,1}, Wen-Ya Wu ^{a,1}, Longgang Tao ^b, Cun Wang ^b, Qiang Zhu ^{a,b,c,*}, Jie Bu ^{b,**}

^a Institute of Materials Research and Engineering, A*STAR (Agency for Science, Technology and Research), 2 Fusionopolis Way, Innovis, #08-03, Singapore 138634, Singapore

^b Institute of Sustainability for Chemicals, Energy and Environment, A*STAR (Agency for Science, Technology and Research), 1 Pesek Road, Jurong Island, Singapore 627833, Singapore

^c School of Chemistry, Chemical Engineering and Biotechnology, Nanyang Technological University, 21 Nanyang Link, Singapore 637371, Singapore

ARTICLE INFO

Keywords:

Carbon dioxide capture
Absorption
Adsorption
Chemical absorption
Physical absorption
Porous materials
Carbon capture and storage
Climate change mitigation

ABSTRACT

In the face of escalating global climate challenges, effective carbon dioxide (CO₂) capture techniques remain at the forefront of mitigating anthropogenic greenhouse gas emissions. This comprehensive review elucidates the latest advancements in CO₂ capture, emphasizing two predominant methodologies: absorption and adsorption. We delve into the mechanisms underlying each process, highlighting the novel materials and technologies that have emerged over recent years. For absorption, the focus is placed on the material design strategy, and identifying new materials in the class of amines, ionic liquids (ILs) and nanofluids for enhanced CO₂ capture capacities and reduced energy requirements. In the realm of adsorption, the synthesis of innovative adsorbents, such as metal organic framework (MOF), organic polymers, inorganic adsorbents, silicon-based adsorbents, and biochar and byproducts from biomass with superior selectivity and stability, is explored. Additionally, the review addresses the challenges associated with each method, offering insights into potential avenues for further research. By providing a holistic overview of the current landscape of CO₂ capture, this article serves as a pivotal resource for researchers and industry professionals aiming to advance sustainable solutions to combat climate change.

1. Introduction

Climate change is a global issue that has gained increasing attention and concern in recent years. The current state of our planet is characterized by rising global temperatures, melting polar ice caps, more frequent extreme weather events, and shifting climate patterns [1]. The Intergovernmental Panel on Climate Change (IPCC) reported that global temperatures have risen by about 1 °C above pre-industrial levels in 2017, and is expected to increase at a rate of 0.2 °C every decade [2]. Though there are strategies targeting buildings [3], batteries [4] and materials such as phase change materials [5], thermoelectric materials [6] etc. to reduce the impact of such high temperatures, it does not resolve

the root cause of it. The cause has been attributed to human actions which release excessive greenhouse gases into the atmosphere, with CO₂ being a chief contributor. Since the industrial revolution, CO₂ emissions levels have risen by 50% to 420 ppm [7], and the United Nations have warned against the detrimental effect to ecosystems and climate should global temperatures rise 1.5°C above pre-industrial levels [8]. CO₂, primarily released through the combustion of fossil fuels, deforestation, and various industrial processes, acts as a potent greenhouse gas by trapping heat and intensifying the natural greenhouse effect. Anthropogenic sources of CO₂ emissions, predominantly stemming from energy production, transportation, and industrial activities, accelerated the pace of global warming and led to ocean acidification, putting

* Corresponding author at: Institute of Materials Research and Engineering, A*STAR (Agency for Science, Technology and Research), 2 Fusionopolis Way, Innovis, #08-03, Singapore 138634, Singapore.

** Corresponding author.

E-mail addresses: debbie-soo@imre.a-star.edu.sg (X.Y.D. Soo), johnathan_lee@imre.a-star.edu.sg (J.J.C. Lee), wuwy@imre.a-star.edu.sg (W.-Y. Wu), tao_longgang@isce2.a-star.edu.sg (L. Tao), wang_cun@isce2.a-star.edu.sg (C. Wang), zhuq@imre.a-star.edu.sg (Q. Zhu), bu_jie@isce2.a-star.edu.sg (J. Bu).

¹ The authors contribute equally to this work.

<https://doi.org/10.1016/j.jcou.2024.102727>

Received 4 January 2024; Received in revised form 26 February 2024; Accepted 3 March 2024

Available online 8 March 2024

2212-9820/© 2024 The Author(s). Published by Elsevier Ltd. This is an open access article under the CC BY-NC-ND license (<http://creativecommons.org/licenses/by-nc-nd/4.0/>).

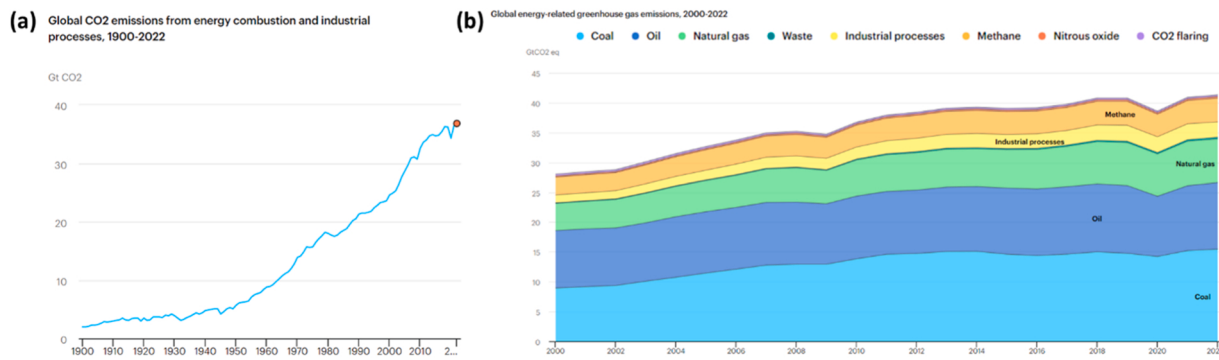


Fig. 1. (a) Global CO₂ emission contributed by combustion from energy related applications and industrial processed between 1900 and 2022. (b) Volume of CO₂ emission between 1900 and 2022 from combustion of different type of fuels [42].

tremendous stress on biodiversity. As a result, countries have pledged the Paris Agreement to limit the rise in global temperature to 1.5 °C above pre-industrial levels [8]. Therefore to mitigate the impact of CO₂ emissions on our climate, efficient CO₂ capture technologies need to be developed with an ambitious goal of net zero emissions by 2050 [9], so as to limit the impact of global warming [10].

Intercepting and sequestering CO₂ emissions from various sources, including power plants, industrial facilities, and transportation, can prevent a significant volume of CO₂ from being released into the atmosphere, thereby reducing its warming effect [11]. In the context of industrial facilities and power plants, CO₂ sequestering can be pre [12] or post-combustion [13], or using oxy-fuel combustion [14]. CO₂ from the respective flue gas streams can then be removed via different techniques, including absorption and adsorption techniques, membrane technology, yogens, microalgae and chemical looping [15]. These technologies are then installed in various industrial components, such as in absorption columns or towers and stripping units, adsorption beds, membrane modules or gas treatment equipment for CO₂ capture. Overall, post-combustion CO₂ capture offers the least disturbance to the existing industrial processes, as the CO₂ capture component can be retrofitted into the existing infrastructure.

Of all the different techniques, absorption and adsorption are the two most commonly researched and widely used techniques, with the former taking a lead in the carbon capture scene. Absorption involves CO₂ dissolving into a solvent, which may react chemically with the solvent (chemical solvents) or bound by weak van der Waals forces (physical solvents). Rectisol [16] was one of the earliest physical solvent to be developed by Linde A. G. in the 1950s for gas purification purposes. It utilized methanol for synthesis gas (syngas) purification. However, it is limited by methanol's high vapor pressure and yogenic refrigeration which made the process costly. Other physical solvents that were subsequently developed and some even patented, include Selexol [17], Fluor [18], Purisol [19], and Sulfinol [20]. These solvents adhered to Henry's Law which increases in efficiency at high partial pressures and low temperatures. Chemical solvents were then developed around the same period in the mid-20th century, where amines for gas subbing and separation were widely investigated. This led to the development of 30 wt% monoethanolamine (MEA) [21], which was found to have good CO₂ absorption selectivity, capacity and rate, and was subsequently widely employed in various power plants. However, energy consumption for solvent regeneration was at a high, accounting for 65% of the total power plant energy consumption [22], which is about 3.7 GJ/ton CO₂ [23]. Nevertheless, it is still widely employed, and often used as a benchmark for new absorbent materials. Efforts were made in exploring different classes of absorbents such as amines blends [24], ILs [25], nanofluids [26] to tackle challenges like solvent degradation and high regeneration energy. Each method has its own advantages and disadvantages, of which many shows good CO₂ capture performance. Nevertheless, high cost and insufficient data are the main factors that

hold them back from being employed on an industrial scale.

Adsorption on the other hand works based on the adherence of CO₂ onto a solid surface, which involves both physisorption and chemisorption, depending on the surface functionality. The inspiration in using adsorption techniques for CO₂ capture stems from initial explorations in gas separation processes using solid adsorbents such as activated carbon and zeolites. The absorbent materials are usually porous materials with maximized large surface areas for effective CO₂ capture. Pore size, degree and type of functionalization is expected to affect the CO₂ capture capacity and rate [27]. Common classes of adsorbent materials such as MOF, zeolites, silicates, activated carbon, organic and inorganic polymers and biochar involve physisorption [15,28], and an increase in pressure is expected to enhance CO₂ loading [29]. Grafting amines to adsorbent materials was later introduced in the early 1990s [30], which brought in the concept of chemisorption for adsorbent materials. Amine-based adsorbent material have higher efficiency in CO₂ capture, and less affect by pressure and moisture [28c,30]. Ongoing research focuses on improving the performance, cost-effectiveness and scalability of adsorption systems, exploring new novel materials for integration into existing industrial infrastructure for larger-scale CO₂ emission mitigation. Continuous effort is needed in improving the efficiency of existing technologies so as to lower the material and process cost for feasible employment into the industry.

With increasing attention on lowering carbon emissions to limit the effect of global warming, high emission sources such as power plants and industrial factories are key areas targeted for CO₂ removal [31]. New novel materials using wastes [32], polymers [33] and different synthetic techniques [34] have been developed over the years to overcome these limitations, aiming to enhance efficiency, reduce costs, minimize environmental impact, and drive innovation in CO₂ capture technologies. Some materials have proved more efficient than traditional materials used for CO₂ capture. Nevertheless, scalability and cost has hindered their employment in power plants. In addition, some of the more recent methods are not well understood, and a collective pool of up-to-date data for comparison is needed. In addition, comparing between the two most widely used techniques, absorption and adsorption, would be interesting for researchers to identify new design mechanisms and materials that may complement each other. So far, reviews have concentrated in introducing the more technical aspect on different methods of CO₂ capture, but does not give much depth on the type of material used in each technique and the material design efficiency for CO₂ capture [35]. Other reviews are more method specific, focusing on material design and function, and give detailed analysis on factors affecting the CO₂ capture performances. They dedicate the entire review to a particular class of material such as amines [36], ILs [25,37], nanofluids [38] etc. for absorption, and MOFs [39], zeolites [40], silica [41], biochar [32e-g] etc. for adsorption. Not many reviews have summarized absorption and adsorption in detail on material design and function and make a comparison on their efficiency and challenges.

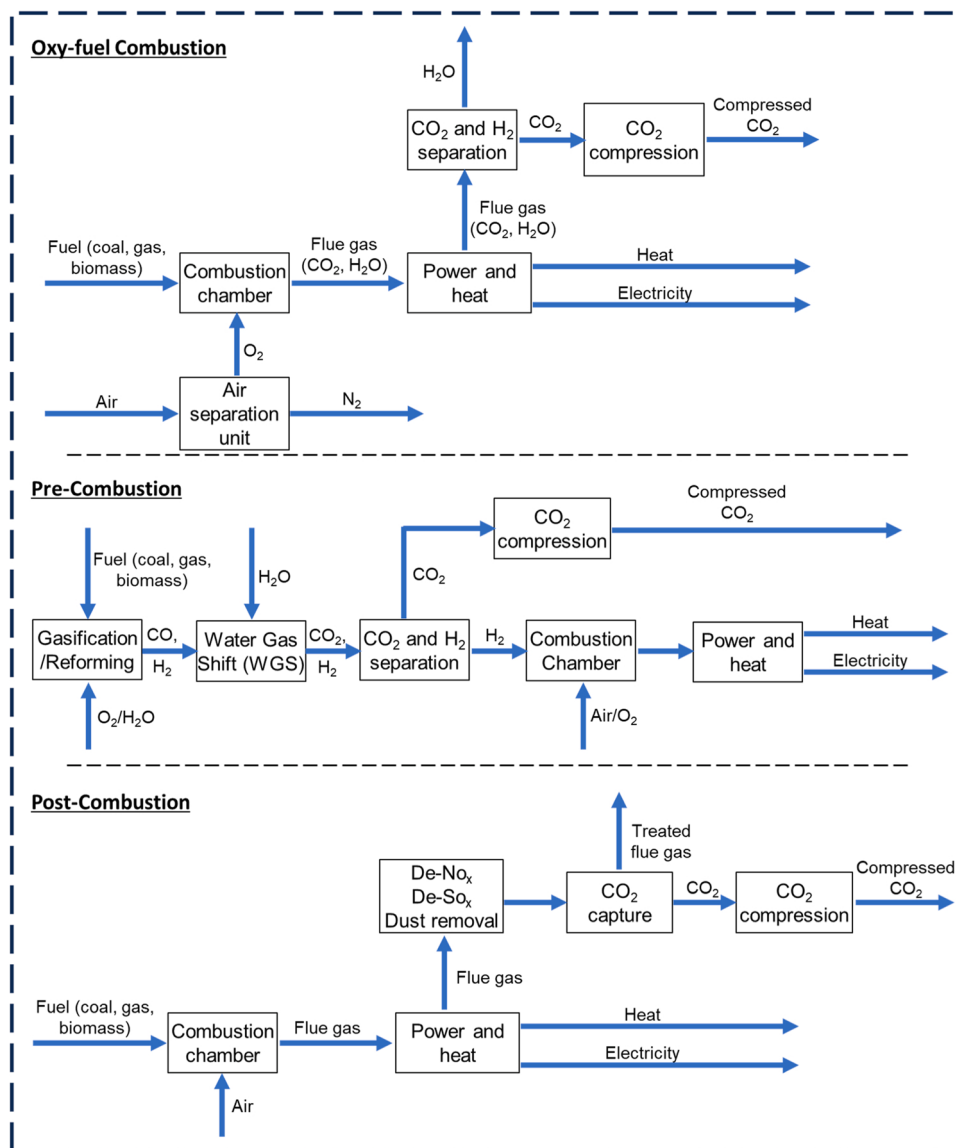


Fig. 2. Graphical illustration of the process flow for power generation via oxy-fuel combustion, pre-combustion and post-combustion CO₂ capture. Readapted with permission [35a]. Copyright 2022 MDPI Journal.

These are the two most promising materials that can be employed on an industrial scale, and it deserves our attention to be aware of and identify new materials to improve the current CO₂ capture efficiency. As such, in this review, we aim to evaluate absorption and adsorption methods for CO₂ capture, identify the challenges and existing research gaps, and note the possible future directions to take. We will first share the importance of reducing CO₂ emissions through carbon capture techniques to slow down the rise in global temperatures and give a brief overview of the current CO₂ capture techniques. The environmental and economic implications of current large scale CO₂ capture facilities will be introduced. This is followed by a detailed exploration of the different materials developed in recent years for absorption and adsorption techniques, and technological advancements will be highlighted. The challenges in this field of CO₂ capture will be presented, and we will end off with a conclusion and future outlook for this sector.

2. Current outlook of CO₂ capture facilities

Global CO₂ emissions has risen rapidly since 1990 (Fig. 1a). With the economy recovering from the Covid-19 period, emissions grew to a new high of 36.8 Gt in 2022. A 2022 report by the International Energy

Agency (IEA) found that CO₂ emitted due to energy related processes/consumption increased by 1% compared to 2021 to a high of 41.3 Gt CO₂, where energy combustion and industrial processes make up 89% of it. Coal was found to be the greatest contributor to the emissions, followed by oil and natural gas (Fig. 1b [42]). Given the increasing CO₂ emissions despite effort in using cleaner fuel, clean energy and reusable energy, the carbon capture, utilization, and storage (CCUS) scheme is widely encouraged for power plants and industries to adopt. CCUS involves capturing CO₂ emissions from large CO₂ emissions applications and either directly or indirectly using the captured CO₂ (eg. feedstock for products or services), or transporting it to storage facilities such as underground geological formations [9].

The cost of CO₂ capture can vary depending on the flue gas composition and technology employed. It can cost less at about USD 15–25 ton⁻¹ CO₂ when sequestering from highly concentrated CO₂ streams (eg. ethanol production), or at a higher range of USD 40–120 ton⁻¹ CO₂ when sequestering from lower CO₂ concentration streams (eg. power plants, cement plants) [43]. Despite its high cost, which is also a hindering factor preventing a faster pace of CCUS facilities being setup, it is noted that CO₂ capture might be one of the most viable option for certain sectors. For example, in the industrial process of cement

production, 67% of the CO₂ emissions are released from heating of the limestone compared to only 33% from burning fuels for power generation. Therefore, reduction of CO₂ emission can only come from CCUS processes. Also, when comparing using CO₂ capture technology with other new technologies such as electrolytic hydrogen, the former is much more affordable. Incorporating CO₂ capture technology in processes with CO₂ lean and rich waste gas streams, overall cost is estimated to increase by < 10% and 20–40% respectively. But for electrolytic hydrogen, cost can rise by 35–70% and 50–115% respectively [43a]. Therefore with the urgency reduce CO₂ emissions from the different processes, CO₂ capture technologies might be the “expensive” solution to consider.

With IEA taking the lead, currently 40 commercial facilities are actively involved in CO₂ capture with an annual 45 Mt CO₂ captured. A couple of the new bigger CO₂ capture facilities were operational since the beginning for 2022, and two were built in United States, one in Belgium, and four in China. Currently, these new facilities are estimated to capture 100,000 ton CO₂ per year. Over 500 projects are in place at different stages across the CCUS value chain, and industry developers have targeted to add 50 new operational CO₂ capture facilities by 2030 which estimates to capture 125 Mt CO₂ per year. Nevertheless, it is acknowledged that deployment of the projects is slow, and it is still far from the net zero emissions by 2050 target set by countries. Though current facilities show the ability to remove about 90% of CO₂ from flue gas, to enhance the capture capacity above 98% would require high energy input, larger facility and more complicated steps [9]. Replacement of coal and oil with cleaner fuels or renewable energy would require much time and effort, given the high cost and scale of infrastructure to be built. Therefore, in the meantime, more efforts can also be pumped in to improving CO₂ capture efficiency.

3. Fundamentals of CO₂ capture

CO₂ emissions from industrial processes, particularly power plants and various industrial facilities, are major contributors to the ongoing global environmental and climate crisis. To combat this issue, significant efforts have been made to develop and implement technologies aimed at capturing CO₂ before its release into the atmosphere. These approaches can be categorized into oxy-fuel combustion, pre-combustion, and post-combustion CO₂ capture (Fig. 2), where each strategy targets to sequester CO₂ emissions at different stages of the combustion process. Nevertheless, each strategy has its advantages and disadvantages.

Oxy-fuel combustion involves burning fuels in an oxygen-enriched environment instead of air. This results in the production of flue gas that is primarily made up of CO₂ and water vapor, simplifying CO₂ capture through condensation of water vapor and subsequent separation from other gases [14]. However the separation of oxygen from the air to create an oxygen-rich environment for combustion is energy and cost intensive, and may even reduce the overall efficiency of the power generation or industrial process [44].

While pre-combustion CO₂ capture involves converting fossil fuels, in particular coal and biomass, into syngas before combustion. Techniques such as gasification are used to produce syngas mainly composed of H₂ and CO. Subsequently H₂ and CO₂ produced via water-gas shift reactions, and H₂ is used as clean source of fuel to power the gas turbines. While CO₂ is separated from this mixture through pressure swing adsorption or membrane-based methods, enabling CO₂ capture before the combustion process. The CO₂ concentration and partial pressure in this process tends to be high, making the removal of CO₂ more effective [12,35a]. However, gasification requires intricate and expensive infrastructure and is energy intensive.

Post-combustion CO₂ capture on the other hand stands as one of the most established methods, focusing on removing CO₂ from flue gases after combustion. The biggest advantage is that post combustion capture allows minimal changes to existing infrastructures while retrofitting the CO₂ capture technology to the appropriate section of the plant.

Nevertheless, flue gas from powerplants often contain low CO₂ partial pressures (CO₂ make up 13 – 15% of flue gas under atmospheric pressure) which reduce the efficiency of CO₂ capture, and presence of other waste gas and solvents complicates the CO₂ capture process [13]. As such, new techniques need to work on improving the selectivity and CO₂ capture capacity to ensure effective removal of this greenhouse gas.

Absorption and adsorption are two distinct mechanisms commonly employed in CO₂ capture technologies. Each technique offers a unique approach to capturing CO₂ from industrial emissions. Absorption captures CO₂ via two mechanisms, physisorption and chemisorption. It involves the dissolution or chemical reaction of CO₂ molecules within a solvent. CO₂ is captured from the waste gas and is diffused into the solvent. Physical solvents interact with CO₂ via weak van der Waals, and therefore dissolve CO₂ into its liquid media. The process follows Henry's law, where CO₂ solubility in the solvent and thus absorption rate, is directly proportional to the CO₂ partial pressure in the gas phase, where an equilibrium is established between the gas and liquid phases. On the other hand, these two factors are inversely proportionate to temperature. This may be seen as a drawback, as solvent systems would require high pressures and extremely low temperatures of below subzero degree Celsius for effective CO₂ capture, which leads to high operating cost [18, 45]. Common classes of physical solvents include alcohols [46] and glycols [47]. While chemical solvents react with CO₂ to form carbamates or bicarbonates, making them more selective towards capturing CO₂ and increasing the capture capacity and rate. Chemical solvents are often unaffected by acid gas partial pressure, and is able to capture CO₂ at ppm concentrations [48]. However, compared to physical solvents, chemical solvents' selectivity between acid gases are lower, and they require adequate heat for CO₂ capture with the possibility of side reaction occurring, and higher energy for solvent regeneration [48]. Common classes of chemical solvents include amines [24], ILs [25], nanofluids [26] etc., where systems involving water, though effective, are often frowned upon as they would need an even greater amount of energy for solvent regeneration. This is due to water's high heat capacity and enthalpy of vaporization, where temperatures would need to be heated above it for CO₂ desorption [49]. Nevertheless, chemical absorption is one of the most mature CO₂ capture techniques with high CO₂ absorption rate and capacity, and good system stability [50]. In particular, 30 wt% MEA, has been widely employed in existing power plants, and commonly compared with in literature due to its excellent capture performance. Still, energy requirement for solvent regeneration can be improved due to it being an aqueous system, and researches are actively experimenting different types and blends of solvent for effective CO₂ capture [51]. Therefore appropriate selection of solvent, tuning of operating conditions, good reactor design and improving surface area for contact can improve the efficiency of CO₂ absorption.

Adsorption, in contrast, involves the adherence of gas molecules such as CO₂, onto the surface of a solid substrate, known as an adsorbent. These solid adsorbent materials are seen to be advantageous over liquid based absorbents, where they are less toxic, yield less waste, and is able to withstand higher operating temperatures [28b]. The adsorbents are usually porous materials with large surface areas to maximize the contact with CO₂ for carbon capture. In addition, pore size and degree and type of functionalization of the pores and surface can also influence the CO₂ capture capacity and rate [27]. Adsorption of CO₂ also involves both physisorption and chemisorption, with similar working principle as absorption. Most materials such as MOFs, activated carbon, zeolites or silicate materials involve physisorption, and therefore CO₂ capture capacity increases at higher pressure. The common mechanisms employed in physical adsorption includes hydrogen bonding, electrostatic interaction, acid-base interactions, diffusion, molecular penetration, weak complex formation etc [29]. Consequently, desorption of CO₂ also requires lower energy compared to conventional materials [52], making adsorption techniques a desirable alternative for CO₂ sequestration. However, since adsorbents utilize their surface to adsorb CO₂, they are highly sensitive to moisture. Especially for adsorbents that have

hydrophilic surfaces, water molecules may occupy the active sites and reduce the capacity for CO₂ capture. Therefore design of the adsorbent's surface is highly important, given the abundant presence of water vapor in air and flue gas streams [30]. On the other hand, when adsorbents are modified with amine functionalities, CO₂ adsorption process involves chemisorption, and properties are enhanced with higher CO₂ capture rates and capacity. Amine functionalized adsorbents are effective at low pressures, and also more tolerant to moisture, of which moisture may even aid in enhancing the CO₂ capture rate and improve their stability [28c,30]. Therefore appropriate selection and design of the adsorbent material can provide effective CO₂ capture with low regeneration energy.

Various targets and benchmarks are being pursued to enhance the efficiency and feasibility of adsorption-based CO₂ capture technologies. Firstly, which is also the main feature of the adsorbent, is to achieve high CO₂ adsorption capacities to make the process economically viable. The benchmark values for adsorbents to achieve CO₂ adsorption capacities range from 3 to 10 mmol/g which are commonly observed in most MOFs and amine functionalized moieties [53]. Secondly, is to enhance the efficiency of PSA processes for CO₂ capture. PSA systems with recovery rates exceeding 90% [54] are being targeted to maximize the utilization of adsorbents which are showcased in most of the examples as mentioned earlier. Then selectivity of adsorbents for CO₂ over other gases in mixed streams should also be factored as an important parameter, current status aims to achieve selectivity ratios of at least 20:1 for CO₂ over competing gases in flue gas or industrial emissions [55]. Lastly on the techno-economical aspect, the ultimate goal of R&D research will always aim for the implementation into large scale commercial application. Adsorption processes are currently pursuing cost targets of 40–60 \$/tCO₂ to remain a practical and affordable large-scale deployment [56].

The key difference between absorption and adsorption lies in the fundamental mechanisms by which CO₂ molecules are captured: absorption involves the dissolution or reaction of CO₂ in a liquid phase, while adsorption involves the adherence of CO₂ molecules to the surface of a solid material. Yet they both rely on the equilibrium between gas and liquid phases (for absorption) or gas and solid surfaces (for adsorption). Each mechanism has its advantages and limitations, and below we will take a look at the different materials developed for CO₂ absorption and adsorption techniques, methods and design, its efficiency and scalability to the industry. Properties of the materials analyzed are summarized in Table 3 (absorption materials) and Table 4 (adsorption materials).

4. Absorption as a CO₂ capture method

CO₂ absorption techniques are one of the most extensively studied methods for CO₂ capture. It boasts of good CO₂ absorption selectivity, capacity, and rate, and is widely employed in various power plants and industrial processes [57]. Below we will take a closer look at four different classes of absorbent material, physical solvents, amines, ILs and nanofluids.

4.1. Physical solvents

Physical solvents for CO₂ capture are designed to absorb and separate CO₂ from gas mixtures using reversible physical interactions without undergoing a chemical reaction. The efficacy of the absorption process is based on the solubility of CO₂ in the solvent, which follows Henry's Law where it is significantly influenced by partial pressure, and to a lesser extent, temperature [15]. Physical solvents are known to operate at high pressure but low temperature due to the weak interactions between CO₂ and solvent molecules. Therefore, depending on the strength of the physical interaction, the release of CO₂ and regeneration of the solvent may involve flashing to lower pressure, or stripping with inert gas at elevated temperatures for stronger interactions

Table 1

Physical solvents in proprietary or commercial processes, and the respective operating conditions and applications.

Process	Physical Solvent	Operating Conditions for CO ₂ Absorption	Application	Ref.
Rectisol	Methanol	-34.4 to -73.3 °C 2.8–7.0 MPa	Purification of syngas derived from coal, LNG plants or other carbon-rich feedstocks to remove CO ₂ and sulfur gases	[18, 45]
Selexol	Dimethyl ether of polyethylene glycol (DMPEG)	5–40 °C 2.0–12.0 MPa	Natural gas sweetening for removal of CO ₂ , sulfur-based and aromatic compounds, and water. Effective when under high acid-gas partial pressures	[58].
Fluor	Propylene carbonate	As low as -28.9 °C Up to 6.9 MPa	Natural gas sweetening and flue gas purification to pipeline quality, with bulk CO ₂ removal, H ₂ S, and H ₂ O	[18, 59].
Purisol	N-Methyl 2Pyrrolidone (NMP)	-15–40 °C	Syngas purification from gas turbines with CO ₂ removal and high selectivity for H ₂ S under high pressure.	[19, 60]

[18]. Over the years, several physical solvents and their specific processes have been patented and licensed, and the common processes are summarized in Table 1.

Many of the research today has drawn inspiration from these processes, where physical solvents of the same family, such as alcohols [46], ethers [61], esters [62] are used in pure physical solvent systems, blended with chemical solvents, or in aqueous systems. Slight modification in the solvent's functional group such as the length of alkyl chains or addition of hydrophobic or hydrophilic groups were common, and some attained better performance than the traditional physical solvents. Gui et al. [63] studied dimethyl carbonate as physical solvent and found that it had higher CO₂ solubility than propylene carbonate and methanol when performed at the same temperature. Noteworthy was when the experiment was conducted at room temperature (298.47 K), dimethyl carbonate attained a comparable CO₂ solubility as methanol at 263.15 K, which allows for lower energy requirement to maintain the system, indicating a potential as a green physical solvent for CO₂ capture. While Heintz et al. [64] investigate perfluorine solvents; perfluoro-perhydrofluorene (PP10), perfluoro-perhydrophenanthrene (PP11), and perfluoro-perhydrobenzyltetralin (PP25), for selective CO₂ capture. Though PP25 was found to have the lowest volumetric mass-transfer coefficient due to its high viscosity, its large number of fluorine atoms which increased the number of weak interactions with CO₂ resulted in it having the highest CO₂ solubility. This was further supplemented with its high molecular weight and large ring size, which makes it a potential as a physical solvent. Mixture of physical solvents were also studied, where Li et al. [62] blended two physical solvents, poly(propylene glycol) monobutyl ether (Mw 340) (PPGME340) and propylene carbonate (PC), where the former was targeted for CO₂ absorption and the latter for decreasing overall viscosity. The PC-PPGME340 system with PC at 0.2501 mass fraction though achieved 19% lower CO₂ solubility of 0.2798 mol mol⁻¹ compared to PPGME340, but the kinematic viscosity reduced by 67% to 11.466 × 10⁶ m² s⁻¹, which was better than several commercial solvents. Other combinations

include glycerol with alcohols [65], sulfolane with alcohols [66], ILs [25] (more will be elaborated in the below section) etc.

Physical solvents are also often blended with other solvents or additives to improve solvent selectivity, or enhance CO₂ solubility. Sulfinol [20], a proprietary solvent blend developed by Shell Global Solutions, showcased the benefits of using a physical-chemical solvent blend which harnessed advantages of both solvents. It comprises of a mixture of tetrahydrothiophene 1–1 dioxide (sulfolane) as physical solvent, diisopropanolamine (DIPA) as chemical solvent, and water for thorough removal of CO₂, H₂S and COS. The ratio of 40%: 40%: 20% sulfolane: DIPA: water, also known as Sulfinol-D, generally absorbs 1.5 mol of acid gas. Varying the ratio of sulfolane and DIPA can change the degree of solubility of CO₂ [58a]. It is commonly used for natural gas processing and refining for the removal of CO₂, sulfur-based compounds, mercaptan derivatives, and effective when under high acid-gas partial pressures. Sulfinol-M was subsequently produced, which replaces DIPA with methyldiethanolamine (MDEA) in similar ratio, to enhance the selectivity of H₂S over CO₂ and COS [67]. Therefore the same physical solvents can be seen to function for different systems and paired with different chemical solvents. Xu et al. [68] thus tested four different physical solvents; diethylene glycol dimethyl ether (DGM), dimethyl sulfoxide (DMSO), sulfolane and n-propanol with three different chemical solvents; 1,4-Diaminobutane (BDA), MEA, and diethylenetriamine (DETA), and found that the nature of the physical solvents had minimal effect on the CO₂ absorption loading. Nevertheless, the system of 2.5DETA-4sulfolane attained better performance than conventional 30 wt% MEA, with a cyclic loading of 0.994 mol mol⁻¹ and cyclic capacity of 4.486 mol L⁻¹. Physical solvents have also been used to replace water fully or partially in aqueous solvent, so as to lower heat capacity and enthalpy of vaporization for reduction of the energy required in solvent regeneration [49], or concentrate the carbamate or bicarbonate in one phase for easy separation and regeneration of CO₂ [68]. These help to reduce the overall operation cost and many research work has been carried out in these areas. More details and examples will be elaborated in the next few sections.

The use of physical solvents on its own or in hybrid systems offer advantages of enhanced selectivity for different gases, require low heat for CO₂ release and solvent regeneration, tunable properties and improved solvent stability [20]. However, it is acknowledged that challenges exist in the need for high CO₂ concentration or high pressures to achieve high CO₂ loading and other process complexities. With appropriate selection of solvents, systems can be optimized to cater to the requirements of different applications.

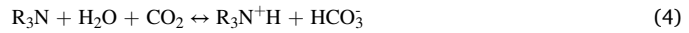
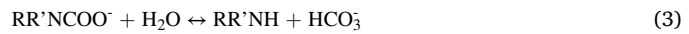
4.2. Amines

Amine-based absorbents have emerged as a prominent and widely adopted solution for mitigating greenhouse gas emissions from industrial processes and power generation, due to their effectiveness in capturing CO₂ from flue gases and other exhaust streams. Amines exhibit a unique affinity for CO₂, forming stable chemical compounds through absorption. Under anhydrous conditions, CO₂ reacts with amines to form ammonium carbamates, while in the presence of moisture forms ammonium carbonate or bicarbonate [69]. CO₂ is thus captured and stored for future use, reducing the emission of greenhouse gas. CO₂ capture in flue gas using amines were developed as early as 1930 s, where they were found to selectively react with CO₂ and easily regenerated the solvents when heated [70]. Term as the first-generation amines for CO₂ absorption, these are aqueous amine solutions which possessed high CO₂ absorption capacity, rapid absorption at low production costs. These include MEA [71], diethanolamine (DEA) [72] and MDEA [73], with 30 wt% MEA as the conventional solution that is widely used at a commercial scale [74]. However aqueous amines have several disadvantages, including being corrosive to equipment, prone to solvent degradation, vapor losses, emit volatile organic compounds, and most urgently requiring our attention is the high amount of energy for

solvent regeneration [75]. This is because of the high heat capacity and enthalpy of vaporization of water in these aqueous amine solutions. In the aspect of conventional 30 wt% MEA, higher heating temperatures are required, amounting to 180 kJ/mol of CO₂ to desorb and release CO₂ from the aqueous solution [49], accounting for around 65% of the total energy consumption of the process [22], which is about 3.7 GJ/ton CO₂ [23]. In general, an aqueous amine system may reduce the efficiency of CO₂ capture and recovery by about 30% as more fuels are burnt to regenerate the solvents, causing more CO₂ emissions [49]. In bid to improve the efficiency of the CO₂ absorption and regeneration systems, different amines structures and advanced solvent systems are developed to address these challenges and enhance the overall sustainability of CO₂ capture technologies.

4.2.1. Amine reactivity – primary, secondary, tertiary, poly

The structure of amines, including its configuration, types of functional groups attached, and the number of amino groups per molecule can potentially influence the amine's reactivity with CO₂ and affect its absorption and desorption properties. Sterically hindered or high degree amines require lower energy for solvent regeneration, as they form weaker chemical bonds with CO₂. A sterically hindered amine is any primary or secondary amine with its amino group attached to a secondary or tertiary carbon atom, for example 2-amino-2-methyl-1-propanol (AMP) [70]. They undergo the same reaction mechanism as primary or secondary amines, where a zwitterion is first formed (Eq. (1)), followed by a stable carbamate ion (Eq. (2)) which allowed for fast reaction rates. These two mechanisms show that 2 mol of amine is used to absorb 1 mol of CO₂, thus CO₂ absorption capacity might not be efficient. However, in the presence of water, the carbamate ion reacts to regenerate the amine and forms a bicarbonate ion (Eq. (3)). Reaction for a stable carbamate from an unhindered primary or secondary amine would be slower compared to an unstable sterically hindered carbamate ion. Hence the regeneration of amine (Eq. (3)) proceeds much faster for sterically hindered amines, and result in higher CO₂ loading and absorption rate [76]. A study by Hüser et al. [77] found that sterically hindered AMP decreased energy and solvent consumption by 20% and 15% respectively, compared to conventional MEA when loaded in amine-subbing units. In fact, the CO₂ absorption and desorption performance can be altered by the molecular structure and alkalinity of amines. A comprehensive study by Liu et al. [78] found that the addition of hydroxyl group causes an inductive on the amino group, resulting in a lower reaction rate with CO₂ but also less energy requirement for solvent regeneration. While the addition of short alkyl chains on or close to the N atom can induce an electron-donor effect on the amino group, and if it contributes to steric hindrance, CO₂ absorption rate is enhanced with a lower regeneration energy needed. However, if there is no increase in steric hindrance, it gives rise to fluidity resistance and CO₂ cyclic performance is reduced.



For tertiary amines, due to the absence of free hydrogen, it reacts with CO₂ and water to form a bicarbonate ion through an indirect hydrolysis (Eq. (4)) [79]. The absence of the formation of a stable carbamate ion results in low CO₂ reactivity, but give rise to a low energy solvent regeneration [80]. The frequently used tertiary amine is MDEA, which had much lower CO₂ absorption rate and capacity compared to MEA [81]. Therefore work has been done to develop new tertiary amines with higher CO₂ removal efficiency in bid to tap on the low cost of solvent regeneration. Rayer et al. [82] found that 3-dimethylamino-1-propanol (3DMA1P), though with similar heat of absorption, had a

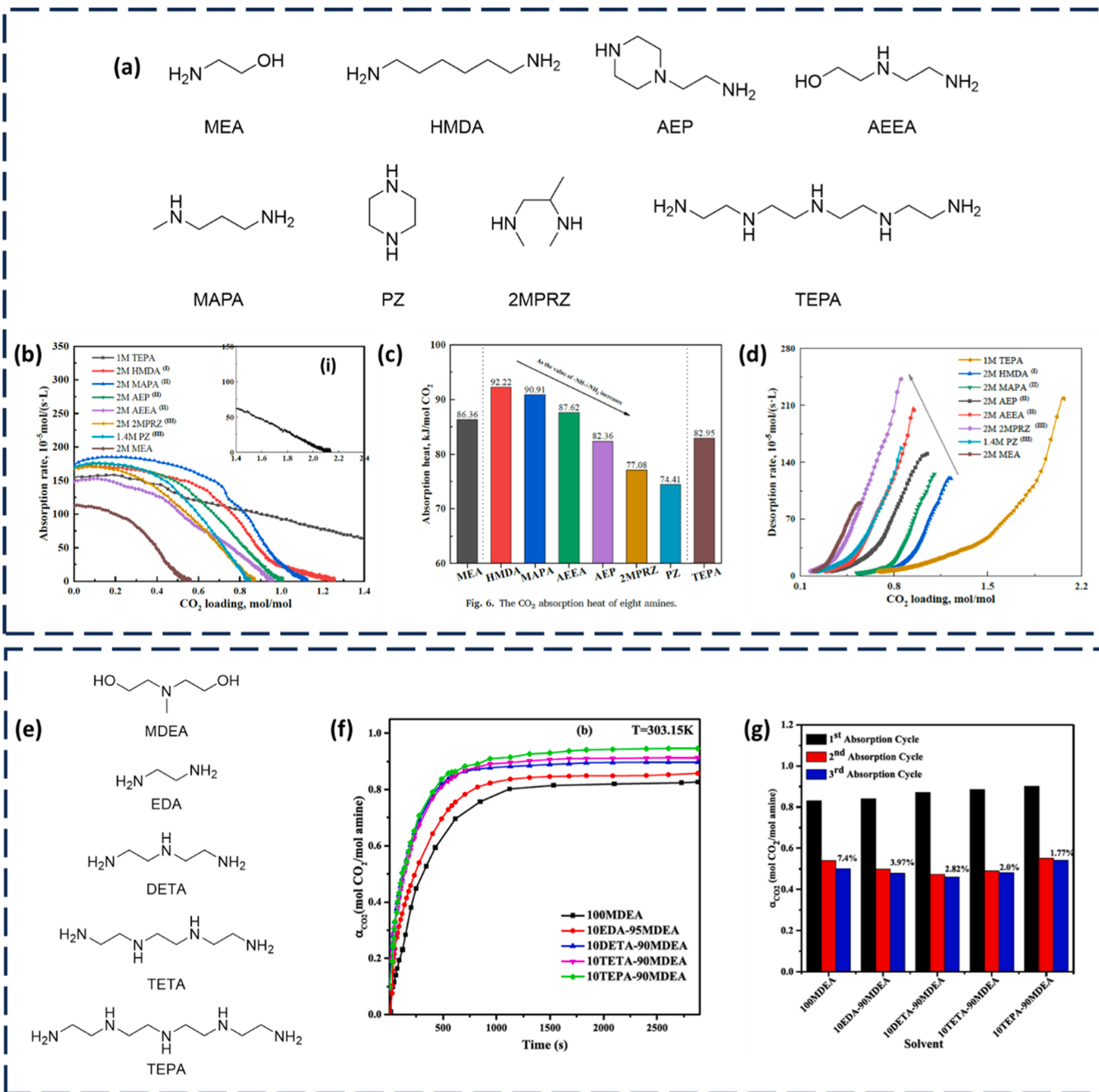


Fig. 3. (a) MEA and polyamines studied in this work. (b) Absorption rate of each polyamine at different CO_2 loading. (313 K, atmospheric pressure, 15% CO_2) (c) CO_2 absorption heat of the respective polyamine. (d) Desorption rate of each polyamine at different CO_2 loading (353 K, atmospheric pressure, pure N_2). Readapted with permission [86]. Copyright 2022 Elsevier B.V. (e) MDEA and polyamines studied in this work. (f) CO_2 absorption rate of MDEA solvent systems loaded with 10 wt% of the respective activator (303.15 K). (g) Cyclic absorption/desorption performance of MDEA solvent systems loaded with 10 wt% of the respective activator (303.15 K). Readapted with permission [88]. Copyright 2019 Elsevier B.V.

higher CO_2 absorption rate and capacity compared to MDEA. The similar structured 1-dimethylamino-2-propanol (1DMA2P) was also found to be better than MDEA, with double the CO_2 absorption capacity of 75 g CO_2/L solution [83], 2.5 times faster reaction kinetics of $70 \text{ m}^3 \text{ kmol}^{-1} \text{s}^{-1}$, and higher mass transfer coefficient at both lean and rich CO_2 loading [84]. Naami et al. [85] on the other hand conducted a lab-scale absorber test, and found that 4-diethylamino-2-butanol (DEAB) had a higher mass transfer coefficient and was more effective in CO_2 removal than MDEA by 1.4 times at 65% efficiency. However, it was less efficient than the conventional MEA which reached 100% efficiency. Nevertheless, DEAB was calculated to be able to offer a 50%

reduction in energy required solvent regeneration, which can potentially reduce the overall CO_2 capture cost by 35%. Therefore, using tertiary amines have a trade-off between CO_2 absorption rate and capacity with reduction in energy and cost for solvent regeneration and careful fine tuning is needed to determine what is best for the system in place.

Polyamines are molecules that contain multiple amino functional groups, and has been found with increased CO_2 absorption rate and capacity and improved selectivity due to presence of multiple reactive sites available for forming chemical bonds with CO_2 [70]. Gao et al. [86] studied seven different polyamines (Fig. 3a) and compared it with MEA.

As expected, tetraethylenepentamine (TEPA), with the highest number of amino groups attained the highest CO₂ loading of 2.239 mol CO₂/mol absorbent and is 3.7 times higher than MEA with the least amino group and the lowest CO₂ loading. The diamines with higher proportion of primary amino groups attained a higher CO₂ loading, and all polyamines achieved a faster CO₂ absorption rate compared to MEA (Fig. 3b). Similarly, when ratio of secondary amino groups in the polyamine increased, CO₂ absorption heat decreased (Fig. 3c), and CO₂ desorption rate increased with higher chance of completion (Fig. 3d). Polyamines thus can be tuned to obtain the desired CO₂ absorption and desorption parameters. However, highly functional polyamines tend to require higher energy for regeneration of polyamine-based, and also more viscous which makes solvent circulation and other challenges in pilot plants challenging [70]. As such, polyamines are frequently used as activators or promoters for tertiary amine solvents of low reactivity, where their multiple amine groups enhance the solution's reactivity towards CO₂, and increase the solubility, absorption rate and loading capacity of CO₂. Jaffary et al. [87] showed that by adding 0.1–0.3 M of polyethylenimine (PEI), TEPA or piperazine (PZ) as activator to 3 M MDEA amine solvent, CO₂ loading and desorption rate improved. This enhancement was greater for the activator molecule with higher amino groups. Therefore, branched PEI performed the best, where CO₂ loading was higher by 33–61% and 29–46%, and desorption rate was faster by 9–18% and 3–7% than PZ and TEPA respectively. Hafizi et al. [88] on the other hand studied four different activators (Fig. 3e): Ethylenediamine (EDA), DETA, triethylenetetramine (TETA) and TEPA, of 10% loading to MDEA, and found similar results of increased CO₂ absorption capacity and rate with increasing amino functional groups per molecule (Fig. 3f). Comparing among the blended solvents, cyclic capacities were increased with increasing ratio of secondary to primary amino groups (Fig. 3g). However as increasing amino groups tend to reduce cyclic capacity, only the solvent system with 10% TEPA that had the highest ratio of secondary:primary amino group performed better than pure MDEA. Therefore, optimization of solvent system is needed to bring out the best performance.

4.2.2. Aqueous amine systems

As mentioned above, the first-generation amines are pure aqueous systems which are low in production costs and effective in CO₂ capture but requiring high regeneration energy. Since aqueous systems will be made up of majority water, it is difficult to bring about a reduction in solvent regeneration energy. Therefore, other aspects of CO₂ capture, such as loading and rate can be improved. Other researchers have explored different aqueous systems, and 8 M PZ system was found to perform better than the conventional 30 wt% MEA [89]. The former was found to have 1.5–2 times higher CO₂ loading, and 2–3 times faster CO₂ mass transfer coefficient than the latter. Also PZ is more resistant to degradation of up to 150 °C compared to MEA [90]. However PZ has low solubility in water of 1.9 mol kg⁻¹, which leads to precipitation at 0.2 mol mol⁻¹ CO₂ loading [91]. As such, Chen et al. [92] studied the effects of CO₂ absorption with different PZ derivatives by substituting it with different groups. It was found that 8 M 2-methylpiperazine (2-MPZ) attained 2–3 times higher CO₂ solubility than 8 M PZ. This is because the methyl group attached beside the active amino group decreases its reactivity and destabilizes the carbamate formed. Nevertheless, 8 M 2-MPZ has a lower absorption rate due to its amino group being slightly hindered by the methyl attached. On the other hand, 8 M 1-methylpiperazine (1-MPZ) with a direct methyl substitution on one of the amino groups, attained similar absorption rate and capacity as 8 M PZ. More bicarbonates were observed for 8 M 1-MPZ. Hadri et al. [93] on the other hand studied 30 different aqueous amine solutions, comprising of primary, secondary and tertiary amines, each dissolved at a concentration of 30 wt%. It was noted that aqueous tertiary amines 3DMA1P, N,N,N',N'-tetramethyl-1,3-propanediamine (TMAD), 2-dimethylaminoethanol (2DMAE), 1DMA2P and MDEA, and secondary amine 2-ethylaminoethanol (2EAE) performed the best with high CO₂

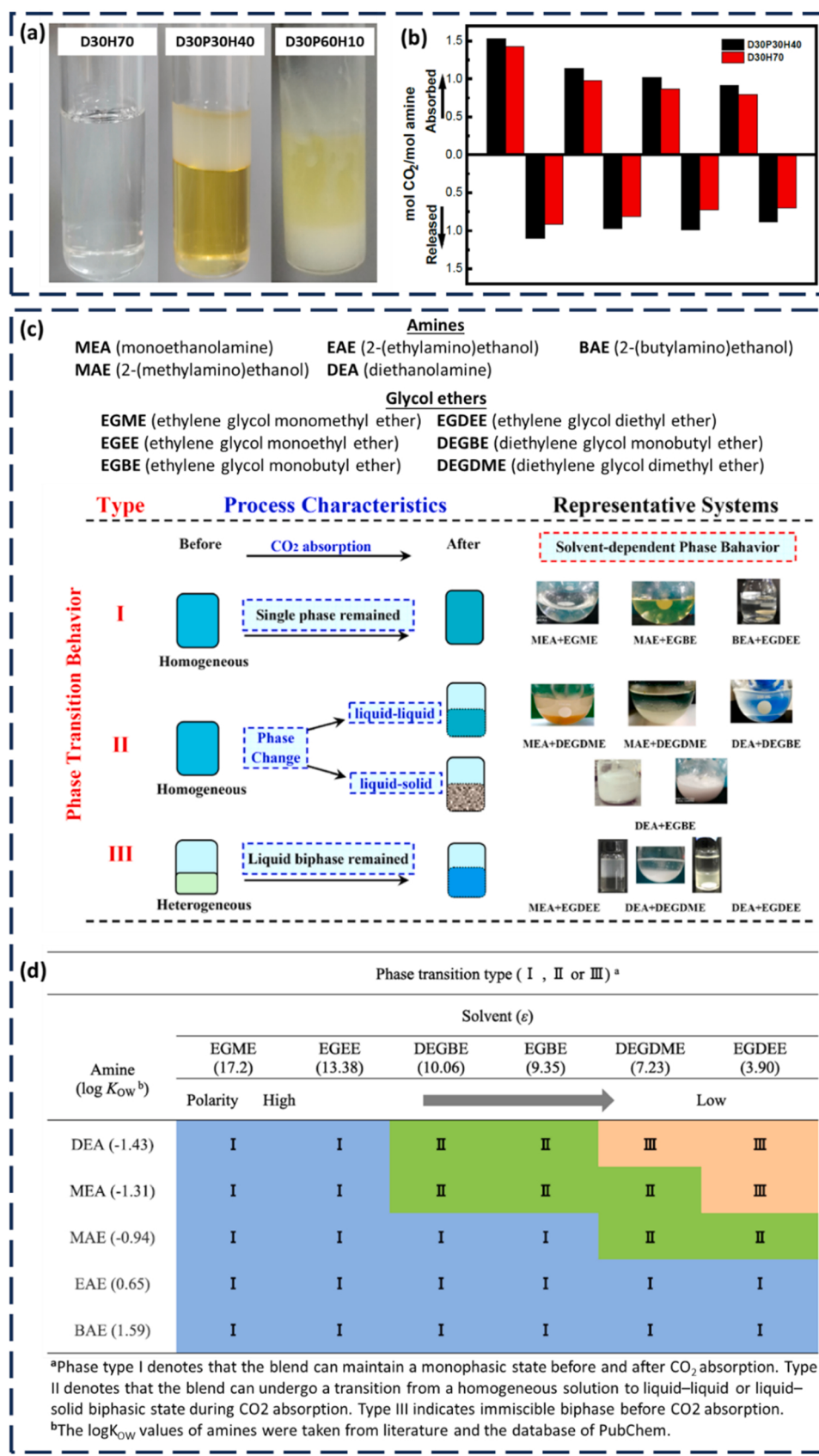
absorption capacity, which is 15–100% higher than conventional 30 wt % MEA. In addition, the 5 tertiary amines have kinetics similar to MEA, which could be due to presence of two tertiary amines for TMAD, and long alkyl chains for the others. While the reaction kinetics for 2EAE was significantly higher than MEA, signifying its potential to replace it. Therefore, efficiency of an aqueous system can be improved with different amines used, and performance depends on the functionality and degree of the amine.

4.2.3. Semi-aqueous amine systems

Apart from choosing the type of amine for the optimal performance, the amine solvent system also influences the absorption and desorption of CO₂. Traditionally aqueous amines, though able to attain high CO₂ loading, require high solvent regeneration energy and is prone to solvent degradation. Amine blends, such as semi-aqueous or non-aqueous amine systems may offer an alternative which balances between CO₂ capture and desorption. Semi-aqueous amine solvent systems contain amine, water and a physical solvent (which could be amine based). This solvent system harnesses the advantages of both chemical and physical absorption, helps to improve the overall amine solubility, reduce solvent corrosion, enhance CO₂ absorption efficiency, stability, and reduce energy requirements during regeneration [94]. The low solubility of PZ [92] can be mitigated by a semi-aqueous solvent system, and thereby improving its absorption capacity. This is demonstrated by Yuan et al. [94] who investigated sulfolane (SUF) and imidazole (IMI) as physical solvents to be added to 5 mol aqueous PZ, with a physical solvent:water ratio of 1:1 and 1:3. Under simulated industry conditions at 40 °C, both SUF and IMI semi-aqueous PZ systems showed an increase in CO₂ absorption efficacy. When operating at over stripping conditions with CO₂ partial pressure of 0.1–5 kPa, the semi-aqueous PZ systems showed a 15–35% higher CO₂ absorption rate. While at natural gas power plant conditions of 0.1–1.5 kPa, a 20–50% improvement was obtained. CO₂ cyclic capacity was also improved by about 10% for these semi-aqueous PZ systems. Similarly, other semi-aqueous amine systems exhibited an improvement in CO₂ absorption and reduction in regeneration energy compared to the conventional 30 wt% MEA, include AMP/1, 5-diamino-2-methylpentane (DA2MP)/H₂O [95], MEA/NMP/H₂O [96], 2-(ethylamino) ethanol (EMEA)/NMP/H₂O [97], and MEA/1DMA2P/H₂O [98].

4.2.4. Non-aqueous amine systems

Non-aqueous amine systems replace water with organics, forming a single-phase amine/physical solvent system. Common non-aqueous solvents includes amine or non-amine based glycols [47], alcohols [46b] and ethers [99]. Non-aqueous systems are gaining popularity as the absence of water reduces the system's heat capacity and vaporization, leading to significant reduction in solvent regeneration energy and cost savings [100]. In addition, amines react with organic solvents to produce non-corrosive products, which is highly valued in industrial settings. However, these systems tend to have poor CO₂ absorption rate and capacity due to the poor gas to liquid mass transfer rate of CO₂ arising from lower CO₂ solubility in and weaker chemical interactions with organic solvents. Also, solvents tend to become viscous with low diffusivity with CO₂ absorption, slowing down subsequent CO₂ capture [47]. Enhancing mass transfer and absorption rates in non-aqueous systems is thus an active area of research. Guo et al. [47] found that blending MEA or DEA with either 2-methoxyethanol (2ME) or 2-ethoxyethanol (2EE) gave a single-phase behavior, and provided a comparable CO₂ loading rate and capacity to 30 wt% MEA, but significantly higher desorption rate and cyclic capacity. MEA non-aqueous systems gave 5–7% lower CO₂ loading, but 62–73% higher cyclic capacity than 30 wt% MEA. While DEA non-aqueous system was slightly lower in CO₂ loading at 24%, but attained a much higher cyclic capacity of 83%. These comparable CO₂ loading capacities of non-aqueous system could be due to formation of carbamate ions when under high CO₂ partial pressure. Overall, these non-aqueous systems were found to improve



(caption on next page)

Fig. 4. (a) Phase separation indications of DETA/1-propanol/H₂O solutions after CO₂ absorption, where the ratio is indicated by the first alphabet of the component followed by the component's percentage. (b) CO₂ absorption/desorption performance for D30P30H40 and D30H70 for 4 cycles. (Conducted at 20 °C and 120 °C for absorption and desorption respectively). Readapted with permission [23]. Copyright 2021 Elsevier B.V. (c) Amines and glycol ethers used it the study, and the different phase transition behavior during CO₂ absorption: Type I: single phase before and after CO₂ absorption; Type II: single phase to biphasic (liquid-liquid or liquid-solid) after CO₂ absorption; Type III: liquid dual phase before and after CO₂ absorption. (d) Type of phase transition for the respective amine-glycol ether system during CO₂ absorption [105]. Readapted with permission. Copyright 2022 Elsevier B.V.

energy saving by about 55%. While Bihong et al. [101] showed that with the help of activators, CO₂ absorption rate and capacity of non-aqueous amine systems can be enhanced with reduction in corrosiveness. AMP in inert NMP solvent system was investigated, where CO₂ loading was only 1.16 mol kg⁻¹, much lower than the conventional 30 wt% MEA at 1.8 mol kg⁻¹. However, with the addition of AEEA as activator, the CO₂ loading was significantly increased to 1.65 mol kg⁻¹. The overall AMP/AEE/NMP system achieved a 4% higher cyclic capacity of 1.64 mol CO₂ kg⁻¹, 76% lower solvent loss of 0.14 kg.CO₂.kg⁻¹, and 45% lower total heat duty of 2.09 GJ ton⁻¹ CO₂ than 30 wt% MEA at 393.15 K. Other systems such as MEA/Methanol [46b] and 2-(butylamino)ethanol (BAE)/ 2-butoxyethanol (EGBE) [99] also shows energy reduction of up to 50% with other properties comparable to 30 wt% MEA. This signals the potential of non-aqueous solvent systems for CO₂ capture.

4.2.5. Phase change amine-based systems

In view of high energy and cost of solvent regeneration, another method for efficient CO₂ capture with reduced regeneration energy is using phase change solvents. These solvents are initially single phase before CO₂ absorption, and form dual phase, either liquid-liquid or solid-liquid, after loading with CO₂. The higher loading CO₂ rich phase can be a solid or liquid, while the lower loading CO₂ lean phase is a liquid phase. Solvent regeneration is only conducted for the CO₂ rich phase, therefore it would require less energy to heat a smaller amount of solvent for regeneration [102]. In addition, the CO₂ rich phase would generate a higher CO₂ partial pressure in the stripper, which reduce the energy required for water vaporization and CO₂ compression work [103]. Therefore the overall energy requirements for solvent regeneration is reduced, which makes it biphasic solvents a topic of interest for CO₂ capture. Biphasic solvents involve a phase separation promoter, usually a primary or secondary reactive amine species, which alters the polarity, hydrogen bond or ionic strength, or hydrophilicity etc. to encourage transition of the CO₂ based species into a specific phase or be precipitated out [103]. Both aqueous and non-aqueous amine systems are capable of attaining phase separation.

4.2.5.1. Aqueous amine-based systems as phase change solvents. Aqueous amine systems generally involve a reactive primary or secondary amine for CO₂ absorption, water, and a phase change promoter solvent (physical solvent) such as tertiary or lipophilic amines, alcohols, ethers, sulfolane, hydrophobic ILs etc. to act as a CO₂ sink [23]. The main reason for phase separation is due to a significantly greater solubility of the amine-CO₂ products in one of the solvent, usually the more polar solvent eg. water, over the other. Solvation energy of the products could be used as a gauge, where the greater the difference between the solvent energy of the products in the two solvents (water and physical solvent), there is a higher chance for phase separation occurring. Li et al. [23] studied three different amines MEA, AMP and DETA in 1-propanol/water system, where the difference in solvation-free energy of the amine-CO₂ between 1-propanol and water was about double for DETA-CO₂ compared to the other two at 12.5 kcal mol⁻¹. Optimizing the ratio of the components found that absence of the physical solvent (D30H70) does not result in a phase change after CO₂ absorption, while precipitation occurred when 1-propanol is more than 60% of the system. Hence the optimized system was found to be DETA/1-propanol/H₂O at a ratio of 30/30/40 (D30P30H40) with good phase separation (Fig. 4a) and CO loading was 1.53 mol CO mol⁻¹. Also, comparing D30P30H40

and D30H70 after 4 cycles, the former had better performance of about 15% promotion compared to the latter (Fig. 4b). While Liu et al. [24] studied an aqueous amine-amine system, where 2-(diethylamino)-ethanol (DEEA, 50 wt%) was used as the physical solvent, and several amines were seen for the CO₂ capture. It was found that primary amines are more likely to result in phase separation after CO₂ capture as they form more stable carbamate products. MEA(25%)/DEEA (50%)/H₂O and AEEA(25%)/DEEA(50%)/H₂O were identified as 2 successful systems which exhibited phase separation after CO₂ capture and attained higher CO₂ absorption (38% and 54% respectively) and desorption (34% and 58% respectively) capacity than conventional 30 wt% MEA. AEEA(25%)/DEEA(50%)/H₂O achieved a low regeneration energy of 2.58 GJ ton⁻¹ CO₂, which was 32.1% lower than conventional 30 wt% MEA. Hu et al. [104] on the other hand explored an secondary amine- tertiary amine blend of 2-(methylamino) ethanol (MAE) and 3DMA1P in a DGM/water solvent system. The addition of a tertiary amine (3DMA1P) was to reduce the viscosity and solvent regeneration energy. Tertiary amines produce carbonate and bicarbonate ions when reacted with CO₂, and it requires less energy for regeneration and is less viscous compared to MAE based carbamates generated. The cyclic capacity with the addition of the tertiary amine (MAE/3DMA1P/DGM/H₂O) was 1.59 mol kg⁻¹, which was 52.5% higher than the system without tertiary amine (MAE/DGM/H₂O), and 74.2% higher than conventional 30 wt% MEA. Viscosity also decreased by 59% with the addition of 3DMA1P to 13.12 mPa.s for MAE/3DMA1P/DGM/H₂O with MAE:3DMA1P ratio of 2:1.5, and solvent system of DGM:H₂O 7:3. The regeneration energy was lowered to 2.8 GJ ton⁻¹ CO₂, which could be further decreased when altering the MAE:3DMA1P ratio to 2:2–2.33 GJ ton⁻¹ CO₂, achieving 26–39% lower energy requirements than conventional 30 wt% MEA. Therefore, with different amine and solvent blends, aqueous based phase change solvents can help to reduce the solvent regeneration energy.

4.2.5.2. Non-aqueous amine-based systems as phase change solvents. In bid to further reduce desorption energy and operational costs, non-aqueous amine phase change systems are gaining popularity given the of absence of water which require high heat for solvent regeneration. Similar to aqueous systems, non-aqueous amine systems phase separate due to difference in polarity of the amine-CO₂ products in the solvent system, resulting in immiscibility [103]. The concept was beautifully showcased by Shen et al. [105] which used a single solvent system of different glycol ethers and blended it with different alkanolamines of different polarities. The different blended combinations gave different phase separation results (Fig. 4c). Highly polar amines (DEA and MEA) with low partition coefficient (K_{ow}) show great immiscibility with low polarity glycol ethers (DGM and EGDEE), and results in phase separation even before CO₂ absorption (Type III) phase transition. While highly non-polar amines (BAE and EAE) remain a single phase through the process with all glycol ethers (Type I). With appropriate matching of polarity between amines (DEA, MEA, MAE) and glycol ether solvents, Type II phase change was attained, where a single phase amine-glycol ether mixture phase separated from the immiscible amine-CO₂ products, making them potential biphasic absorbents (Fig. 4d). Amine carbamates were detected in the CO₂ rich lower phase, while glycol ethers solvent made up the CO₂ lean upper phase. Systems with Type II phase transition were more efficient in solvent regeneration, more than 95% of CO₂ was absorbed in the CO₂ rich phase, and regeneration energy required was reduced by 50–60%. The overall best performing phase

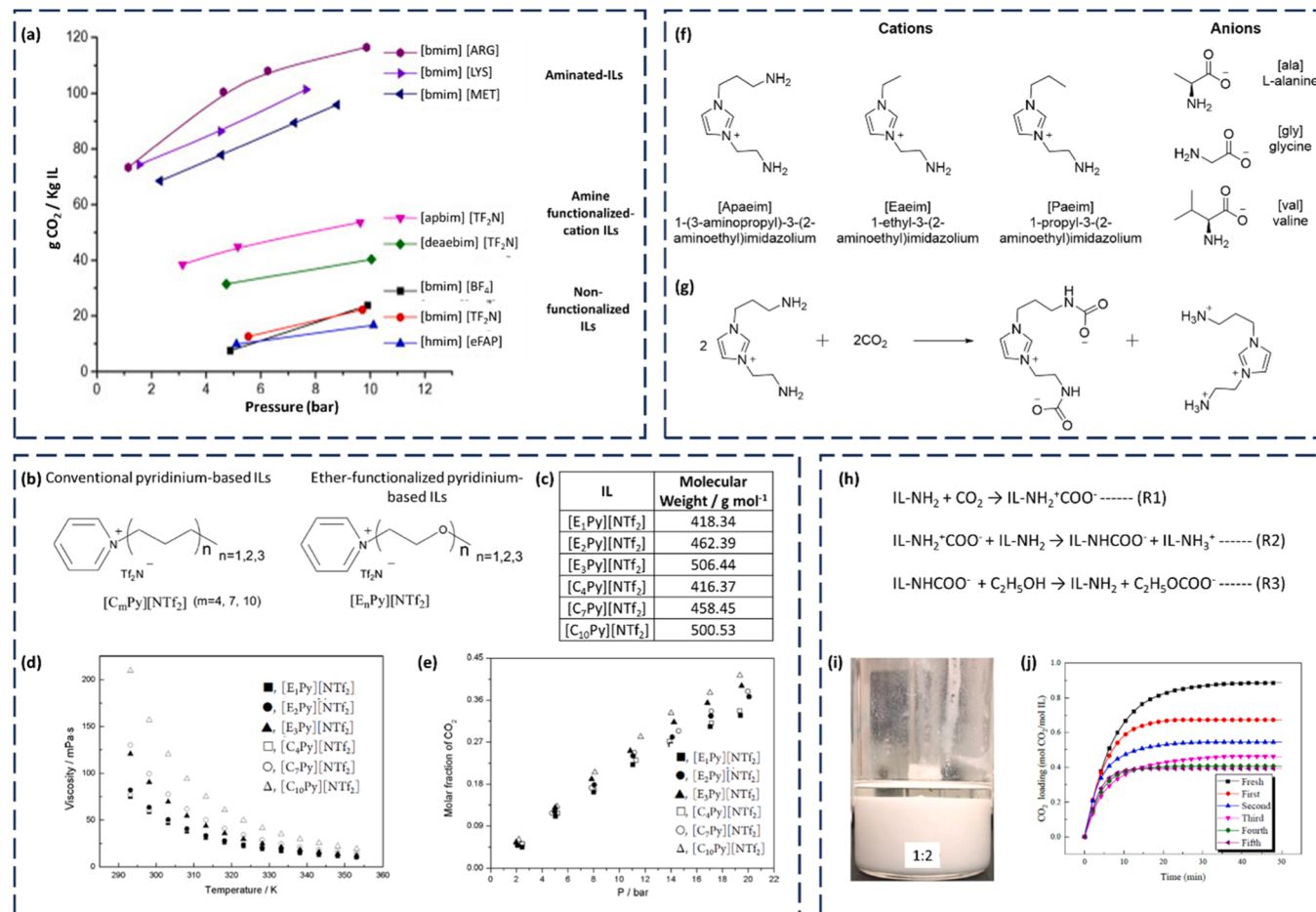


Fig. 5. (a) CO₂ uptake by mass for aminated-ILs, amine functionalized-cation ILs and non-functionalized ILs. Readapted with permission [114]. Copyright 2014 Elsevier B.V. Chemical structures of [CmPy][NTf2] and [EnPy][NTf2]. (c) Molecular weight of the respective ILs. (d) Change in viscosities of the ILs with respect to temperature. (e) Change in CO₂ solubility of the ILs with respect to pressure. Readapted with permission [117]. Copyright 2015 American Chemical Society. (f) Chemical structures of cation and anions used in the IL system. (g) Reaction scheme between [Apaeim] and CO₂ to produce imidazolium cation. Readapted with permission [113]. Copyright 2019 Elsevier B.V. (h) Reaction scheme for CO₂ absorption with [N1111][Gly]/ethanol. (i) Phase separation of CO₂-rich precipitate lower phase and CO₂-poor supernatant upper phase for [N1111][Gly]/ethanol mass ratio 1:2. (j) CO₂ loading of the respective successive regeneration solution. Readapted with permission [118]. Copyright 2021 Elsevier B.V.

change system was MAE/DGM which achieved 4.5–4.9 mol kg⁻¹ CO₂ loading in the rich phase, with 1944 kJ·kg⁻¹ CO₂ energy consumption (at 393 K desorption temperature) which correspond to 59% reduction in energy consumption as compared to conventional 30 wt% MEA. Zhou et al. [106] on the other hand studied a more common three component non-aqueous system consisting of 2-((2-aminoethyl)-amino)ethanol (AEEA) as the reactive amine species, and DMSO and N,N,N',N'',N''-pentamethyldiethylenetriamine (PMDETA) as the solvents. Carbamate and carbamic acid were formed during CO₂ absorption, and these highly polar products were more soluble and stabilized by hydrogen bonding in DMSO than PMDETA, resulting in a liquid-liquid dual phase formation. 1.0 M of AEEA dissolved in a 4:6 DMSO:PMDETA was found to be the optimal system, where a high CO₂ loading of 1.75 mol·mol⁻¹ was attained, and 96.8% of it was contained in the CO₂ rich lower phase which occupied about half of the total volume. Cyclic loading of AEEA/DMSO/PMDETA was 1.20 molmol⁻¹ and heat duty was significantly lowered to 1.66 GJ·ton⁻¹ CO₂ (393.15 K), which was 5 times higher and 54% lower than conventional 30 wt% MEA respectively. While Liu et al. [107] used an amine blend of AMP/MEA as the reactive species, and experimented with sulfolane and DGM as the phase change promoter. MEA-carbamate is first formed with CO₂, and at high CO₂ loading, hydrolysis of AMP-carbamate dominates. These carbamates and other products formed favors dissolution in water and also draws water out from the promoter solvent, while unreacted AMP/MEA remains in the

promoter solvent, resulting in a difference in polarity which caused phase separation. It was noted that CO₂ absorption rates for systems with physical solvents were greater than aqueous AMP/MEA systems due to higher CO₂ solubility and amine activity in physical solvents. Also, these physical solvent systems required much lower solvent regeneration energy compared to conventional 30 wt% MEA. The overall best performing system was AMP/MEA+50% DGM achieving the lowest regeneration energy of 2.55 GJ ton⁻¹ CO₂, and CO₂ absorption capacity of 1.82 mol kg⁻¹, which was 35% lower and 52% higher than conventional 30 wt% MEA. From these examples, non-aqueous amine phase change systems proved their ability to reduce regeneration energy while achieving comparable CO₂ loading capacity compared to its aqueous counterpart. Nevertheless, there are still different considerations for the choice of amine blends and type of solvent system such as the specific application, the concentration of CO₂ in the gas stream, economic considerations, and the desired purity of the captured CO₂. There are many ongoing research efforts on other materials for CO₂ capture, and we will take a look in the below sections.

4.3. Ionic liquids (ILs)

ILs are a specialized class of low temperature molten salts composed entirely of anions and cations with special functional groups that are promising as solvents for capturing and removing CO₂ from industrial

gas emissions. These solvents offer unique properties such as low volatility and energy consumption for solvent regeneration, high CO₂ solubility and thermal stability, tunable chemical structures, and the ability to be tailored for enhanced CO₂ absorption capacity and selectivity [25]. This potentially leads to more effective CO₂ capture, reduced solvent loss and lower operational costs. Researchers are exploring their potential in CO₂ capture and storage initiatives, and different types of IL modification and blending systems are studied for CO₂ capture. The interaction of ILs with CO₂ is similar to the other solvents, involving physical interaction and chemisorption. Conventional ILs include imidazolium, pyridinium and quaternary ammonium cations paired with halides, hexafluorophosphate ([PF₆⁻]), bis(trifluoromethylsulfonyl) imide ([NTf₂⁻]), acetate, formate, and other organic anions [25]. These ILs were initially utilized as physical solvents, and the CO₂ solubility can be altered by the cations or anions used. Anions were found to have a more significant effect on CO₂ solubility [108], and both anions [108, 109] and cations [110] that contained more fluor groups or have longer alkyl chains can enhance the solubility. However CO₂ absorption capacity for physical IL was no match for amine based solvents, which ranged at about 0.5–10 mol/mol IL [111]. Hence, functionalization of these ILs were developed as chemisorption absorbents, of which the conventional cations and anions allow for suitable modifications to tailor the IL properties in the aspect of viscosity, CO₂ solubility, polarity etc, optimizing them for specific CO₂ capture requirements.

4.3.1. Functionalization of ILs

Given the great success of amine-based solvents in CO₂ capture and regeneration, tethering amines to ILs was a popular move to improve CO₂ absorption, where amine based ILs react with CO₂ to form carbamates [112]. The amine functionality can be added to cations of ILs, and most commonly on imidazolium. Multiple amine groups can be added, such as 1-(3-aminopropyl)-3-(2-aminoethyl)imidazolium [Apaeim] and 1-ethyl-3-(2-aminoethyl)imidazolium [Eaeim] [113], where increasing functionality enhances CO₂ capture. While amine functionalized-anions usually comes in the form of amino acid anions. Sistla et al. [114] studied different amino acid anions (amine) with butylmethyl imidazolium ([bmim]⁺) and found that amine with increasing amine sites attain a higher CO₂ loading. Overall, [bmim][ARG] performed the best due to easy access of the amine groups, where it has the highest CO₂ solubility of 0.62 mol CO₂/mol IL. These aminated-ILs were compared with primary ([apbim][TF₂N]) and tertiary ([deabim][TF₂N]) amine functionalized-cation ILs and non-functionalized ILs ([bmim] cation with [TF₂N], and [BF₄] anion, and [hmim][eFAP]) (Fig. 5a), of which aminated-ILs was superior in terms of CO₂ uptake by mass, with 70%, 150% and 600% higher than the respective categories. In addition Shahrom et al. [115] also found that polymerizing amino acid based ILs was able enhance the CO₂ absorption capacity. He investigated vinylbenzyltrimethylammonium [VBTMA] with different amino acids of which all achieved an increase in CO₂ loading after polymerization. [VBTMA][Arg] gave the highest CO₂ loading of 0.83 mol/mol, which increased by 37% to 1.14 mol/mol after polymerization. In addition, a 100% desorption was achieved in the 1st cycle, followed by a subtle decrease to 86% on the 5th cycle. Despite the good performance of amino-functionalized ILs, they are often highly viscous due to hydrogen bonds present. Therefore, non-amino ILs involving ether or carboxylate functionalities can help to reduce the viscosity while improving the CO₂ capture performance [116].

Ether [119] and carboxylate-functionalized [120] ILs tend to exhibit lower viscosity due to the introduction of flexible ether (-O-) or carboxylate (-COO-) groups, reducing intermolecular interactions and enhancing molecular mobility. This lower viscosity promotes better mass transfer and increased diffusion rates, enhancing CO₂ absorption by facilitating quicker interactions between the IL and CO₂ molecules. Additionally, the altered fluidity allows for improved solvation properties, potentially enhancing the IL's ability to interact with and capture CO₂ molecules more effectively compared to higher viscosity

conventional ILs. Zeng et al. [117] compared ether functionalised [E_nPy][NTf₂] IL with conventional [C_nPy][NTf₂] IL (Fig. 5b) of the same molecular weight (Fig. 5c), where n is the number of repeating -CH₂CH₂O- and -CH₂CH₂CH₂- units respectively. Viscosity was lower for the former when compared with its conventional counterpart. However, it must be noted that when the number of ether functionality increased, the alkyl chain length also increased which contribute to a gradual increase in viscosity. Nevertheless the viscosity was by a smaller extent for [E_nPy][NTf₂] compared to [C_nPy][NTf₂] (Fig. 5d), and CO₂ solubility was almost the same for all ILs (Fig. 5e). Therefore, inclusion of the ether groups in ILs help to resolve the high viscosity problem. Viscosity converges to a low of 10–15 mPa.s when temperature increased to 353.15 K, and CO₂ solubility increased with small differences between the 2 types of IL when pressure increased. Hussain et al. [121] continued to study the effects of varying the anions, tricyanomethane ([C(CN)₃]⁻), dicyanamide ([N(CN)₂]⁻), and thiocyanate ion [SCN]⁻ with 1-(2-methoxyethyl)-Pyridinium cation ([E₁Py]⁺), and found that CO₂ solubility increased with more cyanide groups present. This is due to increased lewis acid and base interaction between the anion and CO₂, giving rise to a higher CO₂ solubility for ILs with [C(CN)₃]⁻ > [N(CN)₂]⁻ > [SCN]⁻, with CO₂ mole fraction of 0.40, 0.35, 0.16 respectively at 313.15 K and 14 bar. In addition, the viscosities of the ILs also followed the same trend with [E₁Py][C(CN)₃] having the lowest viscosity of about 10 mPa.s, and they are about three times lower than non-functionalised ILs, indicating the tunability of CO₂ solubility by changing the anions.

4.3.2. Solvent blending with ILs

Other than the tuning of chemical structure or changing counter ions of ILs, studies have shown that IL-solvent blending can substantially reduce the viscosity. This includes blending ILs with water or/and organic solvents, or with different IL systems, of which has shown potential in improving the viscosity. IL-water blends [122] have shown potential in providing tunable properties, improved solubility, reduced viscosity, and potential environmental advantages, making them versatile for various applications while requiring careful optimization for specific uses due to altered properties. Kang et al. [113] studied on a 30 wt% dual amino functionalized imidazolium amino acid IL-aqueous system, and compared with the conventional 30 wt% MEA, where three different imidazolium cations were blended with three amino acids [ala], [gly], [val] (Fig. 5f). Cations functionalized with a higher number of amino groups attained higher CO₂ absorption capacities. Therefore, ILs consisting of [Apaeim] as cations achieved a higher CO₂ loading than [Eaeim] and [Paeim] and conventional 30 wt% MEA as there are amino groups to react with CO₂ to form imidazolium cations (Fig. 5g). On the other hand, anions with different steric effects but the same number of amino groups had minimal influence on the overall performance. Characteristic of ILs, the cyclic capacity and CO₂ desorption rate of the samples were significantly better than 30 wt% MEA, and [Apaeim][ala] was found to perform the best overall, with CO₂ loading, desorption rate and cyclic capacity higher than 30 wt% MEA by 39%, 127% and 120%. Blending IL with organic solvents [123] tends to involve alcohol which lowers the viscosity and also heat capacity, leading to a reduction in solvent regeneration energy; or ethers for regulating the volatility of the overall system and reduce precipitation of insoluble absorption products. Liu et al. [124] blended tetraethylene-pentamine 2-methylimidazolium IL ([TEPAH][2-MI]) with n-propanol (NPA) and ethylene glycol (EG) to produce a non-aqueous system in bid to reduce solvent regeneration energy and enhance CO₂ capture efficiency. The IL system contained 0.5 mol·L⁻¹ [TEPAH][2-MI] in a NPA/EG solvent system of 8:2. This solvent ratio helps to reduce the system's overall viscosity and prevents precipitation of insoluble products during CO₂ absorption. The CO₂ absorption rate was 0.118 mol·mol⁻¹·min⁻¹, and CO₂ absorption capacity and regeneration efficiency were 3.2 times and 8.5% higher than conventional 30 wt% MEA at 1.72 mol·mol⁻¹ and 95.9% (1st cycle) respectively. In addition, viscosity of the system was 3.66 mPa·s, which is much lower than

traditional nonaqueous absorbents.

Another common system is the IL-amine solvent blend [125] that combines IL and amine-based solvents to enhance CO₂ capture and various applications by leveraging the unique properties of both components, aiming to optimize efficiency and tailor properties for specific processes. Xiao et al. [126] studied non-functionalized [BMIM][BF₄] and [BEIM][BF₄] at 30 wt% in MDEA, and found that there was solely physical interaction between the IL and CO₂, but chemical reaction between MDEA and CO₂ significantly enhanced the CO₂ absorption performance. The CO₂ loading for [BMIM][BF₄]/MDEA and [BEIM][BF₄]/MDEA was 0.0526 and 0.0517 g CO₂/g absorbent respectively, and the viscosity was 49.46 and 49.79 cP respectively, which about 2.5 times larger and 50% lower than its pure IL. The cycling capacity was comparable at 91.5%, which dropped slightly to 84.6% after 2 cycles. There have also been ternary systems of IL-amine-water systems [127] or IL-organic solvent-water systems [128], which favors the addition of water to help reduce the overall viscosity and improve CO₂ capture. The addition Zalewski et al. [129] showed that by adding 33 wt% of water to the amine containing system 1-ethyl-3-methylimidazolium octylsulphate [emim][OcSO₄]/DBU can help to reduce the viscosity by 50%. While [Hmim][Gly]/AMP/H₂O hybrid system studied by Zhou et al. [130] showed improved viscosity CO₂ solubility and loading, with a regeneration capacity of 94.07% at the third cycle. IL-amine-water systems provides tailored solvation behavior and enhanced CO₂ absorption efficiency, while the IL-organic solvent-water systems offer tunable polarity, improved solvation power, and reduced viscosity, among other properties, depending on the specific organic solvent utilized.

4.3.3. IL-IL blends

There have also been studies on IL-IL mixtures for CO₂ capture, and one of the motivations was to increase CO₂ absorption capacity and rate by harnessing the benefits of conventional and functional ILs through the blend. Functional ILs have higher absorption rate and capacity, but are often very viscous and require higher regeneration energy. Conventional ILs on the other hand, though have poorer performance in CO₂ capture, its less viscous, its low viscosity can help to improve the overall viscosity and improve CO₂ gas-liquid mass transfer rate [131]. As such, Wang et al. [131] blended amine functionalized [NH₂e-mim][BF₄] and conventional [bmim][BF₄], and found with a [NH₂e-mim][BF₄] mole fraction of 0.4 gave the best performance. CO₂ loading was 1.3 times higher than conventional [bmim][BF₄] of about 0.07 mol mol⁻¹, viscosity was a low of about 400 cP, and cyclic capacity after five cycles was 75–85%. Another motivation was to improve the selectivity of CO₂. As the composition of flue gas consists of about 2% SO₂, being higher in polarity, it has greater affinity to with ILs and thus competes with CO₂ for the reactive sites. While there are other works studying SO₂ tolerance [132], Wu et al. [133] studied a blend of ILs [C₄mim][OAc]/[NH₂emim][BF₄] under simulated flue gas condition of 15% CO₂/ 2% SO₂ / 83% N₂, and attained a CO₂ absorption loading of 0.4 mol CO₂ mol⁻¹ IL. This was more than double the amount of CO₂ captured if [C₄mim][OAc] (0.204 mol CO₂ mol⁻¹ IL) and [NH₂emim][BF₄] (0.180 mol CO₂ mol⁻¹ IL) were to be utilized alone. It was found that [NH₂emim][BF₄] had greater affinity with SO₂, and [C₄mim][OAc] was able to desorb CO₂ easily, hence complementing each other in the system.

4.3.4. Phase change IL-based systems

Phase change solvents are also common amongst IL, which still involves a reactive amine species, and swaps the physical solvent for IL. The phase separation mechanism is similar, where the amine captures CO₂ to form carbamates, which are insoluble in the IL component. Hence it dissolves in water or the more polar solvent, leading to a phase separation [134]. Meng et al. [134] worked on a amine-IL-water system of (30 wt%)MEA-(40 wt%)[BMIM]BF₄-H₂O which showed the importance of the IL presence for phase separation to occur. The presence of [BMIM]BF₄ in close weight fraction to MEA and around 40 wt%, helps to

promote rapid phase change within 5 min. Increasing or decreasing the wt% of [BMIM]BF₄ either results in no stratification or takes more than 72 h for it to occur. The MEA-[BMIM]BF₄-H₂O system attained a CO₂ absorption capacity of 0.581 mol CO₂/mol amine with CO₂ regeneration rate of 56.46%, and viscosity was significantly reduced by 90% to 5.9832 mPa.s (303.15 K) compared to pure [BMIM]BF₄. Overall, regeneration energy required was 2.16 GJ ton⁻¹ CO₂, which was 43.19% lower than conventional 30 wt% MEA. While Jiang et al. [118] studied a non-aqueous system, and utilized an amine functionalized IL, tetramethylammonium glycinate ([N₁₁₁₁][Gly]), which take the role of the reactive amine species and IL, and ethanol as solvent. The addition of ethanol to [N₁₁₁₁][Gly] reduced the overall viscosity which allowed for increased diffusivity and solubility of CO₂, leading to higher CO₂ loading and absorption rate. IL reacted with CO₂ to produce carbamate (Fig. 5h, R1 and R2), which was regenerated by reacting with ethanol to form ethyl carbonate (Fig. 5h, R3). Hence, [N₁₁₁₁][Gly]/ethanol with a mass ratio of 1:2 allowed for an enhanced CO₂ loading of 0.85 mol CO₂/mol IL, which was 2.1 times more than pure [N₁₁₁₁][Gly]. The formation of this insoluble carbamate led to a phase separation of CO₂-rich precipitate lower phase and CO₂-poor supernatant upper phase (Fig. 5i), which makes regeneration of CO₂ for energy efficient as only the form phase needs to be treated. By heating at 120 °C and purging with N₂, 80.54% of CO₂ was recovered, which decreased with each subsequent regeneration (Fig. 5j).

ILs are highly versatile as there are different ways to tune its properties including matching different cations and anions, functionalizing the respective ions, and blending it with different solvent systems. The advantages of amines can also be included into ILs by adding amino groups to its ions or using an amine solvent. Though high viscosity might be one of its main drawbacks, optimizing its formulation can produce an IL system with low volatility, good thermal stability, low corrosiveness and reduced regeneration energy. There are works which gave better CO₂ capture performance than conventional 30 wt% MEA, therefore with continued research and development and careful optimization, cost of IL production could be lowered in the future and be a potential material for commercial CO₂ capture.

4.4. Nanofluids

Nanofluids are nanoparticles dispersed in base fluids, which facilitate a larger interfacial area between the solvent and CO₂, promoting faster and more effective mass transfer [38a]. This leads to enhanced rates of absorption and desorption of CO₂, resulting in higher CO₂ selectivity and capture. In addition, it helps to increase solvent stability and reduce its vapor pressure [135]. Base fluids are usually the different physical or chemical solvents used in current CO₂ capture technologies. While nanoparticles include metal and metallic oxide nanoparticles [136], graphene oxides [137], carbon nanotubes (CNT) [26], silica nanoparticles [138], or modified nanoparticles [139]. There are several proposed mechanisms for enhanced CO₂ capture performance by nanofluid. One would be the shuttle effect, where nanoparticles adsorb CO₂ and transport it across the gas-liquid interface to be desorb into the nanofluid system [140]. The nanoparticles were also suggested to create a velocity disturbance fields from microconvections or Brownian motion for enhanced CO₂ absorption [135]. In addition, these motions may induce turbulence at the gas-liquid interface for enhanced hydrodynamic effects, and increase CO₂ transfer through the interface [140]. Or the presence of nanoparticles lead to the formation of smaller gas bubbles which gives a larger mass transfer area for CO₂ to diffuse into the bulk liquid [141]. These mechanisms may work together for the improved performance of nanofluids. There are two main strategies for making nanofluids. First, is to disperse the original nanoparticles whether alone or mixtures, into base fluids. And the second, is to modify the nanoparticles with functional groups such as amines or hydrophilic/hydrophobic groups to increase CO₂ selectivity and capture, and improve nanoparticle's interaction with the environment.

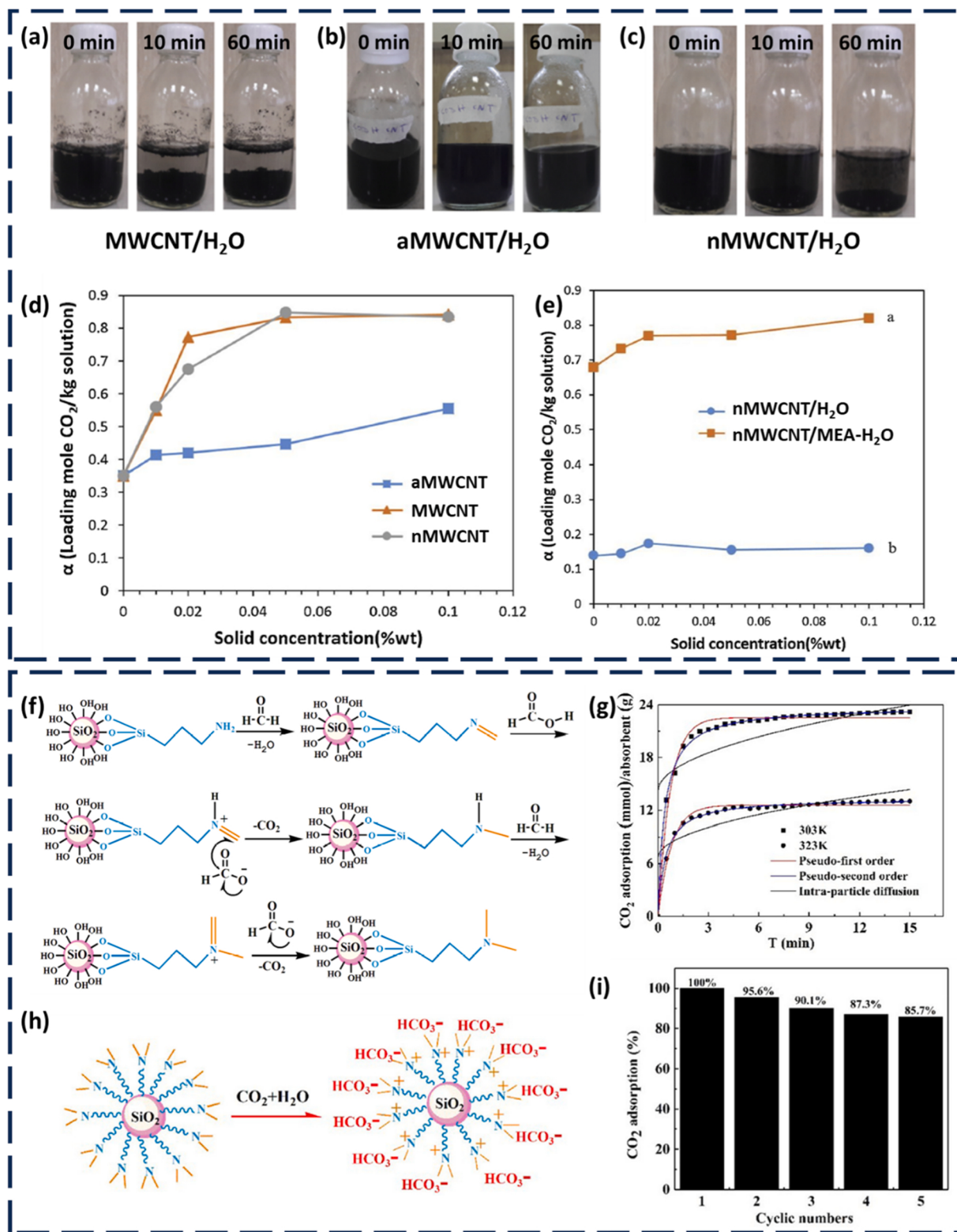


Fig. 6. (a) MWCNT/H₂O, (b) aMWCNT/H₂O and (c) nMWCNT/H₂O nanofluids just after preparation at 0 min, and left standing 10 min and 60 min after preparation. (d) CO₂ loading in 10 wt% MDEA nanofluids dispersed with different MWCNT concentrations ($P_{\text{gas}} = 18.8$ bar, $T = 313$ K) (e) CO₂ loading in nanofluids with different nMWCNT concentrations dispersed in H₂O and 10 wt% DEA ($P_{\text{gas}} = 18.8$ bar, $T = 313$ K). Readapted with permission [26]. Copyright 2019 Elsevier B.V. (f) Schematic illustration of the reaction mechanism of NR₂-SiO₂. (g) Kinetic studies of different CO₂ adsorption models at 303 K and 323 K. (h) Schematic illustration of the reaction between tertiary amine functional groups and CO₂. (i) Cyclic capacity of 0.1 wt% NR₂-SiO₂/H₂O. Readapted with permission [144]. Copyright 2020 Frontiers in Chemistry.

4.4.1. Nanoparticle dispersion in base fluids

The enhanced performance has led many researchers to study nanofluid systems through varied nanoparticles and base fluids, in bid to improve CO₂ capture capacity. Rahmatmand et al. [142] studied different nanoparticles SiO₂, Al₂O₃, Fe₃O₄, and CNTs dispersed in pure water, and found all nanofluid systems enhanced CO₂ absorption compared to water which was a relatively weak absorbent. Interestingly, SiO₂ and Al₂O₃ were found to be more effective in CO₂ capture at higher concentrations of 0.1 wt%, while Fe₃O₄ and CNT at lower concentration of 0.02 wt%. The improvement in CO₂ loading is 21%, 18%, 24% and 34% respectively, and the mechanism was attributed to the shuttle effect since rate of CO₂ absorption was not significantly affected at the start of the reaction. CNT was also found to be effective in improving strong chemical solvents, 5 and 10 wt% aqueous MDEA and DEA. Since aqueous MDEA was a weaker chemical absorbent compared to aqueous DEA, the improvement in CO₂ absorption with an addition of 0.02 wt% CNT was greater for the former by 20–23%. While Devakki et al. [136] investigated nanofluids containing TiO₂ and Al₂O₃ dispersed in deionised water, where the optimum concentration for maximum CO₂ absorption was 0.1 wt% and 0.14 wt%, and the maximum relative absorption index was 39.81% and 22.3% respectively. Above these optimum concentrations, CO₂ loading drops as the nanofluid systems become increasingly viscous and hinders the Brownian motion of nanoparticles. The higher efficiency of TiO₂ can be attributed to its hydrophobic nature, where its entire surface is available for CO₂ absorption. Whereas Al₂O₃ is hydrophilic in nature which causes water molecules adhering to part of its surface area, therefore decreasing the effective surface area available for CO₂ absorption. In addition, increasing saline conditions of base fluids increasingly destabilize the nanofluid system, causing the nanoparticles to coagulate and settle at the bottom of the container. The hydrophobic TiO₂ nanoparticles were more affected compared to hydrophilic Al₂O₃. CO₂ absorption decreased by 11.93% and 5.68% respectively when salt concentration rose from 1 to 3.1 wt%. Irani et al. [137] also showed that 0.1 wt% of graphene oxide (GO) dispersed in 40 wt% MDEA was able to enhance the CO₂ absorption capacity by 9.1%. This was attributed to the oxygen rich functional groups, such as hydroxyl, carbonyl or carboxylic acid groups on GO provides a large number of activated sites for CO₂ absorption. While Elhambakhsh et al. [143] showed that a mixture of nanoparticles CeO₂/SiO₂/TiO₂ of between 0.05–0.15 wt% dispersed in different types of solvent: distilled water, chemical solvent MDEA and a physical solvent NMP was effective in enhancing CO₂ capture properties. Compared with their base fluids of water, MDEA and NMP, the CeO₂/SiO₂/TiO₂/base fluid nanofluid system improved the CO₂ absorption by 23.47%, 8.71%, and 13.5% respectively. In addition, these systems with concentration lower than 0.1 wt% displayed good stability.

4.4.2. Nanoparticles modification

Modified nanoparticles can be in the form of surface functionalization for improved interactions with the base solvent and reacting components, or attaching CO₂-philic groups or polymers (eg. tethered with amine groups) for enhanced CO₂ capture. CO₂ capture rate and capacity depends on the type and amount of reactive functional groups attached, which are similar to the factors discussed in the previous sections. Rahimi et al. [26] beautifully demonstrated this concept of modifying CNT to improve its dispersion and stability in base fluids. Multi-walled CNT (MWCNT) was acid (aMWCNT) and amine (nMWCNT) functionalized to produce MWCNT of different degree of hydrophilicity and dispersed in water. MWCNT being hydrophobic and thus incompatible with water showed signs of coagulation at the start and settled to the bottom after 10 min of standing (Fig. 6a). While hydrophilic aMWCNT with carboxylic acid groups maintains good stability after 60 min (Fig. 6b), and slightly less hydrophilic nMWCNT which was stable through 10 min and showed signs of settlement at 60 min (Fig. 6c). Nevertheless, varying the pH of base fluid can also improve the nanofluid's stability, where using 10 wt% aqueous MEA or MDEA increased the

zeta potential with lower tendency of agglomeration. Despite the excellent stability of hydrophilic aMWCNT, the adhesion of water molecules to its surface in the system decreases the active surface for CO₂ absorption, resulting in lower CO₂ loading compared to the other two (Fig. 6d). While comparing MWCNT and nMWCNT, the latter shows slightly better results in CO₂ absorption, with 0.05 wt% optimal loading achieving a 141.6% improvement at $\alpha_{10\text{ min}}$ (CO₂ absorption after 10 min), corresponding to 0.72 mol kg⁻¹. And 10 wt% MEA improved by 13.71% to give a $\alpha_{10\text{ min}}$ of 0.771 mol kg⁻¹ (Fig. 6e). The team also showed that nMWCNT was able to improve the CO₂ capture performance in both weak and strong absorbent solvents. 0.05 wt% nMWCNT dispersed in weak absorbent, water, improved CO₂ capture by 11.51%. While in strong absorbents, a mixture of 10 wt% MDEA + 5 wt% DEA enhanced CO₂ loading by 20.5% to $\alpha_{10\text{ min}}$ of 0.738 mol kg⁻¹, and 10 wt % MDEA + 5 wt% Pz by 37% to $\alpha_{10\text{ min}}$ of 0.885 mol kg⁻¹. Therefore, appropriate nanoparticle surface modification can aid in CO₂ capture and system stabilization, improving the overall performance.

Amines are known to be highly efficient in CO₂ capture, and many research [139c] has been done to tether amine groups or polymers to nanoparticles. Lai et al. [144] functionalized nano SiO₂ with a tertiary amine by first attaching 3-aminopropyltrimethoxysilane to the core, followed by methylation of the primary amine to give a modified silica nanoparticle (NR₂-SiO₂) (Fig. 6f). 0.1 wt% NR₂-SiO₂ dispersed in water gave a CO₂ adsorption capacity of 25 mmol CO₂ g⁻¹ at 25 °C. The nanofluid systems' low viscosity before and after saturation of 2.23 and 2.96 mPa·s respectively, led to insignificant influence in CO₂ capture performance. It was found that chemisorption was the main mechanism for CO₂ capture by NR₂-SiO₂ with the reaction kinetics following a pseudo second order model (Fig. 6g). Bicarbonate was thus formed from the reaction between CO₂ and the tertiary amines (Fig. 6h). The nanofluid system also showed good cyclic capacity, where CO₂ adsorption capacity dropped slightly by 14.3% after five cycles (Fig. 6i). The team further went on to show that the use of dispersants helped to enhance the CO₂ capture performance. 0.1 wt% PEG 400 enabled better dispersibility of the NR₂-SiO₂ nanoparticles, which reduced the NR₂-SiO₂ diameter distribution by 54% to 56.7 nm. This exposed more active sites for CO₂ absorption, and the CO₂ adsorption capacity increased by 4.5 times to 105.34 mmol g⁻¹. While Irani et al. [139b] attached PEI to GO (PEI-GO) to introduce amine functionalization to the nanoparticles. 0.1 wt% PEI-GO dispersed in 40 wt% MDEA gave a 15% enhancement in CO₂ absorption, where maximum CO₂ solubility is 4.497 mol kg⁻¹ at 2000kPa and 303.15 K. Under the same conditions and base fluids, 0.1 wt% GO attained a 5.3% lower CO₂ solubility of 4.269 mol kg⁻¹. It was noted that both nanofluid systems follows the ideal gas law, where increase in pressure increase CO₂ absorption capacity, while increasing the temperature decreases it. The better performance of PEI-GO nanoparticles is due presence of reactive amine species (PEI) in a tertiary solvent system (MDEA) which increases the rate and capacity of CO₂ absorption.

4.4.3. Magnetic nanoparticles

The application of external magnetic fields to influence magnetic nanoparticles in nanofluid systems for CO₂ capture has gained more attention in the last decade as researchers investigate innovative ways to improve the process efficiency and effectiveness. Darvanojoghi et al. [145] studied the influence of different voltages of alternating (AC) and direct (DC) current magnetic fields on 1 wt% Fe₃O₄/H₂O systems. In both AC and DC magnetic fields, CO₂ absorption and average molar flux was enhanced, demonstrating the effectiveness of applying an external magnetic field. It was found that AC magnetic fields were more superior in enhancing CO₂ capture performance, where the mass transfer coefficient and rate were observed to be almost equivalent when AC magnetic field intensity (350 gauss) was half that of DC magnetic field intensity (720 gauss). This was due to increased interactions by Brownian motions of Fe₃O₄ particles at the gas-liquid interface when AC magnetic field was applied. In addition, the DC magnetic field leads to higher degree of nanoparticle aggregation at the interface, reducing the

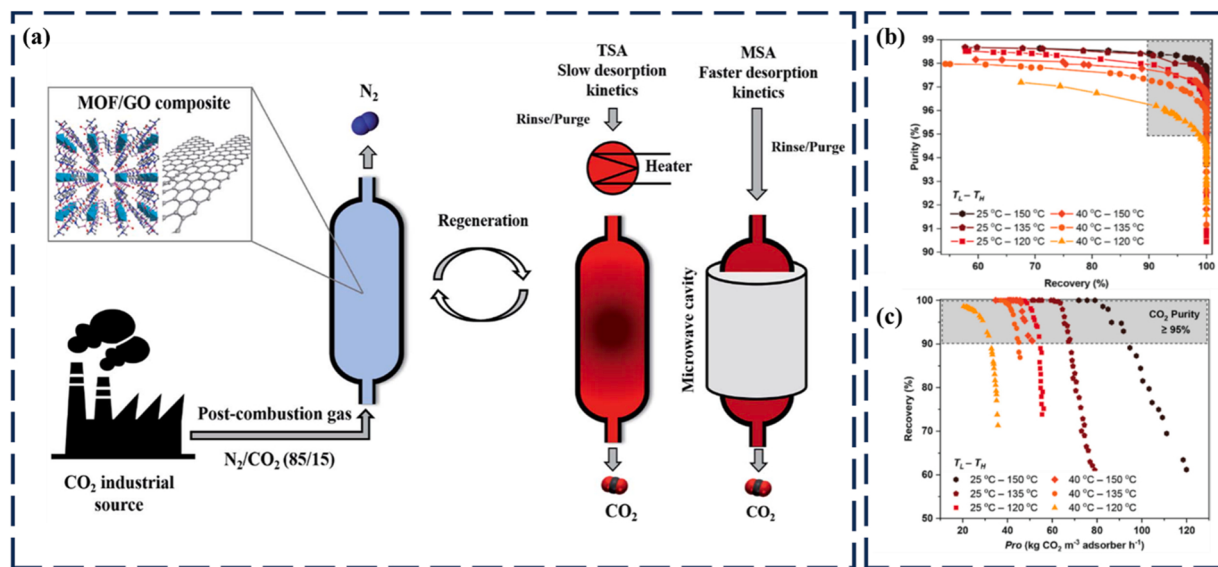


Fig. 7. (a) Overall flow scheme of post combustion gas through the adsorbent column and its regeneration mechanism. Readapted with permission [148]. Copyright 2021 The Royal Society of Chemistry. (b) Plot of purity against recovery and (c) recovery against productivity for a five-step thermal swing adsorption (TSA) cycle using various temperature and feed. Readapted with permission [149]. Copyright 2021 Elsevier Ltd.

active surface for CO₂ capture. While Park et al. [139a] modified Fe₃O₄ with ascorbic acid (AA-Fe₃O₄), and dispersed it 0.005 vol% into methanol for CO₂ capture properties with and without an external rotating magnetic field. Modifying Fe₃O₄ with AA improved the particle dispersibility and stability in the nanofluid system. The average nanoparticle cluster diameter for AA-Fe₃O₄ reduced by 42 times to 397 nm, and zeta potential of the system increased by 21 times to 45.6 mV compared to Fe₃O₄. In addition, AA-Fe₃O₄ particle surface area was increased by 28 times to 231 m² g⁻¹, increasing the number of active sites for CO₂ capture. Though AA-Fe₃O₄/MeOH increase the CO₂ absorption by 6.8% compared to the base fluid, it was rather insignificant compared to Fe₃O₄/MeOH which enhanced the CO₂ capture by 6.7%. However, with the application of a rotating magnetic field, CO₂ absorption increased by 23.3% to 0.157 mmol g⁻¹ for AA-Fe₃O₄/MeOH, which is 2 times higher than Fe₃O₄/MeOH. This is due to the formation of a flux linkage from the aligned AA-Fe₃O₄ nanoparticles, that collides with CO₂ bubbles and encourages its absorption. Also, with AA-Fe₃O₄ improved dispersibility, stability and large surface area, the shuttle effect becomes more prominent. The presence of the external magnetic flux also aids in CO₂ regeneration, where it is more clearly seen in Fe₃O₄/MeOH at which regeneration ratio increased by 6.5% to 0.973. The magnetic field increases collision between the Fe₃O₄ nanoparticles and also increases thermal conductivity, promoting CO₂ regeneration. However, in the case of AA-Fe₃O₄/MeOH, regeneration ratio decreased by 1.3% to 0.898, as its surface morphology that limits the surface effect for such enhancements. Detailed experimentation is therefore needed to identify a system to suit the requirement of the application.

Nanoparticles dispersed in both weak and strong base fluids have been shown to improve CO₂ capture performance. Modification of the nanoparticles to improve their dispersibility and system's stability help to increase their overall active surface for CO₂ absorption. Tethering the particles with amine functional groups may even help to further increase the CO₂ capture capacity. In addition, external influences such as applying a magnetic field can also enhance CO₂ absorption and regeneration. Although further research is ongoing to address scalability, cost-effectiveness, and environmental impact concerns, nanofluids represent a promising avenue in advancing the efficacy of CO₂ capture technologies.

5. Adsorption as a CO₂ capture method

CO₂ adsorption techniques delve into various methodologies employed for the capture of carbon dioxide from industrial emissions and gas streams. It boasts of high selectivity and considerable adsorption capacities, providing versatility and potential for efficient gas separation processes. Reversible swing cycling processes are typically employed to assess its efficiency of gas sorption where purity and recovery rate can be calculated [146]. Below we will take a closer look at five different classes of adsorbent material, MOFs, organic polymers, inorganic adsorbents, silicon-based adsorbents, biochar and byproducts from biomass.

5.1. Metal organic framework (MOF) adsorbents

MOF based adsorbents comprises of metal centers and organic linkers which are coordinated to form a continuous network. One of their primary application and function are in gas separation and capture, due to its versatility in synthetic approach to tailor and tune pore sizes for gas capture, such as CO₂, CH₄ and H₂O, have garnered much interest and attention over the recent years [147]. Conventionally, these frameworks can be tuned to the ideal sizes for the capture of specific gas molecules.

Treatment of flue gases were demonstrated by Serre et al. [148] using a composite MOF based adsorbent consisting of a water stable titanium bisphosphate, MIL-91(Ti), with graphene oxide (GO) as additive to increase its thermal and electrical conductivity for CO₂ capture. The pictorial flow of the CO₂ capture was summarized in

Fig. 7a. The properties of MOF/GO exhibit excellent post combustion CO₂ capture and the microwave swing adsorption test show the desorption efficiency of the MOF. The adsorption test was conducted by filling and saturating the column with 15:85 mixture of CO₂/N₂ gas, then subsequent irradiation of the column with microwave allows desorption of the captured CO₂ and an evaluation of the amount collected was assessed. The advantage of using microwave irradiation is that the desorption requires shorter time of 150 s as compared to conventional heating of about 240 s, furthermore, conventional heating was more prone to mechanical damage of the structure which ultimately, lowers the adsorption capacity in a long run.

Zhao et al. on the other hand showcased a MOF-based sorbent, UTSA-16, with CO₂ capture selectivity [149]. The MOF stands out as a carbon

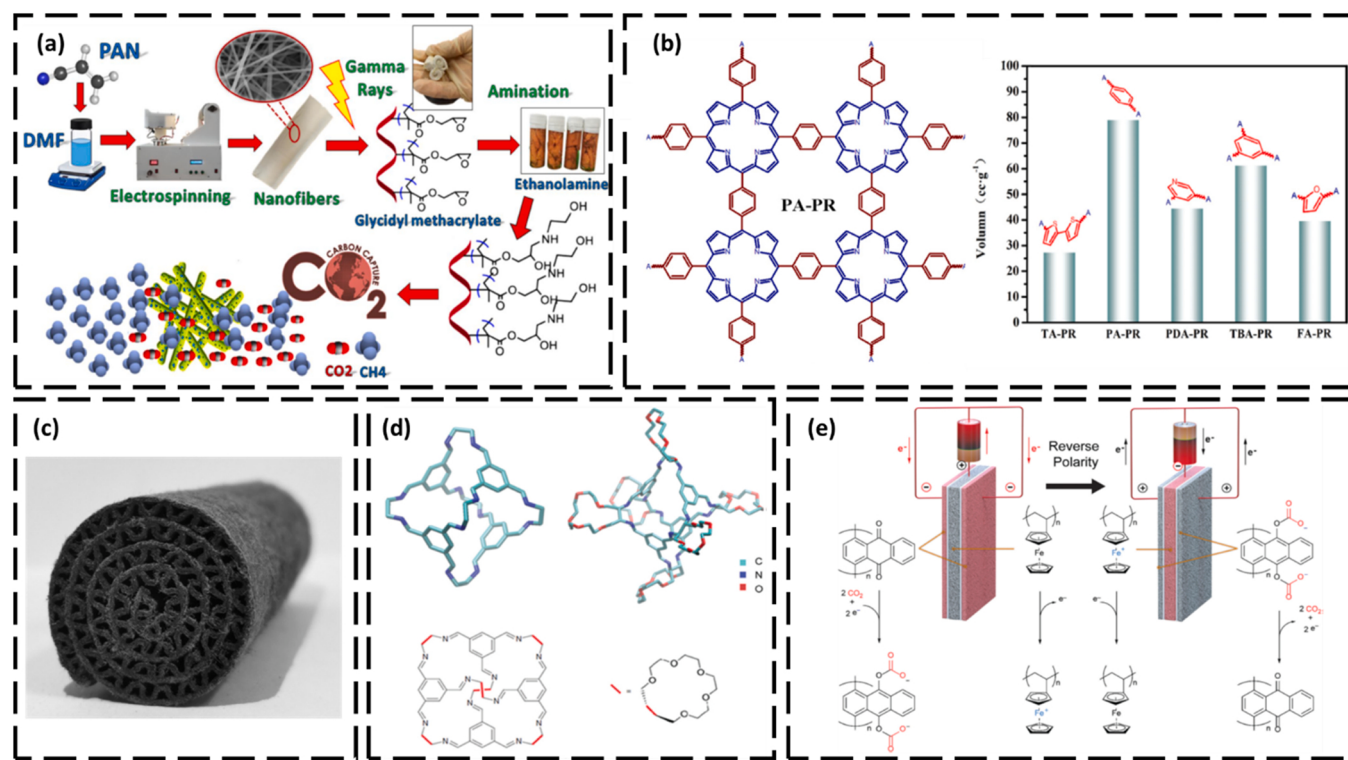


Fig. 8. (a) Flow scheme of grafting of PAN nanofibers to its adsorption application. Readapted with permission [33a]. Copyright 2023 Springer Nature Limited. (b) Structural unit of the porphyrin COF with benzenoid linkers (PA-PR) and its adsorption capacity as compared to other linkers. Readapted with permission [151]. Copyright 2021 Elsevier Inc. (c) Photo of composite adsorption fiber medium fabricated from blending kraft pulp and basalt fiber. Readapted with permission [152]. Copyright 2021 Elsevier Ltd. (d) 3D and 2D structural representation of the covalent organic cage systems. Readapted with permission [153]. Copyright 2021 The Royal Society of Chemistry. (e) Redox schematic of the poly-1,4-anthraquinone during the faradaic electroswinging adsorption mechanism. Readapted with permission [154]. Copyright 2019 The Royal Society of Chemistry.

capture candidate due to its innate desiccant property as it exhibits moisture absorption during capture conditions. UTSA-16 comprises of citrate-based linkers coordinated to tetranuclear Co metal clusters. They form a mioporous framework with diamondoid 3D cages of about 4.5 Å and the application of UTSA-16 was best demonstrated to separate wet flue gas as its structure was selective to accommodate CO₂ over N₂ and CH₄ molecules in high density at near room temperatures and ambient conditions. Detailed simulation test using different modeling techniques and even a large-scale application based on its techno-economic feasibility was conducted in two separate reports. Overall, UTSA-16 operates optimally using a multistep thermal swing adsorption cycle at regeneration temperatures of 150 °C achieve 95% purity (Fig. 7b) and 90% (Fig. 7c) recovery of flue gas feeds at ambient conditions and at slightly elevated temperature of 40 °C. Its productivity under the regeneration temperature, were comparable and sensitive when benchmarked with commercial molecular sieves with similar operating mechanism to UTSA-16 such as 13X zeolite.

A fundamental challenge in CO₂ capture technologies is the perpetual debase in its capacity over a long run during continuous wet cycles. Hong et al. [150] addresses this fundamental issue using a diamine functionalized Mg₂(dobpc) MOF coated with alkylated epoxy and silanes imparting hydrophobicity via epoxy ring opening reaction. Due to its hydrophobicity, it prevents moisture from entering the micropores of the MOF. The maximum adsorption capacity of the MOF to CO₂ was also noted to be 2.82 mmol g⁻¹ at 40 °C under wet flue gas condition consisting of 15% CO₂, 80% N₂ and 5% water. Overall, the post synthetic modified MOF achieved a high selectivity for CO₂ and its integrity was maintained over 100 adsorption desorption cycles. This work highlighted synthetic strategies to impart hydrophobicity using post synthetic modifications with the help of appending long hydrophobic chains using efficient ring opening reactions with epoxides.

5.2. Organic polymers

The effective adsorption and capture of CO₂ were also demonstrated in organic polymers of which some are in the form of organic covalent framework containing mioporous cavity to accommodate the CO₂ molecules while others present itself in forms of long chain with specific orientation of functional groups containing sites of adsorption for the CO₂ molecules [155]. Organic polymers omit the use of metal nodes or clusters which, in some cases, may ease the synthetic procedure and characterization as many of the transition metal complexes are sensitive to moisture and air under ambient conditions.

Poly(acylonitrile) (PAN) nanofibers were fabricated via electrospinning by Ali et al. [33a] the nano fibers were then grafted via gamma ray irradiation with glycidyl methacrylate and modified with epoxy ring opening reaction using different substituted amines. A general scheme of the fabrication process was illustrated in Fig. 8a showing the general flow of synthesize the polymer to the application of it as a CO₂ capture material. Its adsorbent properties were then investigated when incorporated onto a fixed bed adsorption column and flushed with CO₂ and CH₄ gases. In terms of its performance, the maximum adsorption capacity of the polymer modified with ethanolamine was 2.84 mmol g⁻¹. Furthermore, they demonstrated its integrity by attaining negligible changes after 5 cycles of adsorption and desorption at 80 °C.

Apart from linear polymers, Song et al. [151] synthesized a covalent organic framework containing conjugated porphyrin rings connected by different heterocyclic and benzenoid linkers. In addition to the different linkers, they utilized their synthetic expertise to also fabricate 3D analogs using similar linkers with increased sites of propagation. The synthetic approach made use of the polymerization of the chosen aromatic aldehyde and pyrrole with the catalysis with propionic acid and FeCl₃. The various spherical COFs synthesized exhibited high CO₂ capture

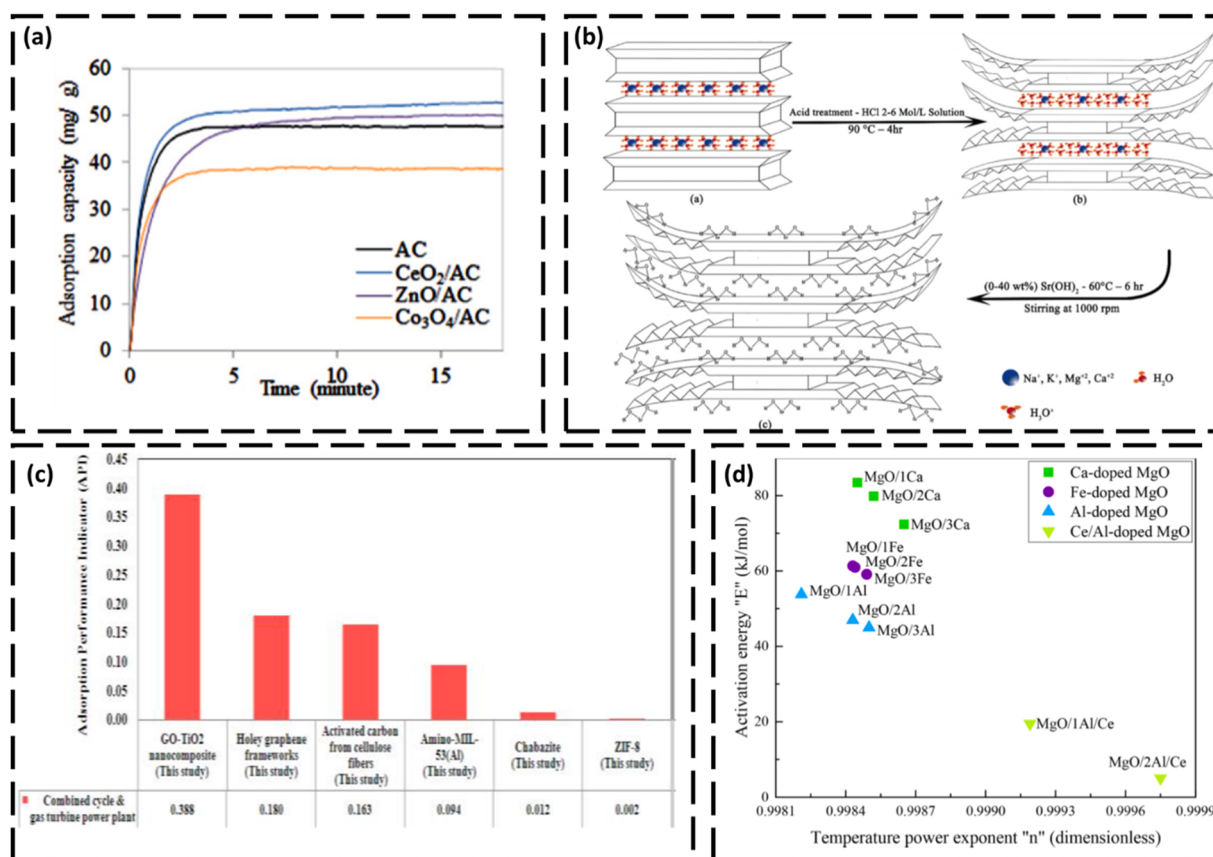


Fig. 9. (a) Plot of adsorption capacity against time for different metal oxides with activated carbon (AC). Readapted with permission [157]. Copyright 2020 Acta Chimica Slovenica. (b) Flow schematic of activating the montmorillonite (MMT) clay with acid and Sr(OH)₂. Readapted with permission [158]. Copyright 2023 Informa UK Limited. (c) Adsorption performance indicator of GO-TiO₂ as compared to different components of the nano composite and ZIF-8. Readapted with permission [159]. Copyright 2019 Iranian Journal of Chemistry and Chemical Engineering. (d) Plot of activation energy against temperature power exponent. Readapted with permission [160]. Copyright 2022 Elsevier B.V.

capacity with terephthalic aldehyde linker (PA-PR) showing the highest performance COF with 79 mg g⁻¹. A structural representation of a unit of PA-PR was illustrated in Fig. 8b, where the bar chart indicates that COF PA-PR exhibited the best performance out of the five polymers synthesized. Other than CO₂ capture, they also showed high iodine capture which could be used in aiding with nuclear waste of radioactive iodine.

Zhang et al. [152] recently made use of a composite adsorption fiber medium fabricated from blending kraft pulp and basalt fiber (Fig. 8c). Thereafter when the structure has formed, it is exposed to polyvinyl alcohol and melamine phosphate to form the composite fiber medium. The composite fiber was supposed to function as a low energy gas capture for dry flue gas separation. To showcase its functionality, it was subjected to CO₂ adsorption performance testing by varying gas flow rate and pressure through a pressure swing adsorption test. The results concluded that the composite was able to separate and capture CO₂ gas at 40% purity and a high recover rate of 96.55%. The composite was benchmarked with several materials such as zeolite 13X molecular sieve [156] in terms of the energy consumption and was superior in consuming the least energy as it requires only 414.8 kJ kg⁻¹ CO₂. Future developments of this work were in upscaling of processes in practical and real-life power plants.

Moving on from experimental study that uses different types of materials for CO₂ capture, Srebnik et al. [153] dwelled deeper into optimizing the gas sorption and maximizing the gas uptake. This is carried out by the pore cavity of a novel 3D covalent organic cage system which they developed using a synergy of synthetic and computational simulation. Through the use of theoretical modeling, they were able to

carefully optimize the capacity of CO₂ uptake given the versatility in functional groups and linker molecules that was explored in the process of the cage synthesis. The cage was synthesized from the imine condensation of EDA and Benzene-1,3,5-tricarboxaldehyde and compared with an analog with 15-own-5 ether substituted on the vertices of the cage (Fig. 8d). They also optimized the molecular density on the exterior and interior of the cavity by mapping the potential energy on the different faces along the geometry of the cage showing its gas sorption dynamics towards pressure and temperature swing behavior. The studies elucidated that external gas uptake would show the highest adsorption capacity and sensitivity to temperature and pressure.

Hatton et al. [154] on the other hand, made use of the advantage of faradaic electro swing adsorption to study the adsorption dynamics of a polymer containing 1,4-antraquinone moiety (Fig. 8e). The use of conjugated polymers allows them to be electrically conductive due to the overlapping of π orbitals. The study consists of a sealed chamber of flow cells fabricated to capture CO₂ when a gas stream is passed through it. The cells contain the poly-1,4-antraquinone which upon electro redox activation and deactivation allows adsorption and desorption of CO₂. As seen in the CO₂ capture mechanism (Fig. 8e), the driving force was due to the rearomatization of the anthraquinone to an anthracene upon reduction. The oxides then serve as nucleophiles to CO₂ to afford bis (carbonate) dianion salts. The faradaic electro swing study afforded 100% purity and recovery of the CO₂ gas with great durability and integrity showing less than 30% capacity loss when exposed to 7000 electrochemical redox cycles.

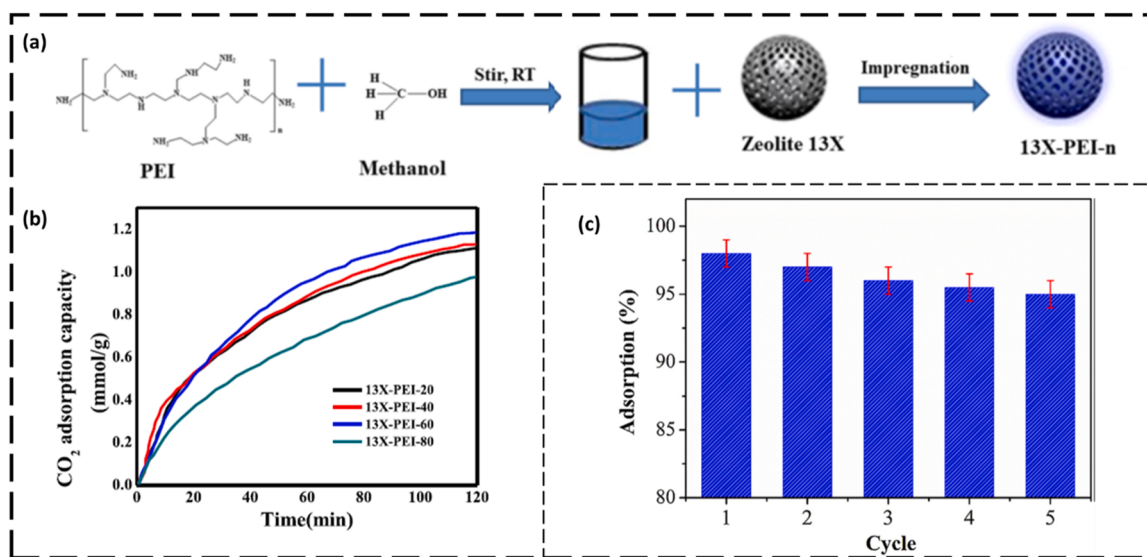


Fig. 10. (a) Synthetic route of impregnating Zeolite 13X with PEI and (b) the adsorption capacity of different weight percentages f PEI loading in Zeolite 13X. Readapted with permission [162]. Copyright 2019 American Chemical Society. (c) adsorption over different cycles of a mesoporous silicon foam incorporating PEI. Readapted with permission [163]. Copyright 2018 Elsevier B.V.

5.3. Inorganic adsorbents

The use of inorganic materials is also well studied as adsorbents for CO₂ capture. Typically, in the form of inorganic salts or natural minerals, they are incorporated into support or additive matrix using impregnation methods to impart mechanical and thermal stability. Inorganic adsorbents are defined as those containing metallic components such as metal oxides, hydroxides, metallic salts, and minerals etc., of which some are naturally found in the environment and thus, omitting the need for tedious inorganic synthesis. They often interact with CO₂ via acid base reaction since metallic oxides and hydroxides are basic and CO₂ is acidic.

One example of basic metallic oxides used as adsorbent was demonstrated by Lahuri et al. [157] using CeO₂ incorporated in activated carbon using wet impregnation. A comparison study was conducted and the superior adsorbent properties of CeO₂ were highlighted when compared with other oxides such as ZnO and Co₂O₃. The highest adsorbent capacity was observed to be 52.68 mg g⁻¹ under near ambient conditions of 30 °C (Fig. 9a). The excellent performance of CeO₂ as a metal oxide adsorbent was attributed to its ability to reactivate the activated carbon to allow more efficient chemisorption for CO₂ uptake since activated carbon only allows physisorption through weak van der Waals' forces. Integrity and reliability of the adsorbent was also highlighted when only 6.53% mass loss was observed when subjected to 5 cycles of adsorption and desorption. A relatively low desorption temperature was also required for the release of CO₂ of about 160 °C, inferring that the process was not energy consuming.

The use of minerals as an additive support was reported by Ghaemi et al. [158] as they showcased a modified montmorillonite (MMT) clay by incorporating basic Sr(OH)₂ after acid treatment as a surface modification technique for CO₂ adsorption. A synthetic scheme is illustrated in Fig. 9b showing the structural modification and decomposition of the clay to amorphous silicate upon exposure to acid where existing cations were replaced with H⁺. This was followed by activation of the acid treated clay with Sr(OH)₂. Both components are able to interact with CO₂ well at an optimum loading of 16% of Sr(OH)₂, where the clay was believed to exhibit optimum adsorption capacity of 102.21 mg g⁻¹ at ambient temperature. In addition, cyclic thermal stability test was carried out and the adsorption desorption process did not impede the integrity of the modified clay as there were negligible losses in the adsorption capacity measured after 10 cycles of the thermal cycling. The

excellent thermal stability was attributed to the Sr(OH)₂ incorporated in the clay as its high thermal stability is imparted to the clay.

Another carbonaceous additive used as a mechanical support for inorganic adsorbent was shown by Reza et al. [159] by incorporating mesoporous graphene oxide (GO) with TiO₂ by colloidal blending and ultrasonication. The study assimilates thermal power plant capture of CO₂, exposing the GO/TiO₂ nanoparticle to flue gas compositions gas mixtures (15:85, CO₂:N₂) and assessing the performance of the nanoparticle via PSA. TiO₂ and GO are good adsorbents since TiO₂ has been studied to be a well-known photocatalyst for CO₂ reduction in solvents such as water or methanol while the pores of GO have been studied to adsorb pollutants and specific small molecules such as CO₂. The adsorption capacity was compared to commercial adsorbent such as zeolites like ZIF-8 and more. The adsorption capacity achieved a value of 0.508 m mol g⁻¹ which was the best performing adsorbent in an assimilated gas turbine and combine cycle power plant condition as evident in the bar chart showing the performance of the different isolated components and commercially used ZIF-8 (Fig. 9c).

Apart from studies using external support, Zhuo et al. [160] reports the use of Al and Ce dopants directly on the surface of MgO to change the transition state energy barrier and create potential wells as sites for accelerated CO₂ adsorption and capture. They claim that the use of these dopants reduced the energy barrier to near zero, thereby allowing efficient and easy adsorption of CO₂ on the surface. The study was first conducted when the first dopant, Al, was chosen to be the best performing candidate when compared to iron and calcium atoms when compared to pure MgO, Al-MgO exhibited the largest dip in potential energy reduction as seen in the plot of Fig. 9d. The resultant Al-MgO was then further modified by doping with Ce atom as Ce was claimed to possess good CO₂ catalytic properties and it was also able to further decrease the potential energy for accelerated CO₂ adsorption.

5.4. Silicon-based adsorbents

Silicon-based materials are a class of inorganic adsorbents that have been specially highlighted in this section due to its wide range of applications as porous materials. The use of silicon containing adsorbents has been well established. They are chemically and physically stable, resistant and widely studied due to its mesoporous versatility in different forms, such as zeolites, porous silica and other molecular sieves [161]. Mesoporous silica or silicon-containing minerals possesses cavity

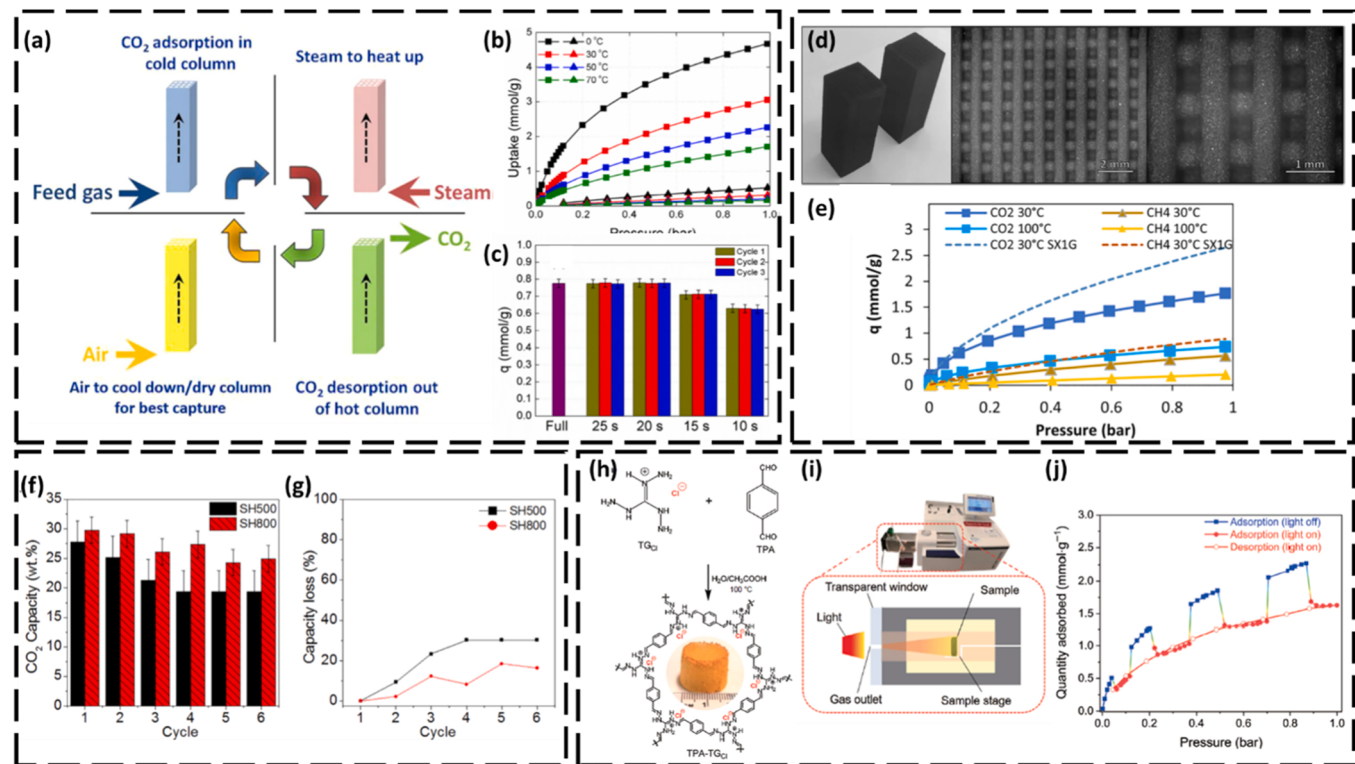


Fig. 11. (a) Flow scheme of using steam and air for the adsorption and release of CO₂ using the novel honeycomb carbon monolith. (b) Plot of adsorption uptake against pressure. (c) Comparison of different cycles of exposure of heating to the base case. Readapted with permission [166]. Copyright 2019 Elsevier B.V. (d) SEM imaging of the 3D printed carbon monolith. (e) Comparison of the adsorption capacity against pressure of the 3D carbon monolith to different gases at various temperatures. Readapted with permission [167]. Copyright 2022 Elsevier B.V. (f) Bar chart of the adsorption capacity of SH500 and SH800 at different adsorption-desorption cycles. (g) Plot of adsorption capacity loss against the different cycles. Readapted with permission [168]. Copyright 2020 John Wiley & Sons, Inc. (h) Synthetic scheme of terephthalate aldehyde with triaminoguanidinium chloride to form the COF hydrogel and xerogel. (i) Pictorial cross section showing the working mechanism behind intermittent illumination. (j) Adsorption capacity against pressure plot showing the lights on and light off cycle. Readapted with permission [169]. Copyright 2023 Springer Nature.

capable of adsorbing desired molecules. Paired with strategic use of additives, researchers have explored ways to efficiently fabricate composites for selective CO₂ uptake.

Relying on a scaffold to house absorbent is an effective and cost-efficient way to fabricate thermally stable and high yielding composites. Pal et al. [162] impregnated zeolite 13X with PEI in methanol which acts as basic adsorbents to interact with the acidic CO₂ gas from flue gas streams, a general synthetic scheme of the fabrication is illustrated in Fig. 10a. Through assessment of the kinetic parameters using modeling studies, the optimal amount of PEI incorporated was found to be 60 wt% with a working temperature of 75 °C and the maximum adsorption capacity was estimated to be 1.22 mmol g⁻¹ as seen in the adsorption-time graph in Fig. 10b. They highlighted that the rate of adsorption process was rate limited by the intra-diffusion step which prodded further study and analysis in the molecular weight of PEI utilized for such applications.

Another report of PEI as an adsorbent was demonstrated by Ahn et al. [163] using fly ash derived mesoporous silicon foam as the support scaffold. In addition to PEI, they prepared an (ethylenediaminetetraacetic acid) EDTA composite which also possesses basic properties to react with acidic CO₂ as a comparison. The composite achieved a maximum adsorption capacity of 4.7 mmol g⁻¹. Fig. 10c shows that there was negligible change in the adsorption capacity after 5 cycles of adsorption-desorption cycle ensuring the composite's integrity and performance as an efficient CO₂ adsorbent.

While Liu et al. [164] synthesized a molecular sieve (CSMS-12) comprising of cobalt and silicon using hydrothermal methods from colloids. CSMS-12 exhibited the highest adsorption capacity at 1.86 mmol g⁻¹ and showed excellent selectivity when tested with mixture of

gasses that assimilated flue gas conditions. The choice of using cobalt in the mesoporous molecular sieve is that it is an easily polarizable metal that can eat high dispersion potential energy on the surface of the silicon which results in a conductive surface for CO₂ adsorption. They also highlighted that CSMS-12 excelled in basic condition of pH 12 which provided optimal pore volume and surface area for the uptake of CO₂.

5.5. Biochar and byproducts from biomass

This section addresses the use of a class of organic material that is typically found as municipal waste byproduct. The use of biomass byproducts as an upcycled material has been intensely studied over recent years due to the limited finite resources for energy consumption [165]. The rising detriments of burning fossil fuel have raised alarming environmental impact in terms of global warming and greenhouse gas emission. In an effort to relieve greenhouse emissions through reducing waste generation and burning through incineration, giving our everyday waste a “second chance” to be applicable in our lives would help to reduce the use of finite resources as an alternative source. Some of these materials highlighted include lignocellulosic biomass, tar, biochar from burnt carbon sources such as fly ash and natural plant-based materials from oats and wheat. The innovative use of carbonaceous waste materials was made possible through synthetic functionalization and physicochemical characterization about its innate nature for gas sorption and capture as a porous material.

The use of steam was interestingly demonstrated by Denayer et al. [166] on a novel carbon monolith with honeycomb structure that exhibits selective fast CO₂ uptake using accelerated TSA. The study was conducted using hot dry air and steam which highlighted the advantages

of steam in the cyclic adsorption desorption study of the carbon monolith. In general, steam facilitated surface separation of CO₂ and moisture during the desorption process as illustrated in the flow cycle in Fig. 11a. It also serves as a source of low-cost energy for heating in the adsorption column. A maximum adsorption capacity of 1.02 mmol g⁻¹ was attained at ambient temperature (Fig. 11b). Additionally, steam was also able to facilitate the fast heating and cooling cycling of the novel carbon monolith (Fig. 11c), where only 10 s of heating was needed to regenerate 80% of the CO₂ through desorption, and about 25 s to regenerate the full amount. This is more efficient compared to full thermal regeneration which is heated at 140 °C condition as a base case (Fig. 11c).

Another reported work by Denayer et al. [167] highlighted the efficiency of an electrically conductive carbon monolith derived using K₂SiO₃ as binding agent and fabricated with the help of an extruder. 3D printing was used to fabricate and mold the monolith into desired shape and morphologies to maximize homogenous heating and cooling (within 30 s). The intricately printed shape is analysed via SEM (Fig. 11d) to observe the details in micro and nano scale. Electrical swing adsorption was highlighted in this report as an effective testing method as it reduced heat losses in the measurements and process cycling time. The rapid electrical and thermal conduction through Joule heating allowed the activated carbon to achieve a regeneration efficiency of 95%, with a purity of 85% when a high voltage is used. While the fabricated activated carbon achieved an adsorption capacity of 1.04 mmol g⁻¹ as seen in the breakthrough curve in Fig. 11e.

A novel activated carbon flake was fabricated by Anuar et al. [168] using different proportions of starch, urea, Zn(OAc)₂ and FeCl₃ as an activating agent under mild acidic conditions via pyrolysis. The reaction produced a range of porous carbon with different pore sizes, and the best performing mesoporous carbon material was identified as SH800. It functions as a low-cost CO₂ adsorbent for biohydrogen purification in hydrogen power plants to prevent catalyst poisoning while producing H₂. The amine incorporated into the activated carbon works as Lewis base to reaction with acidic CO₂. The porous carbon achieved a maximum adsorption capacity of 6.77 mmol g⁻¹ under ambient conditions. In a real-life study, negligible loss and changes in the CO₂ adsorption capacity were detected after 5 adsorption desorption cycles as evident in the bar chart comparison in Fig. 11f and g, making it a viable option for a cheaper alternative in CO₂ capture.

An interesting use of existing commercial carbon based by-products, tar, derived from biomass was reported by Li et al. [170]. Tar is mostly regarded as a hazardous side product from industrial processes such as gasification. It was chemically treated with bases such as KOH and CaO from eggshells in a one-step synthesis procedure to produce a porous carbon material that was able to efficiently uptake CO₂ gas. The ratio of KOH and CaO used produced products with different porosity, with the best performing porous carbon synthesized at a ratio of 2:3 wt ratio of CaO and KOH respectively. The porous carbon material was able to achieve a maximum adsorption capacity of 5.03 mmol g⁻¹ at 273 K, and a CO₂ recovery rate of 95%. Furthermore, they showed that the gas separation was selective towards CO₂ from the gas isotherms of the flue gas simulation using a mixture of CO₂ and N₂ gas.

On the same topic of using existing materials from biomass or its byproducts, Joan et al. [171] made use of two different plant-based biomass as carbonaceous char for CO₂ adsorption, the plant-based materials were mainly from vine shoots and wheat straw pallets which was subjected to pyrolysis as a reduced rate to produce the biochar. The purpose of using two different biochar was to showcase their efficiency in CO₂ uptake under dry and humid conditions, activated carbon from vine shoots performed better under dry condition while wheat straw pallets faired at humid conditions. The difference in the performance was hypothesized by the amount of hydrophilic functional groups in the organic structure of the materials. The two biomass samples were subjected to cyclic adsorption-desorption testing and there was a minute drop in CO₂ uptake capacity. The best performance after five cycles

achieved 82% retention.

Lignin is one of the largest contributors to municipal waste as its application in our daily lives is ubiquitous and its fate as a waste product often comes in the form of lignocellulosic waste [172]. To reduce the environmental impact, upcycling of lignocellulosic waste has been intensely researched in recent years, given its ease in functionalization from the branched hydroxyl groups. A lignin derived biochar was developed by Zhang et al. [173] where the novel biochar undergone post treatment acid wash followed by ultrasound to enhance the adsorption capability of the material. They claimed that the post treatment method polished the surface of the material by removing blockages and enlarging the existing pore sizes. The increased pore volume from the post treatment extruded organic ashes and allowed the material to achieve a CO₂ adsorption capacity of 178 mg g⁻¹ due to the clearing of the microporous structures. Moreover, its integrity was also sustained as its performance remained at a high 99.46% even after 10 cycles of adsorption desorption.

It is well established that hydrogels could find huge applications due to its porous structure [174]. As previously mentioned of the conventional pressure and thermal adsorption swings and electro adsorption swings, Chao et al. [169] reports a solar adsorption swing made of an activated carbon with high CO₂ capture. The polymer was synthesized by imine condensation of terephthalate aldehyde and triaminoguanidinium chloride under mild acidic condition forming an organic covalent framework in the form of hydrogel or xerogels (Fig. 11h). The adsorption-desorption mechanism works on the basis of intermittent illumination, where “light on” phase is when N heteroatoms are available as Lewis bases for adsorption of CO₂, and “lights off” phase is when CO₂ molecules are released and recovered. The set-up in Fig. 11i depicts the working mechanism of the intermittent illumination, along with the adsorption productivity as observed in Fig. 11j. The increase in adsorption capacity corresponds to the “lights on” phase, and the dips corresponds to the desorption during “lights off”. The fabricated xerogel and hydrogels contain plenty of ultramicropores which are sites for CO₂ capture. Maximum CO₂ capacity reached 0.226 kg_{CO₂} kg_{carbon} h⁻¹ and exhibits high CO₂ selectivity when exposed to flue gas conditions.

6. Comparison of absorption and adsorption techniques

6.1. Cost and efficiency

New CO₂ absorption materials have proved to be efficient in CO₂ capture, many of which have superseded 30 wt% MEA in their CO₂ capture performance. Nevertheless, researchers are still actively finding the perfect material with low cost in terms of material production, operations and energy consumption, and high CO₂ capture efficiency in terms of CO₂ loading, regeneration efficiency, cyclic capacity etc. Traditional amines are known for their good CO₂ solubility, low material cost and established infrastructure and processes. However, its energy-intensive solvent regeneration incurs significant operational costs, which led to research of semi or non-aqueous amine systems. Though these systems reduced the solvent regeneration energy, conventional 30 wt% MEA still attained similar or better performance. Given the cost of changing out MEA from existing plants for similar performance material, it was not highly favored amongst the existing industries. On the other hand, research in ILs offered better CO₂ capture performance with good tunability, high CO₂ solubility, high regeneration efficiency and lower solvent regeneration energy compared to amines. However, they face higher upfront costs due to complex synthesis and scalability challenges. Therefore, much work is needed to lower its production cost before ILs can be comfortably used on an industrial scale. Nanofluids present a potential cost advantage by requiring less material but introduce complexity in nanoparticle production and dispersion. Their enhanced mass transfer kinetics may improve capture efficiency. In addition, the use of magnetic nanoparticles with an external magnetic field applied improved CO₂ absorption and desorption performance,

Table 2
Comparison of absorption and adsorption techniques.

Parameters	Absorption	Adsorption
Thermodynamics	Mostly endothermic.	Mostly exothermic.
Nature of process	Bulk phenomenon, concentration eventually becomes uniform throughout the system.	Surface phenomenon, internal concentration differs from surface concentration.
Rate of reaction	Uniform reaction rate.	Steady incease and reaches an equilibrium.
Temperature influence	Temperature independent.	Favored by lower temperature.
Cyclic Capacity	<ul style="list-style-type: none"> - Typically > 3 – 5 cycles - 30 wt% MEA: 0.841 mol kg⁻¹ / 0.254 mol mol⁻¹. - Absorbents in general: 0.6 – 2.7 mol kg⁻¹ / 0.2 – 3.1 mol mol⁻¹. 	<ul style="list-style-type: none"> - Cycling adsorption-desorption swing test typically ranging from 5 – 10 cycles. - Typically, 3–10 mmolg⁻¹ for adsorbents. - A 7000-cyclic swing test was demonstrated by et al. using faradaic electroswing adsorption mechanism. - Typically, 2.5–4GJ ton⁻¹ for adsorbents. - However, desorption and regenerative process may require high heat and pressure to recover adsorbent for reuse.
Energy consumption (Productivity)	<ul style="list-style-type: none"> - 30 wt% MEA: 3.80 GJ ton⁻¹ CO₂. - Other absorbents: 1.6 – 2.8 GJ ton⁻¹ CO₂. 	
Regeneration efficiency	70 – 100%.	70 – 100%.
CO ₂ Loading (Maximum Adsorption Capacity)	<ul style="list-style-type: none"> - 30 wt% MEA: 2.2 mol kg⁻¹, 0.614 mol mol⁻¹. - Other absorbents: 0.5 – 25 mol kg⁻¹ / 0.6 – 4.7 mol mol⁻¹. 	0.5 – 6.77 mmolg ⁻¹ .
Desorption mechanisms	<ul style="list-style-type: none"> - Desorption conditions range from 298 – 393 K, 0.5 – 101.325 kPa. - Aqueous systems usually require higher temperature. 	<ul style="list-style-type: none"> - Usually, around 320 – 370 K for desorption, 100–500 kPa. - Inorganic and metal containing adsorbents may require high temps at 400 – 500 K.
Material	Liquids (Aqueous, semi-aqueous, non-aqueous)	<ul style="list-style-type: none"> Solid composites, mostly porous cages and cavity that allow housing and uptake of small molecules. Mostly require simple synthetic procedures to functionalize pore sites to attach functional groups for chemisorption.
Preparation (e.g. is synthesis required)	<ul style="list-style-type: none"> - Amines: Often considered as low material cost. Bulk cost are from the infrastructure, equipment and operational expenses. - Ionic Liquids: Higher synthesis costs due complex chemical processes and higher purity requirements. - Nanofluids: Potential cost advantages due to the lower amount of material required compared to bulk solvents. Bulk cost in production. 	

signaling a potential for higher efficiency and cost reduction compared to the other two materials. However, nanofluids are still a rather new area of research, and challenges remain in ensuring stable nanoparticles and efficient regeneration processes. Phase change solvents, which is more common for amines and ILs systems, offer an improved CO₂ capture efficiency and lower solvent regeneration energy, reduced solvent loss. Given the current developmental stages of each material, amines are still the best choice for industrial scale applications as it is the most

mature and reliable material at present. Amine based phase change solvents or semi and non-aqueous amines solvents which gives better overall performance can slowly replace the conventional MEA solvent or trialed in new plants. Meanwhile, more work can be carried out with ILs and nanofluids to reduce its cost of production and improve its stability. When these main issues are resolved, they can have a higher chance of replacing amine solvents in the future.

Adsorption on the other hand has a much diverse and versatile selection of materials as the research in porous materials have been heavily researched over the past few decades. Currently, the best performing adsorbents stems from classes in MOFs, zeolites and activated carbons [175]. The innate desirable properties in these materials such as high thermal stability, wide availability and tunable pore size distribution, makes them attractive for molecular sieves for CO₂ capture [176]. Furthermore, their versatility in adsorption processes is highlighted in their ability to be functionalized with different functional groups for interaction between the adsorbent and the adsorbate. A common strategy is to dope the adsorbents with heteroatoms such as N and O doping to increase affinity towards CO₂ capture [177]. However, the cost of wet synthesis in terms of solvent cost and handling, hampers the practicality of pilot scale implementation of the materials. For future prospectus, more research should be directed towards the upcycling and use of biomass byproducts alternative as possible porous materials. Not only does this expand the field of research in sustainable CO₂ technology but also help in reducing carbon footprint in the process.

Taking a deeper dive into the insights of two different processes, a comparison of the techniques can be seen in Table 2. Adsorption processes often have lower initial capital costs compared to absorption processes. The cost of absorption materials varies, and amine absorbent are relatively low in comparison to ILs and nanofluids. Some of the more diverse classes of adsorbents such as activated carbon, silica gel, and zeolites have varied costs based on their specific chemical modification tailored for the CO₂ adsorption process. Generally, the more cost effective classes of adsorbents are mostly polymeric materials and activated carbons, while the more expensive ones tend to be complex MOFs and functionalized zeolites [176]. In the regenerative processes, absorption systems, especially aqueous systems, require high solvent regeneration energy, which may make up the major cost of the CO₂ capture process. Equipment such as pumps and heat exchangers may need to be regularly maintained or replaced due to corrosion from adsorbents such as ionic liquids or amines, contributing to operational costs. Adsorption systems on the other hand may incur high costs from regeneration agents, energy input, equipment, constant monitoring, and replacement of faulty adsorbents so as to regenerate high quality adsorbents required for efficient CO₂ capture.

The efficiency and turnover rates of the materials used in the two processes are also critical factors to be considered. Absorption is effective for gases or solutes that are highly soluble in the chosen absorbent. Efficiency depends on the solubility characteristics of the substances involved. Efficient mass transfer between the gas or liquid phase and the absorbent is crucial for high absorption efficiency. Adsorption on the other hand can achieve high efficiency in capturing specific molecules or contaminants. Efficiency depends on the affinity between the adsorbent and adsorbate. Adsorption processes can be designed for selective capture, enhancing their efficiency in targeted applications. In cases when porous materials are used such as zeolites or MOF cages, the low density nature of such materials results in a lighter weight in the overall set up facilitating ease of handling and potentially allow higher additive loading.

Absorption and adsorption costs vary based on the materials used, energy requirements, and regeneration processes. Both techniques can be highly efficient, with adsorption offering selectivity and absorption relying on solubility and mass transfer characteristics.

6.2. Scalability

As of the current state of technology, high cost, poor stability, low efficiency, and insufficient data has hindered most materials' application to the industry. The scalability of absorption and adsorption processes depends on various factors, including the nature of the sorbate, the available technology, and economic considerations. While physical pilot plants are ideal in assessing the scalability and economic feasibility of a material for CO₂ capture, utilization of simulation softwares such as Aspen Plus, Aspen Dynamic, Aspen Plus methodology etc. to aid in accurate prediction of the total annualized cost in using a new materials for CO₂ capture also provide helpful insights. The softwares are able to vary parameters such as input material, CO₂ composition, flow rate, pressure, temperature, position of CO₂ capture (eg. pre or post combustion) etc. to identify the most cost-efficient material and conditions for CO₂ capture.

Amines are the most matured amongst the materials, and its affordable cost has allowed for applications in many industrial plants and physical scale up pilot plants. Several commercially available and novel amine solvents were tested in pilot plants against conventional 30 wt% MEA. Cost of MEA-based pilot plants were found incur a cost of 51–147 \$/tCO₂ for post combustion processing [178]. While BASF OASE® blue solvent was tested in a 1.0–1.5 MW_e scale slipstream post combustion pilot plant, and found with higher CO₂ capture efficiency of 28.0% compared to MEA at 24.9%, and a cost of 38.8–57.4 \$/tCO₂ [179]. New amines were also tested where a mixture of newly synthesized amine with commercially available amine was tested in a 10 ton CO₂ per day Mikawa CO₂ capture pilot plant. the system was highly stable with low solvent regeneration energy of 2.4 GJ ton⁻¹ CO₂ and 90% CO₂ capture [180]. Evidently amines are feasible to be scaled up and tested in pilot plants prior to applying it to industries. On the other hand, high cost of ILs of up to \$5000 kg⁻¹ makes its uneconomical for industrial applications [181]. ILs are also plagued with high viscosity, which may add onto the operational cost. Nevertheless, it requires much lower energy for solvent regeneration compared to traditional 30 wt% MEA, and almost free from solvent degradation [182]. As such, several researchers have modeled different ILs in pilot plants, and the cost range from 62 to 270 \$/tCO₂ [178c,183]. The CO₂ capture cost-efficiency improves with increase in plant size, greatly benefitting from economy of scale [178c]. While there is much potential in nanofluids for CO₂ capture, more work needs to be done in maintaining the stability of nanofluids, especially maintaining a homogeneous nanoparticle dispersion and stability across large volumes over long periods. There are few studies on large pilot plants, nevertheless lab scale tests shows high CO₂ absorption and regeneration efficiency. Therefore we see amines as the most feasible for scaling up for an industrial scale. But in the long run, other materials may be able to attain the same performance and cost as amines, and provide a more efficient CO₂ capture.

In adsorption systems, processes are often modular and can be scaled up by adding more adsorption units or increasing the size of existing units to cater to industrial scaling needs. Different types of adsorbents can be tailored to specific adsorbates, providing flexibility in addressing diverse applications. The issue lies in the complexity and intricacy of the synthetic modification. If the process of modifying the adsorbents require tedious purification and stringent reaction conditions, then large scale production will not be feasible due to the impracticality. The typical cost ranges from 40 to 60 \$/tCO₂ ranges around in adsorption processes [184]. Capital cost for industrial infrastructure typically range from 1000 to 2000 \$/tCO₂. Svante is an example for the world's first pilot scale plant using adsorbent processes for carbon capture and their cost for CO₂ capture is about 60 \$/tCO₂ [185]. Perhaps exploring in alternative methods of upscaling such as designing for a continuous or batch operation will allow for adaptability of the adsorption process to vary in scales. In current advances in adsorption technologies, adsorption is widely employed in large-scale applications, such as clean water treatment [186], air purification [187], and industrial processes such as

petrochemical, food and beverage, and pharmaceuticals [188]. The scalability of adsorption processes is assessed by the economic feasibility of regenerating, reusing adsorbents and considering if it is suitable for continuous operations on a large scale.

6.3. Environmental impacts

CO₂ capture technologies strive to reduce the emission of greenhouse gases, and thereby reducing global warming and other ecological and environmental impacts. However, the materials and techniques used for CO₂ capture may lead to a different set of environmental impacts, where inappropriate choice of materials and technique may lead to overall more pollution.

The environmental impact of materials used for CO₂ absorption depends on the specific material, production process, usage, and disposal methods. Traditional amine-based solvents, such as monoethanolamine (MEA), diethanolamine (DEA), and methyldiethanolamine (MDEA), that are widely used for CO₂ absorption in industrial applications, are corrosive and toxic [189]. This poses a risk of environmental damage if accidentally released into the environment. Also, their production may involve energy-intensive processes and chemical reactions that generate pollutants. This would reduce its overall efficiency in CO₂ sequestering. ILs may be less toxic and environmentally damaging compared to amines. However, its complex synthesis may generate harmful waste materials that could be highly damaging to the environment [25]. More energy may also be required to produce the ILs. In addition, large scale production may lead to extensive resource consumption and high volume of waste generation. For nanofluids, common nanoparticles used are MWCNT and Fe₃O₄, which are said to possess low toxicity. Therefore, the degree of damage would also depend on the nanoparticles used. Nevertheless, the small size of nanoparticles causes them to interact with biological systems and penetrate biological barriers more readily, posing a potential risk of bioaccumulation in workers during production [190]. Also, they have higher environmental persistence, and if accidentally released into the environment, may lead to ecological impacts and bioaccumulation in terrestrial and aquatic ecosystems. Therefore, proper management and disposal of waste materials plays an important role in reducing the risk of accidental release that pollutes the environment.

While for CO₂ adsorption materials, similarly, production of the materials may release harmful waste materials in the process and use large amounts of energy. But with appropriate usage of the material, they are generally not considered damaging to the environment. MOFs are generally considered environmentally benign. However metal ions or organic ligands attached to the MOF structure may pose an environmental concern if released into the environment during production or disposal. Also, its complex synthesis coupled with purification, processing, transport and storage results in high energy consumption, large amount of waste solvent generated and harmful vapors release [191]. Similarly, organic polymers are generally considered safe for the environment. Some organic polymers may be derived from fossil fuels or use toxic chemicals during manufacturing, which can contribute to environmental pollution if not properly managed. While silicon-based materials are typically inert and non-toxic, their production may be energy intensive which leads to added carbon emissions. Biochar on the other hand, produced from the pyrolysis of biomass, is generally considered a sustainable material with minimal damage to the environment. In fact, biochar is considered environmentally beneficial to soil health and climate change mitigation [192]. Its environmental impact would depend on feedstock selection, pyrolysis conditions, and land use practices. Proper processing of biochar can bring significant environmental benefits.

Overall, both absorption and adsorption techniques have environmental impacts associated with their materials, processes, and energy requirements. Adsorption materials and techniques are considered to be less harmful to the environment and require lower energy compared to

absorption techniques. They do not involve energy-intensive solvent regeneration processes and solid sorbents may have lower greenhouse gas emissions associated with their production and disposal compared to solvents used in absorption techniques. As such, with solvents as their medium to absorb CO₂, absorption materials experience solvent degeneration, solvent loss and unwanted emissions of volatile organic compounds or toxic waste materials, polluting the environment [15]. Additionally, the production and disposal of solvent materials may contribute to environmental pollution and resource depletion. Compared to adsorption materials which use a solid composite material to lock CO₂ in, disposal of the material is simpler and less prone to spillage. In addition, waste materials such as lignin, ash, tar can be upcycled into adsorption materials for mechanical strength enhancement, allowing sustainable production of adsorbents. While absorption materials and techniques may be more toxic to the environment, the large extent of the environmental impact from both techniques depends on the methods of material production and waste disposal. Certain absorbent and adsorbent materials require complex synthesis which may lead to release of pollutants. Also, improper handling or disposal of the materials will severely affect the environment, regardless of the toxicity of the material. Therefore, to minimize the environmental impact of materials used for CO₂ capture, environmentally friendly solvents and sorbents can be used, and sorbent material production process can be optimized to reduce energy consumption and emissions. Proper handling and disposal procedures need to be put in place, and a thorough lifecycle environmental impact assessment of each material can be conducted to minimize damage to the environment. Ongoing research and development can also be carried out to identify and develop new processes and materials with improved environmental performance.

7. Challenges/limitations and opportunities

Lastly, in this section we address some challenges and limitations as well as research gaps that are potential opportunities for further research and development in the absorption and adsorption techniques. We hope to provide readers with more in-depth discussion about current problems that are limiting the advances in the field of CO₂ capture technologies and a concerted effort from the global scientific community in tackling these fundamental challenges will greatly push the boundaries of CO₂ capture technologies to new heights.

The first hurdle is to overcome upscaling of research approaches stemming from the techno-economic aspect as some technologies incorporated into the approaches are impractical and costly when conducted in a large-scale setting. These examples include the use of toxic and specific catalysts that are expensive and require highly stringent and specific conditions for its operation, albeit its highly yielding performance. On another hand, apart from the materials, techniques and characterization methods can also pose as a limiting factor in terms of its cost of operation when conducted in large scale. One example of such technology involves the use of direct air capture which incurs costly fabrication procedure. Ge and Wang et al. [193] strategically made use of a concise three-step procedure in order to circumvent this issue of cost. They made use of the temperature vacuum-swing adsorption test with the use of steam. Interestingly, they realized that the adsorption of moisture from steam during the heat purging step was capable of regenerating CO₂ during heat release. The procedure was able to efficiently capture CO₂ in ambient air and was competitive with current post-combustion CO₂ capture technologies if the heat energy is derived from solar energy or waste heat from industry.

Apart from improving current synthetic and fabrication procedures in the approaches, the use of computational simulation allows us to tackle issues and gaps that are identified before conducting the actual experiments. This greatly helps to prevent wastage of resources for trials. The use of theoretical modeling allows us to optimize conditions, thermodynamic behavior of the reaction and time spent on the research.

In fact, some of the aforementioned examples have incorporated the use of theoretical modeling and computational analysis in their studies. A special highlight to Thomas et al. [194] who not only revolve its analysis of CO₂ capture on theoretical modeling, but also made use of thermodynamic modeling of CO₂ adsorption behavior in several organic bases under aqueous conditions. The novel simulation method was able to predict using correlation data from phase equilibrium measurements and thermal characteristics of CO₂ when compared to data in the literature. Following up, the simulations were also applied in large scale pilot production settings to further validate their findings.

The future outlook for adsorption processes in research and development (R&D) as well as in various industries is promising, driven by advancements in materials science, environmental concerns, and the increasing need for sustainable efficient separation and purification technologies. Hybrid technologies, combining adsorption with other separation techniques or processes, should be explored for synergistic effects which will improve overall performance [195]. As mentioned earlier, the utilization of solar energy to activate the adsorbents for capture and deactivation for release of CO₂ makes use of natural sunlight instead of additional energy cost for the adsorbent activation.

The pressing issue of reducing carbon footprint will emphasize the need for sustainable practices which drive research into more energy-efficient and environmentally friendly regeneration methods, promoting the reusability of adsorbents. Research must focus on comprehensive life cycle assessments to evaluate and optimize the environmental footprint of adsorption processes. Ongoing research is focused on developing highly efficient and selective adsorbents through advanced materials and nanotechnology, allowing for customization based on specific molecules. As showcased by Hatton et al., the cycling rate using faradaic electro swing adsorption test of poly-1,4-anthraquinone reports a remarkable 7000 redox electrochemical cycles which out-performs most of the materials in terms of cycling rates. Such materials should be explored further to tailor for potential upscaling [154].

One of the major challenges in absorption processes is the inevitable use of solvents in the system. Especially when it is carried out in large scale setting, the approach will generate huge amounts of harmful waste solvents containing heavy elements which will be destined to be disposed into the environment. The result of this detriment will cause toxic side effects and endanger wildlife, which will eventually affect humans down the line. Kim et al. [196] demonstrated the use of a catalytic nickel nanoparticle that was able to absorb more CO₂ into a MEA system as compared to just purely using MEA. The approach reduced the amount of MEA used for CO₂ capture for a given amount of CO₂ since the nickel particle was able to aid in the absorption by reducing the absorption equilibrium significantly.

On the same topic of MEA, most research have been basing their reports to 30 wt% MEA as the benchmark. However due to its high regeneration energy, researchers have been actively looking to improve or find an alternative system with good CO₂ absorption and lower regeneration energy. On average, 3.2–4.0 GJ ton⁻¹ CO₂ is the current regeneration energy that researchers target to overcome. This opened the gates to new classes of absorbents such as amine blends, ionic liquids, nanofluids, phase change solvents etc., which have shown positive results of obtaining CO₂ loading above conventional 30 wt% MEA and lower regeneration energy. But so far none has actually replaced it for wide scale CO₂ capture. The new absorbents are either too costly for scale up, or insufficient data has been generated to give confirmation on their feasibility for usage in power plants. Amine blends in general are toxic, volatile and subjected to degradation. Due to the strong affinity with CO₂, considerable amounts of energy are still needed for solvent regeneration, pushing up the overall operational costs. ILs have significantly helped to reduce solvent regeneration energy. However, the major problem is that they are expensive compared with traditional absorbents, thus curtailing their large-scale employment. Most ILs are synthesized in lab scales using expensive raw materials and scaling up is not feasible. While nanofluids have helped to improve the mass transfer

Table 3
Properties of CO₂ absorption materials.

Material	Experiment CO ₂ Condition	Operating Condition (CO ₂ capture)	CO ₂ Loading (Absorption)	CO ₂ Absorption Rate	Operating Condition (CO ₂ Desorption)	CO ₂ Loading (After Desorption)	CO ₂ Desorption Rate	Energy consumption OR Regeneration efficiency	Cyclic Capacity	Viscosity / cP	Ref.
Amine											
8 M PZ/H ₂ O	Flow rate 5 L min ⁻¹	313.15 K Partial pressure (kPa)*	(mol mol ⁻¹) 0.31 0.39	(mol s ⁻¹ Pa ⁻¹ m ⁻²) 8.5×10^7	313.15 K	-	-	-	(mol kg ⁻¹) 0.79	-	[92]
8 M 1-MPZ/H ₂ O		0.5 (Lean CO ₂) 5 (Rich CO ₂)	0.16 0.26	8.4×10^7	-	-	-	-	0.83	9.6	
8 M 2-MPZ/H ₂ O		*(correspond to each absorption rate)	0.27 0.37	5.9×10^7	-	-	-	-	0.93	10.5	
30 wt% MEA/H ₂ O	13 vol% CO ₂ + N ₂	313 K, 101.325 kPa	(mol kg ⁻¹) 2.198	(mol kg ⁻¹ s ⁻¹) 32.68×10^5	353 K, 101.325 kPa	(mol kg ⁻¹) 1.357	(mol kg ⁻¹ s ⁻¹) 29.11×10^5	-	(mol kg ⁻¹) 0.841	1.58	[47]
MEA/2ME			2.090	34.14×10^5		0.637	43.35×10^5	-	1.453	2.62	
MEA/2EE			2.045	34.09×10^5		0.679	36.73×10^5	-	1.366	3.11	
DEA/2ME			1.662	29.87×10^5		0.123	68.18×10^5	-	1.539	9.06	
3 M MDEA	50% CO ₂ + N ₂ Flow rate 200 mL min ⁻¹	313.15 K, 100 kPa	(mol mol ⁻¹) 0.63	-	373.15 K	-	-	-	(mol mol ⁻¹ min ⁻¹) 0.0313	2.12	[87]
0.1 M PZ/3 M MDEA			0.64	-		-	-	-	0.0328	2.12	
0.2 M PZ/3 M MDEA			0.65	-		-	-	-	0.0350	2.43	
0.3 M PZ/3 M MDEA			0.67	-		-	-	-	0.0352	2.42	
0.1 M TEPA/3 M MDEA			0.66	-		-	-	-	0.0363	2.79	
0.2 M TEPA/3 M MDEA			0.73	-		-	-	-	0.0366	3.98	
0.3 M TEPA/3 M MDEA			0.74	-		-	-	-	0.0372	3.75	
0.1 M PEI/3 M MDEA			0.85	-		-	-	-	0.0388	4.70	
0.2 M PEI/3 M MDEA			0.97	-		-	-	-	0.0395	9.75	
0.3 M PEI/3 M MDEA			1.08	-		-	-	-	0.0385	15.95	
5 m aq PZ	Wetted wall column	313.15 °C Partial pressure* (kPa)	- 0.1–5 0.5–5	(mol s ⁻¹ Pa ⁻¹ m ⁻²) 1.41×10^6 1.13×10^6 2.09×10^6	-	-	-	-	(mol kg ⁻¹) 0.95 0.6 0.78	4.2	[94]
5 m PZ in 1SUF/1 H ₂ O		0.1–1.5 *(correspond to each absorption rate)	-	1.74×10^6 1.28×10^6 2.37×10^6	-	-	-	-	1.06 0.56 0.82	24	
5 m PZ in 1SUF/3 H ₂ O			-	1.99×10^6 0.94×10^6 3.05×10^6	-	-	-	-	1.21 0.56 0.98	10	
5 m PZ in 1IMI/1 H ₂ O			-	1.64×10^6 1.13×10^6 2.42×10^6	-	-	-	-	1.2 0.64 0.87	18	
5 m PZ in 1IMI/3 H ₂ O			-	2.24×10^6 1.08×10^6 3.12×10^6	-	-	-	-	1.26 0.67 0.93	8.3	
7 m MEA (30 wt% MEA/H ₂ O)	Wetted wall column	313.15 °C Partial pressure (kPa) 0.1–5 *(Lean CO ₂ Rich CO ₂)	(mol mol ⁻¹) 0.36–0.50	(mol s ⁻¹ Pa ⁻¹ m ⁻²) 2.0×10^{-6} 3.5×10^{-7}	-	-	-	-	-	-	[96]

(continued on next page)

Table 3 (continued)

Material	Experiment CO ₂ Condition	Operating Condition (CO ₂ capture)	CO ₂ Loading (Absorption)	CO ₂ Absorption Rate	Operating Condition (CO ₂ Desorption)	CO ₂ Loading (After Desorption)	CO ₂ Desorption Rate	Energy consumption OR Regeneration efficiency	Cyclic Capacity	Viscosity / cP	Ref.
7 m MEA in 1NMP/ 3 H ₂ O		*(correspond to each absorption rate)	0.33–0.48	2.5×10^{-6} 4.0×10^{-7}	-	-	-	-	-	-	
7 m MEA in 3NMP/ 1 H ₂ O			0.30–0.47	8.2×10^{-6} 4.0×10^{-7}	-	-	-	-	-	-	
7 m MEA in 19NMP/ 1 H ₂ O			0.29–0.46	35×10^{-6} 4.5×10^{-7}	-	-	-	-	-	-	
30 wt% MEA/H ₂ O	Flow rate of 80 mL min ⁻¹	313.15 K, 101.325 kPa	(mol kg ⁻¹) 1.80	-	393.15 K, 101.325 kPa	-	-	(GJ·ton ⁻¹ CO ₂) 3.80	1.57	-	[101]
AMP/AEEA/NMP			1.65	-				2.09	1.64	-	
AMP/MEA + 50% DGM	12% CO ₂ + N ₂ Flow rate 2 L min ⁻¹	313.15 K, 12 kPa	(mol kg ⁻¹) 1.82	-	368.15 K	-	-	2.07 GJ·ton ⁻¹ CO ₂ (normalized)	(mol kg ⁻¹) ~1.75	-	[107]
30 wt% MEA/H ₂ O	Simulating post-combustion CO ₂ capture for cement plant flue gases	313.15 K, 120 kPa CO ₂ vol%*: 0.4 20	(mol mol ⁻¹) 0.37	-	368.15 K	-	-	-	(mol mol ⁻¹) 0.25 0.17	-	[197]
AMP(30%)/PZ(5%)/ H ₂ O		60	0.52	-				-	0.26	-	
DEA(30%)/PZ(5%)/ H ₂ O	*(correspond to each CO ₂ loading)	0.39	0.52	-				-	0.21	-	
5 M MAE/DGM/H ₂ O (where DGM:H ₂ O is 7:3)	12 vol% CO ₂ + N ₂ Flow rate 1000 mL min ⁻¹	313.15 K	-	-	393.15 K	-	-	-	(mol kg ⁻¹) 1.04	32.12	[104]
MAE/3DMA1P/ DGM/H ₂ O (MAE: 3DMA1P 2:1.5, total 4 M. DGM:H ₂ O is 7:3)			(mol kg ⁻¹) 2.53 (CO ₂ rich phase) 0.08 (CO ₂ lean phase)	-				~2.8 GJ ton ⁻¹ CO ₂	1.59	13.12	
0.5 M MAE/DGM		313 K, 101.325 kPa	(mol kg ⁻¹) 4.589 (CO ₂ rich phase) 0.090 (CO ₂ lean phase)	-	393 K, 101.325 kPa	(mol kg ⁻¹) 1.844 (CO ₂ rich phase) 0.856 (combined phase)	-	1.94 GJ ton ⁻¹ CO ₂	(mol kg ⁻¹) 2.745	-	[105]
0.5 M MAE/EGDEE			4.791 (CO ₂ rich phase) 0.013 (CO ₂ lean phase)	-		2.228	-	-	2.563	-	
AEEA (1.0 M)/ DMSO:PMDETA (4:6)	Flow rate 80 mL min ⁻¹	313.15 K	(mol·mol ⁻¹) 1.75 (CO ₂ rich phase)	-	393.15 K	-	-	1.66 GJ·ton ⁻¹ CO ₂	(mol mol ⁻¹) 1.20	-	[106]
MEA(25%)/DEEA (50%)/H ₂ O	12 vol% CO ₂ + N ₂ Flow rate 2 L min ⁻¹	313.15 K, 12 kPa	(mol kg ⁻¹) 2.423 (CO ₂ rich phase)	-	373.15 K	-	-	-	(mol kg ⁻¹) ~1.9	-	[24]
AEEA(25%)/DEEA (50%)/H ₂ O Ionic Liquids			1.925 (CO ₂ rich phase)	-				2.58 GJ ton ⁻¹ CO ₂	~2.3	-	
30 wt% MEA/H ₂ O	15 vol% CO ₂ + N ₂	313.15 K, 101.325 kPa	(mol L ⁻¹) 3.02 ([mol mol ⁻¹] 0.614)	(mol L ⁻¹ s ⁻¹) 39.98×10^5	353.15 K, 101.325 kPa	-	(mol L ⁻¹ s ⁻¹) 10.11×10^5	-	(mol L ⁻¹) 1.27 ([mol mol ⁻¹] 0.254)	-	[113]

(continued on next page)

Table 3 (continued)

Material	Experiment CO ₂ Condition	Operating Condition (CO ₂ capture)	CO ₂ Loading (Absorption)	CO ₂ Absorption Rate	Operating Condition (CO ₂ Desorption)	CO ₂ Loading (After Desorption)	CO ₂ Desorption Rate	Energy consumption OR Regeneration efficiency	Cyclic Capacity	Viscosity / cP	Ref.
[Apaeim][gly](30 wt %)/H ₂ O			3.89 (4.19)	29.82×10^5	-		25.01×10^5	-	2.62 (2.82)	-	
[Apaeim][ala](30 wt %)/H ₂ O			4.19 (4.72)	29×10^5	-		22.91×10^5	-	2.80 (3.14)	-	
[Apaeim][val](30 wt %)/H ₂ O			3.64 (4.44)	25.78×10^5	-		25.43×10^5	-	2.42 (2.95)	-	
[Eaeim][gly](30 wt %)/H ₂ O			1.99 (1.97)	35.12×10^5	-		31.56×10^5	-	1.93 (1.91)	-	
[Eaeim][ala](30 wt %)/H ₂ O			2.54 (2.44)	26.83×10^5	-		29.54×10^5	-	2.10 (2.09)	-	
[Eaeim][val](30 wt %)/H ₂ O			2.56 (2.90)	36.72×10^5	-		28.29×10^5	-	2.07 (2.35)	-	
[Paeim][gly](30 wt %)/H ₂ O			2.35 (2.45)	30.87×10^5	-		27.52×10^5	-	1.87 (1.95)	-	
[Paeim][ala](30 wt %)/H ₂ O			2.46 (2.67)	39.37×10^5	-		30.87×10^5	-	2.02 (2.19)	-	
[Paeim][val](30 wt %)/H ₂ O			2.50 (2.96)	36.58×10^5	-		27.11×10^5	-	2.23 (2.65)	-	
[VBTMA][Arg]		298 K, 100 kPa	(mol mol ⁻¹) 0.83	-	353.15 K	-	-	-	-	-	[115]
Poly[VBTMA][Arg]			1.14	-		-	-	Regeneration efficiency 86% (5th cycle)	-	-	
27	[N ₁₁₁₁][Gly]/EtOH	Flow rate 50 mL min ⁻¹	303.15 K	(mol mol ⁻¹) 0.85	-	393.15 K	-	-	Regeneration efficiency 80.54% (1st cycle)	-	[118]
[E ₁ Py][C(CN) ₃]	-		313.15 K, 1500 kPa	(Mole fraction of CO ₂) 0.40429	-	-	-	-	-	~10	[121]
[E ₁ Py][N(CN) ₂] [E ₁ Py][SCN]				0.34601 0.16347	-	-	-	-	-	~48 ~175	
[TEPAH][2-MI] (0.5 mol·L ⁻¹)/ NPA/EG	15 vol% CO ₂ + N ₂	313.15 K	(mol mol ⁻¹) 1.72	(mol mol ⁻¹ min ⁻¹) 0.118	393.15 K	-	-	90.7% (5th cycle)	-	3.66	[124]
[BMIM][BF ₄] (30 wt %)/MDEA [BEIM][BF ₄] (30 wt %)/MDEA	Flow rate 20 mL min ⁻¹	298 K	(g g ⁻¹) 0.0526 0.0517		353 K	-	-	-	-	49.46 cp	[126]
0.3 M [Hmim][Gly] + 0.7 M AMP + water	15 vol% CO ₂ + N ₂ Flow rate 120 mL min ⁻¹	303 K	(mol mol ⁻¹) 0.04886		333 K, 0.5 kPa	-	-	Regeneration efficiency 84.6% (3rd cycle)	-	139	[130]
[NH ₂ e-mim][BF ₄]/ [bmim][BF ₄] (ratio 4:6)	Flow rate 60 mL min ⁻¹	303.15 K, 0.1 MPa	(mol mol ⁻¹) 0.07	353.15 K, 0.1 MPa.	-	-	-	Regeneration efficiency 75–85% (5th cycle)	-	400	[131]
[C ₄ mim][OAc]/ [NH ₂ emim][BF ₄] [C ₄ mim][OAc] [NH ₂ emim][BF ₄]	15% CO ₂ + + 2% SO ₂ + N ₂	293 K	(mol mol ⁻¹) 0.4 0.204 0.180	-	-	-	-	-	-	-	[133]
MEA (30 wt %)/[BMIM] BF ₄ (40 wt%)/H ₂ O	-	303.15 K	(mol mol ⁻¹) 0.581		363 K	-	-	2.16 GJ ton ⁻¹ CO ₂	-	5.98	[134]

(continued on next page)

Table 3 (continued)

Material	Experiment CO ₂ Condition	Operating Condition (CO ₂ capture)	CO ₂ Loading (Absorption)	CO ₂ Absorption Rate	Operating Condition (CO ₂ Desorption)	CO ₂ Loading (After Desorption)	CO ₂ Desorption Rate	Energy consumption OR Regeneration efficiency	Cyclic Capacity	Viscosity / cP	Ref.
Nanofluids											
nMWCNT (0.05 wt %)/10 wt% MDEA	-	313 K, 1880 kPa	(mol kg ⁻¹) 0.720	-	-	-	-	-	-	-	[26]
nMWCNT (0.05 wt %)/10 wt% MEA			0.771	-	-	-	-	-	-	-	
nMWCNT (0.05 wt %)/10 wt% MDEA + 5 wt% MEA			0.738	-	-	-	-	-	-	-	
nMWCNT (0.05 wt %)/10 wt% MDEA + 5 wt% Pz			0.885	-	-	-	-	-	-	-	
0.005 vol% AA-Fe ₃ O ₄ /MeOH (without magnetic flux)	In a bubble column, flow rate 0.033 g s ⁻¹	298.15 K, 400 kPa	(mmol g ⁻¹) 0.136	-	333.15 K	-	-	(Regeneration ratio) 0.910	-	-	[139a]
0.005 vol% AA-Fe ₃ O ₄ /MeOH (with magnetic flux)			0.157	-	-	-	-	0.898	-	-	
0.005 vol% Fe ₃ O ₄ /MeOH (without magnetic flux)			0.135	-	-	-	-	0.914	-	-	
0.005 vol% Fe ₃ O ₄ /MeOH (with magnetic flux)			0.141	-	-	-	-	0.973	-	-	
0.1 wt% PEI-GO/40 wt% MDEA	-	303.15 K, 2000kPa	(mol kg ⁻¹) 4.497	-	-	-	-	-	-	-	[139b]
0.1 wt% GO/40 wt% MDEA			4.269	-	-	-	-	-	-	-	
SiO ₂ (0.1 wt%)/H ₂ O	-	308 K, 4000 kPa	(mol kg ⁻¹) 0.53	-	-	-	-	-	-	-	[142]
Al ₂ O ₃ (0.1 wt%)/H ₂ O			0.52	-	-	-	-	-	-	-	
Fe ₃ O ₄ (0.02 wt %)/H ₂ O			0.55	-	-	-	-	-	-	-	
CNT (0.02 wt%)/H ₂ O			0.59	-	-	-	-	-	-	-	
CNT (0.02 wt %)/MDEA (5 wt %)/H ₂ O			0.82	-	-	-	-	-	-	-	
CNT (0.02 wt %)/MDEA (10 wt %)/H ₂ O			0.83	-	-	-	-	-	-	-	
CNT (0.02 wt%)/DEA (5 wt%)/H ₂ O			0.87	-	-	-	-	-	-	-	
CNT (0.02 wt%)/DEA (10 wt%)/H ₂ O			0.90	-	-	-	-	-	-	-	
NR ₂ -SiO ₂ (0.1 wt %)/H ₂ O	Flow rate 1 L min ⁻¹	298.15 K	(mol kg ⁻¹) 25	-	298.15 K	-	-	Regeneration efficiency 85.7% (5th cycle)	-	2.23	[144]
NR ₂ -SiO ₂ (0.1 wt %)/PEG 400 dispersion (0.1 wt %)		303.15 K	23.16 105.34	-	-	-	-	-	-	-	

Table 4
Properties of CO₂ adsorption materials.

CO ₂ Sorbent	Experiment CO ₂ Condition	Feed CO ₂ /N ₂ /H ₂ O	Operating Temperature (K)	Regeneration temperature (K)	Purity	Recovery	Cyclic Adsorption-desorption swing cycles	Productivity	Maximum Adsorption Capacity	Ref.
MOF Adsorbents										
MIL-91(Ti)/GO 2 wt%	Microwave irradiation	15/85/0	300	323	-	-	4	-	-	[148]
MIL-91(Ti)/GO 5 wt%										
MIL-91(Ti)/GO 10 wt%										
MIL-91(Ti)/GO 20 wt%										
UTSA-16	15 mol% CO ₂ + 3–7% H ₂ O at 25 and 40 °C	15/82/3	298	423	95	90	5	(MJ kg ⁻¹ CO ₂) 6.28–7.07	-	[149]
een-MOF/Al-Si	Gas feed rate 5 sccm	15/78/7 15/80/5 15/80/5	313 313 313	413	95 - -	90 71 ~100	5 100 100	7.61–8.68	-	[150]
een-MOF/Al-Si-C17-200								(mmol g ⁻¹) 2.82		
Organic Polymers										
PAN-g-GMA-EA	Gas feed 100 mL/min (95% CH ₄)	5/0/0	-	-	-	94	5	-	(mmol g ⁻¹) 2.84	[33a]
TA-PR	Isothermal adsorption at 0.02–1 bar	100/0/0	273	-	-	-	-	-	(mg g ⁻¹) 27.4	[151]
PA-PR										
PDA-PR										
TBA-PR										
FA-PR										
CAM (composite adsorption fiber material)	Feed flow rate at 1733–1933 NL min ⁻¹	15/85/0	-	-	40.08	96.55	6	(molCO ₂ kg _{ads} ⁻¹ h ⁻¹) 2.40	-	[152]
15-own-5 ether-POC (PAQ-CNT) cathode (PVFc-CNT) anode	-	-	300	-	-	-	2	-	-	[153]
	Electrochemical cell condition at 20 mbar and 294 K, feed rate 10 mL min ⁻¹	15/5/0	298	298	100	100	7000	-	-	[154]
Inorganic Adsorbents										
AC	Purge with CO ₂ at 303 K then purged with N ₂	Purge with CO ₂ then N ₂	303	433–553	99	95.47	5	-	(mg g ⁻¹) 52.01	[157]
CeO ₂ /AC										
ZnO/AC										
Co ₂ O ₃ /AC										
SH-MMT	Absorbent lined bed column purging with N ₂ then CO ₂	Purging with N ₂ then CO ₂	298	373	-	98	10	-	(mg g ⁻¹) 102.21	[158]
GO-TiO ₂	Miotrac Belsorp-max adsorption apparatus	15/85/0	298	393	-	-	-	-	(mmol g ⁻¹) 0.508	[159]
Ca-doped MgO	Feed flow rate 0–1000	-	-	-	-	-	-	-	-	[160]
Fe-doped MgO										
Al-doped MgO										
Ce/ Al-doped MgO										
Silicon-based Adsorbents										
13X-PEI-20	Feed flow rate 50 mL min ⁻¹	Purging with N ₂ then CO ₂	298	348	-	-	-	-	(mmol g ⁻¹) 1	[162]
13X-PEI-40										
13X-PEI-60										
13X-PEI-80										
PEI/MSF-4	1 bar, Flow rate 30 mL min ⁻¹	15/85/0	298	363	-	-	5	-	(mmol g ⁻¹) 4.7	[163]
CSMS-12	200 mm adsorption column, Flow rate 150 mL min ⁻¹	15/85/0	273	-	-	-	-	-	(mmol g ⁻¹) 1.86	[164]
Biochar and byproducts from biomass										

(continued on next page)

Table 4 (continued)

CO ₂ Sorbent	Experiment CO ₂ Condition	Feed CO ₂ /N ₂ /H ₂ O	Operating Temperature (K)	Regeneration temperature (K)	Purity	Recovery	Cyclic Adsorption-desorption swing cycles	Productivity	Maximum Adsorption Capacity	Ref.
Carbon honeycomb monolith	Flow rate 20 mL min ⁻¹	Purging with N ₂ then CO ₂	231	393	-	80	5	-	(mmol g ⁻¹) 1.02	[166]
3D printed carbon monolith	Flow rate 100 mL min ⁻¹	15/85/0	298	423	84.3	95	-	-	(mmol g ⁻¹) 1.04	[167]
SH800	Flow rate 50 mL min ⁻¹	40–50/0/0 (60–50 H ₂)	298	-	99	-	5	-	(mmol g ⁻¹) 6.77	[171]
SH500									-	
PC-1-1	5 °C min ⁻¹ to 300 °C	15/85/0	273–298	-	-	95	10	-	(mmol g ⁻¹) 3.81	[170]
PC-1-2									4.40	
PC-1-3									4.10	
PC-2-1									4.77	
PC-3-1									5.03	
PC-4-1									4.62	
AC VS_600	In a bubble column, flow rate	15/75/10	298–323	323	-	84.1	5	-	(mmol g ⁻¹) 2.35	[198]
AC_VS_600_P	0.033 g s ⁻¹				-	72.9	-	-	2.67	
AC_WS_500					-	68.8	-	-	2.63	
AC_WS_500_P					-	69.6	-	-	2.44	
LB	Flow rate 50 mL min ⁻¹	98/0/0	298	323	-	76.14	10	-	(mg g ⁻¹) 178.75	[173]
LBA						98.19			-	
LBAU1						99.46				
LBAU5						99.14				
LBAU10						94.00				
LBAU20						96.55				
TPA-TG _{Cl}	Flow rate 1 L min ⁻¹	20/80/0	298	373	-	-	-	0.226	(mg g ⁻¹) 102.2	[169]

rate of CO₂ across the gas-liquid interface for faster CO₂ absorption. However, their stability needs to be maintained by addition of surfactants, or surface modification which may be a costly process. Both ILs and nanofluids are a relatively new area of research, and clear, systematic understanding between the interaction between the absorbents and CO₂, their kinetics and thermodynamics are not well established. There are also not many studies that provide data on real industrial conditions, and most experiments are conducted with CO₂ in N₂, which does not simulate the actual composition of flue gas from power plants. This questions the applicability of the results and performance when it is eventually translated up. Research which includes SO₂ (about 2%) in inflow gas indicated lower amounts of CO₂ captured. And this is not adding on to other possible waste gas and degraded solvent that is generated in industrial flue gas. This makes it harder for their translation to power plants. Therefore, in addition to looking for cost-efficient materials for efficient CO₂ absorbents, detailed studies for the CO₂ capture properties and transport behaviors need to be established. In due time, pilot plants for these systems would be needed to provide a more realistic understanding of their operation on an industrial scale.

8. Conclusion

To conclude this review, we have provided an in-depth and thorough discussion by highlighting some examples of recent advances in absorption and adsorption technologies for CO₂ capture. By sequestering CO₂ into the novel materials discussed above, we are able to reduce the consequences of the increasing fossil fuel consumption due to urban development. In the adsorption approaches discussed, innovative use of support material increases mechanical and thermal strength of the composite to prevent decomposition of the material. Researchers have found innovative and energy conservative methods to incorporate adsorbents into porous materials. The sustainable use of byproducts from biomass as porous materials for gas sorption have paved many permutations and combinations of adsorbents to existing waste byproducts which are fated

to be disposed. As such, these materials are in turn upcycled for a greater purpose. One of the most effective approaches in capturing CO₂ was discussed in the chemical absorption techniques which are the most developed, with most research basing off their performance to 30 wt% MEA. The classes of materials discussed have shown remarkable breakthroughs and pushed the frontiers in CO₂ capture. The issue of cost remains a major hurdle from preventing pilot production, and the impracticality of upscaling these intricate approaches calls for a dire need for more streamlined and cost-efficient methodologies in these approaches and techniques. Future direction in the field of CO₂ capture may be focused on the direction of studying and modeling the thermodynamics during the process of capture and conversion of CO₂ as this is an area that as yet to be well established. The use of artificial intelligence (AI) and theoretical simulation is impetus in such forecasting studies.

CRediT authorship contribution statement

Longgang Tao: Writing – review & editing. **Cun Wang:** Writing – review & editing. **Qiang Zhu:** Supervision, Conceptualization. **Xiang Yun Debbie Soo:** Writing – original draft, Visualization. **Johnathan Joo Cheng Lee:** Writing – original draft, Visualization. **Wenya Wu:** Writing – original draft, Visualization. **Jie Bu:** Supervision, Funding acquisition, Conceptualization.

Declaration of Competing Interest

The authors declare that they have no known competing financial interests or personal relationships that could have appeared to influence the work reported in this paper.

Data availability

Data will be made available on request.

Acknowledgment

The authors gratefully acknowledge the National Research Foundation (NRF) of Singapore for funding this research under the Low-Carbon Energy Research Funding Initiative (Project Ref: U2102d2008).

References

- [1] K.O. Yoro, M.O. Daramola, in: *Advances in Carbon Capture*, Woodhead Publishing, 2020, pp. 3–28.
- [2] Intergovernmental Panel on Climate Change.
- [3] (a) P.J. Ong, Y.Y. Lum, X.Y.D. Soo, S. Wang, P. Wang, D. Chi, H. Liu, D. Kai, C.-L. K. Lee, Q. Yan, J. Xu, X.J. Loh, Q. Zhu, *Constr. Build. Mater.* **386** (2023) 131583; (b) J.Z.X. Heng, T.T.Y. Tan, Z. Xing, J.L.Y. Ong, K.S. Lin, X.Q. Koh, W. Jiang, L. Zhang, Q. Zhu, Z. Li, X.J. Loh, J.Y.C. Lim, E. Ye, *Mater. Today Chem.* **31** (2023) 101608; (c) R.J. Yeo, J.C. Yeo, S. Yu Tan, A. Sng, N. Tomczak, J.K. Muiruri, S. Wang, P. Wang, W. Thitsartarn, F. Wang, *Adv. Opt. Mater.* (2023) 2301955.
- [4] (a) B.E. Jia, A.Q. Thang, C. Yan, C. Liu, C. Lv, Q. Zhu, J. Xu, J. Chen, H. Pan, Q. Yan, *Small* **18** (2022) 2107773; (b) Y. Shi, C. Lee, X. Tan, L. Yang, Q. Zhu, X. Loh, J. Xu, Q. Yan, *Small Struct.* **3** (2022) 2100185; (c) F. Wei, B. Cheng, L.T. Chew, J.J. Lee, K.H. Cheong, J. Wu, Q. Zhu, C.C. Tan, *J. Mater. Res. Technol.* **20** (2022) 4130–4136.
- [5] (a) Z.M. Png, X.Y.D. Soo, M.H. Chua, P.J. Ong, J. Xu, Q. Zhu, *J. Mater. Chem. A* **10** (2022) 3633–3641; (b) X.Y.D. Soo, Z.M. Png, X. Wang, M.H. Chua, P.J. Ong, S. Wang, Z. Li, D. Chi, J. Xu, X.J. Loh, Q. Zhu, *ACS Appl. Polym. Mater.* **4** (2022) 2747–2756; (c) J.J.C. Lee, S. Sugianto, P.J. Ong, X.Y.D. Soo, X. Ni, P. Luo, Y.Y.K. Hnin, J.S. Y. See, F. Wei, R. Zheng, P. Wang, J. Xu, X.J. Loh, D. Kai, Q. Zhu, *J. Energy Storage* **56** (2022) 106118; (d) J.J.C. Lee, N.J.X. Lim, P. Wang, H. Liu, S. Wang, C.-L.K. Lee, D. Kai, F. Wei, R. Ji, B.H. Tan, *World Sci. Annu. Rev. Funct. Mater.* **1** (2023) 2230007; (e) X.Y. Soo, J.K. Muiruri, J.C. Yeo, Z.M. Png, A. Sng, H. Xie, R. Ji, S. Wang, H. Liu, J. Xu, *SmartMat* (2023) e1188; (f) Q. Zhu, P.J. Ong, S.H.A. Goh, R.J. Yeo, S. Wang, Z. Liu, X.J. Loh, *Nano Mater. Sci.* (2023); (g) X.Y.D. Soo, S.Y. Tan, A.K.H. Cheong, J. Xu, Z. Liu, X.J. Loh, Q. Zhu, *Exploration*, Wiley Online Library, 2023, p. 20230016; (h) W.Y. Wu, G.M.D. Yeo, S. Wang, Z. Liu, X.J. Loh, Q. Zhu, *Chem. Asian J.* **18** (2023) e202300391.
- [6] (a) Q. Zhu, E. Yildirim, X. Wang, A.K.K. Kyaw, T. Tang, X.Y.D. Soo, Z.M. Wong, G. Wu, S.-W. Yang, J. Xu, *Mol. Syst. Des. Eng.* **5** (2020) 976–984; (b) X. Yong, G. Wu, W. Shi, Z.M. Wong, T. Deng, Q. Zhu, X. Yang, J.-S. Wang, J. Xu, S.-W. Yang, J. Mater. Chem. A **8** (2020) 21852–21861; (c) T. Tang, A.K.K. Kyaw, Q. Zhu, J. Xu, *Chem. Commun.* **56** (2020) 9388–9391; (d) X.Y. Tan, J.-F. Dong, N. Jia, H.-X. Zhang, R. Ji, A. Suwardi, Z.-L. Li, Q. Zhu, J.-W. Xu, Q.-Y. Yan, *Rare Met.* **41** (2022) 3027–3034; (e) X. Wang, X. Huang, Z.M. Wong, A. Suwardi, Y. Zheng, F. Wei, S. Wang, T. L. Tan, G. Wu, Q. Zhu, H. Tanoto, K.S. Ong, S.-W. Yang, A.Q. Yan, J. Xu, *ACS Appl. Nano Mater.* **5** (2022) 8631–8639.
- [7] Vol. 2023, NASA.
- [8] Vol. 2023, United Nations.
- [9] Vol. 2023, International Energy Agency.
- [10] (a) J. Hu, Y. Zou, Y. Zhao, *Int. J. Hydrot. Energy* **58** (2024) 1429–1442; (b) S. Gao, Q. Zhang, X. Su, X. Wu, X.-G. Zhang, Y. Guo, Z. Li, J. Wei, H. Wang, S. Zhang, J. Wang, *J. Am. Chem. Soc.* **145** (2023) 9520–9529; (c) Q. Zhang, S. Gao, Y. Guo, H. Wang, J. Wei, X. Su, H. Zhang, Z. Liu, J. Wang, *Nat. Commun.* **14** (2023) 1147; (d) S. Zhang, X. Bai, C. Zhao, Q. Tan, G. Luo, J. Wang, Q. Li, L. Wu, F. Chen, C. Li, *Earth's Future* **9** (2021) e2020EF001938.
- [11] (a) L. Wang, Y. Yang, W. Shen, X. Kong, P. Li, J. Yu, A.E. Rodrigues, *Chem. Eng. Sci.* **101** (2013) 615–619; (b) L. Wang, Y. Yang, W. Shen, X. Kong, P. Li, J. Yu, A.E. Rodrigues, *Ind. Eng. Chem. Res.* **52** (2013) 7947–7955.
- [12] C.A. Scholes, K.H. Smith, S.E. Kentish, G.W. Stevens, *Int. J. Greenh. Gas Control* **4** (2010) 739–755.
- [13] A. Mukherjee, J.A. Okolie, A. Abdelrasoul, C. Niu, A.K. Dalai, *J. Environ. Sci.* **83** (2019) 46–63.
- [14] L.F. de Mello, R. Gobbo, G.T. Moura, I. Miracca, *Energy Procedia* **37** (2013) 7815–7824.
- [15] U. Khan, C.C. Ogbaga, O.-A.O. Abiodun, A.A. Adeleke, P.P. Ikubanni, P.U. Okoye, J.A. Okolie, *Carbon Capture Sci. Technol.* (2023) 8.
- [16] G. Hochgesand, *Ind. Eng. Chem.* **62** (1970) 37–43.
- [17] Z. Kapetaki, P. Brandani, S. Brandani, H. Ahn, *Int. J. Greenh. Gas Control* **39** (2015) 17–26.
- [18] K. Arnold, M. Stewart, in: *Surface Production Operations: Design of Gas-Handling Systems and Facilities*, second edition, Gulf Professional Publishing, Woburn, 1999, pp. 151–194.
- [19] A. Kohl, R. Nielsen, Houston: Gulf Publishing Company 1997.
- [20] J.G. Speight, in: *Natural Gas* (second edition), Gulf Professional Publishing, Boston, 2019, pp. 277–324.
- [21] E. Gjernes, S. Pedersen, T. Cents, G. Watson, B.F. Fostås, M.I. Shah, G. Lombardo, C. Desvignes, N.E. Flø, A.K. Mørken, T. de Cazenove, L. Faramarzi, E.S. Hamborg, *Energy Procedia* **114** (2017) 1146–1157.
- [22] H.F. Svendsen, E.T. Hessen, T. Mejell, *Chem. Eng. J.* **171** (2011) 718–724.
- [23] X. Li, J. Liu, W. Jiang, G. Gao, F. Wu, C. Luo, L. Zhang, *Sep. Purif. Technol.* **275** (2021) 119181.
- [24] F. Liu, M. Fang, W. Dong, T. Wang, Z. Xia, Q. Wang, Z. Luo, *Appl. Energy* **233–234** (2019) 468–477.
- [25] S. Zeng, X. Zhang, L. Bai, X. Zhang, H. Wang, J. Wang, D. Bao, M. Li, X. Liu, S. Zhang, *Chem. Rev.* **117** (2017) 9625–9673.
- [26] K. Rahimi, S. Riahi, M. Abbasí, *J. Environ. Chem. Eng.* **8** (2020) 103580.
- [27] S.D. Kenarsari, D. Yang, G. Jiang, S. Zhang, J. Wang, A.G. Russell, Q. Wei, M. Fan, *RSC Adv.* **3** (2013) 22739–22773.
- [28] (a) M. Zhao, Y. Yang, X.-S. Gu, *Inorg. Chem. Commun.* (2023) 152; (b) C. Goel, S. Mohan, P. Dinesha, *Sci. Total Environ.* **798** (2021) 149296; (c) E.E. Ünveren, B.Ö. Monkul, S. Sarıoğlu, N. Karademir, E. Alper, *Petroleum* **3** (2017) 37–50; (d) X. Fan, B.H. Tan, Z. Li, X.J. Loh, *ACS Sustain. Chem. Eng.* **5** (2017) 1217–1227; (e) Z. Li, P.L. Chee, C. Owh, R. Lakshminarayanan, X.J. Loh, *RSC Adv.* **6** (2016) 28947–28955; (f) X.J. Loh, *J. Appl. Polym. Sci.* **127** (2013) 992–1000.
- [29] A.A. Abd, S.Z. Naji, A.S. Hashim, M.R. Othman, *J. Environ. Chem. Eng.* **8** (2020) 104142.
- [30] J.M. Kolle, M. Fayaz, A. Sayari, *Chem. Rev.* **121** (2021) 7280–7345.
- [31] (a) M. Shang, J. Luo, *Int. J. Environ. Res. Public Health* **18** (2021) 2101; (b) J. Luo, W. Zhuo, S. Liu, B. Xu, *IEEE Access* (2024).
- [32] (a) J. Cao, Y. Sim, X.Y. Tan, J. Zheng, S.W. Chien, N. Jia, K. Chen, Y.B. Tay, J. F. Dong, L. Yang, *Adv. Mater.* **34** (2022) 2110518; (b) S.S.F. Duran, D. Zhang, W.Y.S. Lim, J. Cao, H. Liu, Q. Zhu, C.K.I. Tan, J. Xu, X.J. Loh, A. Suwardi, *Crystals* **12** (2022) 307; (c) J. Zheng, S.F.D. Solco, C.J.E. Wong, S.A. Sia, X.Y. Tan, J. Cao, J.C.C. Yeo, W. Yan, Q. Zhu, Q. Yan, *J. Mater. Chem. A* **10** (2022) 19787–19796; (d) J.J.C. Lee, N.N.A. Hayat, X.Y.D. Soo, S.Y. Tan, Y.Y.K. Hnin, S. Wang, F. Wei, D. Kai, F. Wang, P. Luo, J. Xu, X.J. Loh, Q. Zhu, *J. Energy Storage* **73** (2023) 109084; (e) A.N. Shafawi, A.R. Mohamed, P. Lahijani, M. Mohammadi, *J. Environ. Chem. Eng.* **9** (2021) 106869; (f) S. Jung, Y.-K. Park, E.E. Kwon, *J. CO₂ Util.* **32** (2019) 128–139; (g) P.D. Dissanayake, S.W. Choi, A.D. Igalavithana, X. Yang, D.C.W. Tsang, C.-H. Wang, H.W. Kua, K.B. Lee, Y.S. Ok, *Renew. Sustain. Energy Rev.* **124** (2020) 109785.
- [33] (a) A.A. Tourzani, F. Hormozi, M. Asadollahzadeh, R. Torkaman, *Sci. Rep.* **13** (2023) 6173; (b) S. Wang, J.K. Muiruri, X.Y.D. Soo, S. Liu, W. Thitsartarn, B.H. Tan, A. Suwardi, Z. Li, Q. Zhu, X.J. Loh, *Chem. Asian J.* **18** (2023) e202200972; (c) J. Kinyanjui Muiruri, J. Chee Chuan Yeo, X. Yun Debbie Soo, S. Wang, H. Liu, J. Kong, J. Cao, B. Hoon Tan, A. Suwardi, Z. Li, J. Xu, X. Jun Loh, Q. Zhu, *Eur. Polym. J.* **187** (2023) 111882; (d) Z.M. Png, C.-G. Wang, J. Yeo, J.J.C. Lee, N.E.B. Surat'man, Y.L. Tan, H. Liu, P. Wang, M.B.H. Tan, J. Xu, *Mol. Syst. Des. Eng.* (2023); (e) R. Liang, X. Yang, P.Y.M. Yew, S. Sugianto, Q. Zhu, J. Zhao, X.J. Loh, L. Zheng, D. Kai, *J. Nanobiotechnol.* **20** (2022) 327.
- [34] (a) W.T. Neo, Q. Ye, M.H. Chua, Q. Zhu, J. Xu, *Macromol. Rapid Commun.* **41** (2020) 2000156; (b) M.H. Chua, S.H.G. Toh, P.J. Ong, Z.M. Png, Q. Zhu, S. Xiong, J. Xu, *Polym. Chem.* **13** (2022) 967–981; (c) S. Wang, P.J. Ong, S. Liu, W. Thitsartarn, M.J.B.H. Tan, A. Suwardi, Q. Zhu, X.J. Loh, *Chem. Asian J.* **17** (2022) e202200608; (d) S. Wang, W.Y. Wu, J.C.C. Yeo, X.Y.D. Soo, W. Thitsartarn, S. Liu, B.H. Tan, A. Suwardi, Z. Li, Q. Zhu, *BMEMat* (2023) e12021; (e) T.P. Vo, M.H. Chua, S.J. Ang, K.L.O. Chin, X.Y.D. Soo, Z.M. Png, T.L.D. Tam, Q. Zhu, D.J. Procter, J. Xu, *Polym. Chem.* **13** (2022) 6512–6524; (f) M.H. Chua, K.L.O. Chin, X.J. Loh, Q. Zhu, J. Xu, *ACS Nano* **17** (2023) 1845–1878.
- [35] (a) P. Madejski, K. Chmiel, N. Subramanian, T. Kuś, *Energies* **15** (2022) 887; (b) N.S. Sifat, Y. Haseli, *Energies* **12** (2019) 4143; (c) S. Kammerer, I. Borho, J. Jung, M.S. Schmidt, *Int. J. Environ. Sci. Technol.* **20** (2023) 8087–8104.
- [36] (a) F. Meng, Y. Meng, T. Ju, S. Han, L. Lin, J. Jiang, *Renew. Sustain. Energy Rev.* **168** (2022) 112902; (b) B. Aghel, S. Janati, S. Wongwises, M.S. Shadloo, *Int. J. Greenh. Gas Control* **119** (2022) 103715; (c) J. Hack, N. Maeda, D.M. Meier, *ACS Omega* **7** (2022) 39520–39530.
- [37] (a) W. Jiang, X. Li, G. Gao, F. Wu, C. Luo, L. Zhang, *Chem. Eng. J.* **445** (2022) 136767; (b) S. Lian, C. Song, Q. Liu, E. Duan, H. Ren, Y. Kitamura, *J. Environ. Sci.* **99** (2021) 281–295.
- [38] (a) W. Yu, T. Wang, A.-H.A. Park, M. Fang, *Nanoscale* **11** (2019) 17137–17156; (b) A. Tavakoli, K. Rahimi, F. Saghafiani, J. Scott, E. Lovell, *J. Environ. Manag.* **313** (2022) 114955; (c) B. Aghel, S. Janati, F. Alobaid, A. Almoslhy, B. Epple, *Appl. Sci.* **12** (2022) 3200.
- [39] (a) M. Younas, M. Rezakazemi, M. Daud, M.B. Wazir, S. Ahmad, N. Ullah, Inamuddin, S. Ramakrishna, *Prog. Energy Combust. Sci.* **80** (2020) 100849; (b) S. Mahajan, M. Lahtinen, *J. Environ. Chem. Eng.* **10** (2022) 108930;

- (c) L. Li, H.S. Jung, J.W. Lee, Y.T. Kang, *Renew. Sustain. Energy Rev.* **162** (2022) 112441.
- [40] (a) W. Rahmah, G.T.M. Kadja, M.H. Mahyuddin, A.G. Saputro, H.K. Dipojono, I. G. Wenten, *J. Environ. Chem. Eng.* **10** (2022) 108707;
- (b) X. Gao, Z. Wang, T. Chen, L. Hu, S. Yang, S. Kawi, *Carbon Capture Sci. Technol.* **5** (2022) 100073;
- (c) S. Kumar, R. Srivastava, J. Koh, *J. CO₂ Util.* **41** (2020) 101251.
- [41] (a) S.S. Fatima, A. Borhan, M. Ayoub, N. Abd Ghani, *J. Mol. Liq.* **338** (2021) 116913;
- (b) A. Cherevotan, J. Raj, S.C. Peter, *J. Mater. Chem. A* **9** (2021) 27271–27303.
- [42] Vol. 2023, International Energy Agency.
- [43] (a) Vol. 2023, International Energy Agency. (b) Vol. 2023, International Institute for Sustainable Development.
- [44] B.J.P. Buhre, L.K. Elliott, C.D. Sheng, R.P. Gupta, T.F. Wall, *Prog. Energy Combust. Sci.* **31** (2005) 283–307.
- [45] (a) T.N. Borhani, M. Wang, *Renew. Sustain. Energy Rev.* **114** (2019) 109299;
- (b) M.M. Martín, in: *Industrial Chemical Process Analysis and Design*, Elsevier, Boston, 2016, pp. 199–297.
- [46] (a) S. Shen, Y. Bian, Y. Zhao, *Int. J. Greenh. Gas Control* **56** (2017) 1–11;
- (b) Y.S. Yu, H.F. Lu, T.T. Zhang, Z.X. Zhang, G.X. Wang, V. Rudolph, *Ind. Eng. Chem. Res.* **52** (2013) 12622–12634.
- [47] H. Guo, C. Li, X. Shi, H. Li, S. Shen, *Appl. Energy* **239** (2019) 725–734.
- [48] T.N. Borhani, E. Oko, M. Wang, *J. Ind. Eng. Chem.* **75** (2019) 285–295.
- [49] M. Asif, M. Suleman, I. Haq, S.A. Jamal, *Greenh. Gases Sci. Technol.* **8** (2018) 998–1031.
- [50] J. Li, P. Tharakarn, D. Macdonald, X. Liang, *Energy Policy* **61** (2013) 1377–1387.
- [51] S.H.B. Vinjarapu, R. Neerup, A.H. Larsen, J.K. Jørsboe, S.N.B. Villadsen, S. Jensen, J.L. Karlsson, J. Kappel, H. Lassen, P. Blinksbjerg, N. von Solms, P. L. Fosbøl, *Appl. Energy* **355** (2024) 122193.
- [52] X. Xu, C. Song, J.M. Andresen, B.G. Miller, A.W. Scaroni, *Energy Fuels* **16** (2002) 1463–1469.
- [53] Y. Belmabkhout, V. Guillerm, M. Eddaudi, *Chem. Eng. J.* **296** (2016) 386–397.
- [54] D. Ko, R. Siriwardane, L.T. Biegler, *Ind. Eng. Chem. Res.* **44** (2005) 8084–8094.
- [55] B.S. Caglayan, A.E. Aksyoju, J. Hazard. Mater. **252** (2013) 19–28.
- [56] C.A. Grande, S. Roussanly, R. Anantharaman, K. Lindqvist, P. Singh, J. Kemper, *Energy Procedia* **114** (2017) 2259–2264.
- [57] Z. Liu, L. Wang, X. Kong, P. Li, J. Yu, A.E. Rodrigues, *Ind. Eng. Chem. Res.* **51** (2012) 7355–7363.
- [58] (a) N. Ghasem, in: *Advances in Carbon Capture*, Woodhead Publishing, 2020, pp. 479–501;
- (b) C. Higman, in: *Advances in Clean Hydrocarbon Fuel Processing*, Woodhead Publishing, 2011, pp. 155–185;
- (c) B.G. Miller, in: *Clean Coal Engineering Technology*, second edition, Butterworth-Heinemann, 2017, pp. 261–308.
- [59] S. Mokhatab, W.A. Poe, J.Y. Mak, in: *Handbook of Natural Gas Transmission and Processing*, fourth edition, Gulf Professional Publishing, 2019, pp. 231–269.
- [60] B. Elvers, *Ullmann's Encyclopedia of Industrial Chemistry*, Vol. 17, Verlag Chemie Hoboken, NJ, 1991.
- [61] (a) Y. Li, Y. You, W. Huang, J. Yang, *J. Chem. Thermodyn.* **130** (2019) 38–46;
- (b) Y. Chen, C. Ma, X. Ji, Z. Yang, X. Lu, *Fluid Phase Equilibria* **504** (2020) 112336.
- [62] Y. Li, Y. You, M. Dai, X. Chen, J. Yang, *J. Chem. Eng. Data* **65** (2020) 896–905.
- [63] X. Gui, Z. Tang, W. Fei, *J. Chem. Eng. Data* **55** (2010) 3736–3741.
- [64] Y.J. Heintz, L. Sehabigae, B.I. Morsi, K.L. Jones, H.W. Pennline, *Energy Fuels* **22** (2008) 3824–3837.
- [65] G.V.S.M. Carrera, Z. Visak, R. Bogel-Lukasik, M. Nunes da Ponte, *Fluid Phase Equilibria* **303** (2011) 180–183.
- [66] S. Xu, Y.W. Wang, F.D. Otto, A.E. Mather, *J. Chem. Technol. Biotechnol.* **56** (1993) 309–316.
- [67] A.L. Kohl, R.B. Nielsen, in: *Gas Purification* (fifth edition), Gulf Professional Publishing, Houston, 1997, pp. 1187–1237.
- [68] M. Xu, S. Wang, L. Xu, *Int. J. Greenh. Gas Control* **85** (2019) 199–205.
- [69] E.S. Sanz-Pérez, C.R. Murdock, S.A. Didas, C.W. Jones, *Chem. Rev.* **116** (2016) 11840–11876.
- [70] F. Vega, M. Cano, S. Camino, L.M.G. Fernández, E. Portillo, B. Navarrete, *Carbon Dioxide Chemistry, Capture and Oil Recovery*, 2018, pp. 142–163.
- [71] P. Luis, *Desalination* **380** (2016) 93–99.
- [72] C.S. Hsu, C.J. Kim, *Ind. Eng. Chem. Prod. Res. Dev.* **24** (1985) 630–635.
- [73] M.Z. Hajji-Sulaiman, M.K. Aroua, A. Benamor, *Chem. Eng. Res. Des.* **76** (1998) 961–968.
- [74] K. Li, W. Leigh, P. Feron, H. Yu, M. Tade, *Appl. Energy* **165** (2016) 648–659.
- [75] V. Buvik, K.K. Hoisater, S.J. Vevelstad, H.K. Knuttila, *Int. J. Greenh. Gas Control* **106** (2021) 103246.
- [76] (a) G. Sartori, D.W. Savage, *Ind. Eng. Chem. Fundam.* **22** (1983) 239–249;
- (b) D. Gómez-Díaz, J.M. Navaza, P. Rodríguez, R. Vega, *Chem. Eng. Technol.* **40** (2017) 1767–1773.
- [77] N. Hüser, O. Schmitz, E.Y. Kenig, *Chem. Eng. Sci.* **157** (2017) 221–231.
- [78] S. Liu, H. Gao, C. He, Z. Liang, *Appl. Energy* **233–234** (2019) 443–452.
- [79] E.B. Rinker, S.S. Ashour, O.C. Sandall, *Ind. Eng. Chem. Res.* **39** (2000) 4346–4356.
- [80] F. Bougie, M.C. Iliuta, *J. Chem. Eng. Data* **57** (2012) 635–669.
- [81] A. Aroonwilas, A. Veawab, *Ind. Eng. Chem. Res.* **43** (2004) 2228–2237.
- [82] A.V. Rayner, A. Henni, *Ind. Eng. Chem. Res.* **53** (2014) 4953–4965.
- [83] F.A. Chowdhury, H. Okabe, S. Shimizu, M. Onoda, Y. Fujioka, *Energy Procedia* **1** (2009) 1241–1248.
- [84] L. Wen, H. Liu, W. Rongwong, Z. Liang, K. Fu, R. Idem, P. Tontiwachwuthikul, *Chem. Eng. Technol.* **38** (2015) 1435–1443.
- [85] A. Naami, M. Edali, T. Sema, R. Idem, P. Tontiwachwuthikul, *Ind. Eng. Chem. Res.* **51** (2012) 6470–6479.
- [86] G. Gao, W. Jiang, X. Li, Z. Zhao, C. Jiang, C. Luo, F. Wu, L. Zhang, *Sep. Purif. Technol.* **306** (2023) 122615.
- [87] B. Jaffary, L. Jaafari, R. Idem, *Energy Fuels* **35** (2021) 8081–8094.
- [88] A. Hafizi, M.H. Mokari, R. Khalifeh, M. Farsi, M.R. Rahimpour, *J. Mol. Liq.* **297** (2020) 111803.
- [89] (a) G. Rochelle, E. Chen, S. Freeman, D. Van Wagener, Q. Xu, A. Voice, *Chem. Eng. J.* **171** (2011) 725–733;
- (b) H.M. Kvamsdal, M.C. Romano, L. van der Ham, D. Bonalumi, P. van Os, E. Goetheer, *Int. J. Greenh. Gas Control* **28** (2014) 343–355.
- [90] (a) R.E. Dugas, *Carbon Dioxide Absorption, Desorption, and Diffusion in Aqueous Piperazine and Monoethanolamine*, The University of Texas at Austin, 2009;
- (b) R. Dugas, G. Rochelle, *Energy Procedia* **1** (2009) 1163–1169.
- [91] S.A. Freeman, R. Dugas, D.H. Van Wagener, T. Nguyen, G.T. Rochelle, *Int. J. Greenh. Gas Control* **4** (2010) 119–124.
- [92] X. Chen, G.T. Rochelle, *Chem. Eng. Res. Des.* **89** (2011) 1693–1710.
- [93] N. El Hadri, D.V. Quang, E.L.V. Goetheer, M.R.M. Abu Zahra, *Appl. Energy* **185** (2017) 1433–1449.
- [94] Y. Yuan, G.T. Rochelle, *Int. J. Greenh. Gas Control* **85** (2019) 182–186.
- [95] C. Nwaoha, P. Tontiwachwuthikul, A. Benamor, *Fuel* **234** (2018) 1089–1098.
- [96] Y. Yuan, G.T. Rochelle, *Chem. Eng. Sci.* **182** (2018) 56–66.
- [97] Z. Qi, F. Liu, H. Ding, M. Fang, *Fuel* **350** (2023) 128726.
- [98] M. Afkhamipour, M. Mofarahi, A. Rezaei, R. Mahmoodi, C.-H. Lee, *Fuel* **256** (2019) 115877.
- [99] T. Ping, Y. Dong, S. Shen, *ACS Sustain. Chem. Eng.* **8** (2020) 18071–18082.
- [100] D.J. Heldebrant, P.K. Koech, V.-A. Glezakou, R. Rousseau, D. Malhotra, D. C. Cantu, *Chem. Rev.* **117** (2017) 9594–9624.
- [101] L. Bihong, Y. Kexuan, Z. Xiaobin, Z. Zuoming, J. Guohua, *Appl. Energy* **264** (2020) 114703.
- [102] F. Barzaghi, F. Mani, M. Peruzzini, *Int. J. Greenh. Gas Control* **60** (2017) 100–109.
- [103] S. Zhang, Y. Shen, L. Wang, J. Chen, Y. Lu, *Appl. Energy* **239** (2019) 876–897.
- [104] H. Hu, M. Fang, F. Liu, T. Wang, Z. Xia, W. Zhang, C. Ge, J. Yuan, *Appl. Energy* **324** (2022) 119570.
- [105] S. Shen, X. Shi, C. Li, H. Guo, Q. Long, S. Wang, X. Yin, *Sep. Purif. Technol.* **300** (2022) 121908.
- [106] X. Zhou, X. Li, J. Wei, Y. Fan, L. Liao, H. Wang, *Environ. Sci. Technol.* **54** (2020) 16138–16146.
- [107] F. Liu, M. Fang, N. Yi, T. Wang, *Energy Fuels* **33** (2019) 11389–11398.
- [108] J.L. Anthony, J.L. Anderson, E.J. Maginn, J.F. Brennecke, *J. Phys. Chem. B* **109** (2005) 6366–6374.
- [109] X. Zhang, Z. Liu, W. Wang, *AIChE J.* **54** (2008) 2717–2728.
- [110] (a) M.J. Muldoon, S.N.V.K. Aki, J.L. Anderson, J.K. Dixon, J.F. Brennecke, *J. Phys. Chem. B* **111** (2007) 9001–9009;
- (b) A. Yokozeki, M.B. Shiflett, C.P. Junk, L.M. Grieco, T. Foo, *J. Phys. Chem. B* **112** (2008) 16654–16663.
- [111] B.E. Gurkan, J.C. de la Fuente, E.M. Mindrup, L.E. Ficke, B.F. Goodrich, E. A. Price, W.F. Schneider, J.F. Brennecke, *J. Am. Chem. Soc.* **132** (2010) 2116–2117.
- [112] M. Aghaie, N. Rezaei, S. Zendehboudi, *Renew. Sustain. Energy Rev.* **96** (2018) 502–525.
- [113] S. Kang, Y.G. Chung, J.H. Kang, H. Song, *J. Mol. Liq.* **297** (2020) 111825.
- [114] Y.S. Sistla, A. Khanna, *Chem. Eng. J.* **273** (2015) 268–276.
- [115] M.S. Raja Shahrom, C.D. Wilfond, D.R. MacFarlane, R. Vijayraghavan, F.K. Chong, *J. Mol. Liq.* **276** (2019) 644–652.
- [116] S.K. Shukla, S.G. Khokarale, T.Q. Bui, J.-P.T. Mikkola, *Front. Mater.* **6** (2019) 42.
- [117] S. Zeng, J. Wang, L. Bai, B. Wang, H. Gao, D. Shang, X. Zhang, S. Zhang, *Energy Fuels* **29** (2015) 6039–6048.
- [118] W. Jiang, F. Wu, G. Gao, X. Li, L. Zhang, C. Luo, *Chem. Eng. J.* **420** (2021) 129897.
- [119] L. Zhou, X. Shang, J. Fan, J. Wang, *J. Chem. Thermodyn.* **103** (2016) 292–298.
- [120] Y. Zhang, X. Zhao, Q. Yang, Z. Zhang, Q. Ren, H. Xing, *Ind. Eng. Chem. Res.* **56** (2017) 7336–7344.
- [121] S. Hussain, H. Dong, S. Zeng, M. Umair Ahmad, F. Khurum Shehzad, H. Wu, Y. Zhang, *J. Mol. Liq.* **336** (2021) 116362.
- [122] (a) G. Wang, W. Hou, F. Xiao, J. Geng, Y. Wu, Z. Zhang, *J. Chem. Eng. Data* **56** (2011) 1125–1133;
- (b) S.P.M. Ventura, J. Pauly, J.L. Daridon, J.A. Lopes da Silva, I.M. Marrucho, A. M.A. Dias, J.A.P. Coutinho, *J. Chem. Thermodyn.* **40** (2008) 1187–1192.
- [123] (a) C. Ma, N. Wang, N. Ye, X. Ji, *Appl. Energy* **304** (2021) 117767;
- (b) Y. Liu, Z. Dai, F. Dai, X. Ji, *Crystals* **10** (2020) 978.
- [124] F. Liu, Y. Shen, L. Shen, C. Sun, L. Chen, Q. Wang, S. Li, W. Li, *Environ. Sci. Technol.* **54** (2020) 3520–3529.
- [125] (a) C. McEllis, S.F.R. Taylor, J. Jacquemin, C. Hardae, *J. Chem. Eng. Data* **61** (2016) 1092–1100;
- (b) I. Iliuta, M. Hasib-ur-Rahman, F. Larachi, *Chem. Eng. J.* **240** (2014) 16–23.
- [126] M. Xiao, H. Liu, H. Gao, W. Olson, Z. Liang, *Appl. Energy* **235** (2019) 311–319.
- [127] B. Lv, C. Sun, N. Liu, W. Li, S. Li, *Chem. Eng. J.* **280** (2015) 695–702.
- [128] Y. Chen, Y. Sun, Z. Yang, X. Lu, X. Ji, *Appl. Energy* **257** (2020) 113962.
- [129] M. Zalewski, T. Krawczyk, A. Siewniak, A. Sobolewski, *Int. J. Greenh. Gas Control* **105** (2021) 103210.
- [130] Z. Zhou, B. Guo, B. Lv, H. Guo, G. Jing, *Int. J. Greenh. Gas Control* **44** (2016) 115–123.

- [131] M. Wang, L. Zhang, L. Gao, K. Pi, J. Zhang, C. Zheng, *Energy Fuels* **27** (2013) 461–466.
- [132] X. Feng, J. Zhu, K. Song, J. Zeng, X. Zhou, X. Guo, K. Lin, Cuihong Zhang, C. Xie, J.-W. Shi, *Sep. Purif. Technol.* **336** (2024) 126285.
- [133] G. Wu, Y. Liu, G. Liu, X. Pang, *Molecules* **25** (2020) 1034.
- [134] F. Meng, T. Ju, S. Han, L. Lin, J. Li, K. Chen, J. Jiang, *Chem. Eng. J.* **462** (2023) 142296.
- [135] S. Krishnamurthy, P. Bhattacharya, P. Phelan, R. Prasher, *Nano Lett.* **6** (2006) 419–423.
- [136] B. Devakshi, S. Thomas, *Int. J. Air-Cond. Refrig.* **28** (2020) 2050017.
- [137] V. Irani, A. Maleki, A. Tavasoli, *J. Environ. Chem. Eng.* **7** (2019) 102782.
- [138] K.R. Chaturvedi, T. Sharma, *Mater. Today Proc.* **46** (2021) 5298–5303.
- [139] (a) J.H. Park, J.W. Lee, S. Kim, R. Xu, Y.T. Kang, *J. CO₂ Util.* **54** (2021) 101753; (b) R. Aghehrochaboki, Y. Aghdoud Chaboki, S.A. Maleknia, V. Irani, *J. Environ. Chem. Eng.* **7** (2019) 103285; (c) V. Irani, A. Tavasoli, M. Vahidi, *J. Colloid Interface Sci.* **527** (2018) 57–67.
- [140] J.H.J. Kluytmans, B.G.M. van Wachem, B.F.M. Kuster, J.C. Schouten, *Chem. Eng. Sci.* **58** (2003) 4719–4728.
- [141] W.-g Kim, H.U. Kang, K.-m Jung, S.H. Kim, *Sep. Sci. Technol.* **43** (2008) 3036–3055.
- [142] B. Rahmatmand, P. Keshavarz, S. Ayatollahi, *J. Chem. Eng. Data* **61** (2016) 1378–1387.
- [143] A. Elhambakhsh, S.M. Mousavi, M.N. Ghasemi, F. Esmailzadeh, P. Keshavarz, K. Asadi, R.K. Haghghi, X. Wang, *Chem. Pap.* **76** (2022) 4817–4834.
- [144] N. Lai, Q. Zhu, D. Qiao, K. Chen, L. Tang, D. Wang, W. He, Y. Chen, T. Yu, *Front. Chem.* **8** (2020) 146.
- [145] M.H. Karimi Darvanooghi, M. Pahlevaninezhad, A. Abdollahi, S.M. Davoodi, *AIChE J.* **63** (2017) 2176–2186.
- [146] D. Jelen, *Electrocore, Inc.*, 2023.
- [147] C. Petit, *Curr. Opin. Chem. Eng.* **20** (2018) 132–142.
- [148] M. Muschi, S. Devautour-Vinot, D. Aureau, N. Heymans, S. Sene, R. Emmerich, A. Ploumistas, A. Geneste, N. Steunou, G. Patriarche, *J. Mater. Chem. A* **9** (2021) 13135–13142.
- [149] S.B. Peh, S. Farooq, D. Zhao, *Chem. Eng. Sci.* **250** (2022) 117399.
- [150] J.H. Choe, H. Kim, M. Kang, H. Yun, S.Y. Kim, S.M. Lee, C.S. Hong, *J. Am. Chem. Soc.* **144** (2022) 10309–10319.
- [151] L. Jiang, Z. Yin, J. Chu, C. Song, A. Kong, *J. Solid State Chem.* **306** (2022) 122771.
- [152] J. Tian, Y. Shen, D. Zhang, Z. Tang, *J. Environ. Chem. Eng.* **9** (2021) 106037.
- [153] Z.J. Li, S. Srebnik, *Phys. Chem. Chem. Phys.* **23** (2021) 10311–10320.
- [154] S. Voskian, T.A. Hatton, *Energy Environ. Sci.* **12** (2019) 3530–3547.
- [155] X. Yu, L. Mao, H. Xie, X. Yao, G. He, Z. Huang, *Langmuir* **39** (2023) 5936–5943.
- [156] L. Wang, Z. Liu, P. Li, J. Yu, A.E. Rodrigues, *Chem. Eng. J.* **197** (2012) 151–161.
- [157] A.H. Lahuri, M.L.N. Khai, A.A. Rahim, N. Nordin, *Acta Chim. Slov.* **67** (2020) 570–580.
- [158] M. Khajeh, A. Ghaemi, *Int. J. Environ. Anal. Chem.* **103** (2023) 5311–5336.
- [159] S. Nazari Kudahi, A. Noorpoor, N.M. Mahmoodi, *Iran. J. Chem. Chem. Eng. (IJCHE)* **38** (2019) 293–307.
- [160] P. Hu, S. Wang, Y. Zhuo, *Sep. Purif. Technol.* **287** (2022) 120518.
- [161] Z. Liu, C. Shen, F.V. Lopes, P. Li, J. Yu, C.A. Grande, A.E. Rodrigues, *Sep. Sci. Technol.* **48** (2013) 388–402.
- [162] S. Karka, S. Kodukula, S.V. Nandury, U. Pal, *ACS Omega* **4** (2019) 16441–16449.
- [163] S. Zhang, S. Ravi, Y.-R. Lee, J.-W. Ahn, W.-S. Ahn, *J. Ind. Eng. Chem.* **72** (2019) 241–249.
- [164] P. Cao, Z. Wang, L. Liu, P. Gao, G. Tian, H. Liu, J. He, *J. Taiwan Inst. Chem. Eng.* **138** (2022) 104444.
- [165] M. Shirzad, M. Karimi, A.E. Rodrigues, J.A. Silva, *Biochar and its Composites: Fundamentals and Applications*, Springer, 2023, pp. 73–105.
- [166] B. Verougstraete, A. Martin-Calvo, S. Van der Perre, G. Baron, V. Finsy, J. F. Denayer, *Chem. Eng. J.* **383** (2020) 123075.
- [167] B. Verougstraete, M. Schoukens, B. Sutens, N.V. Haute, Y. De Vos, M. Rombouts, J.F. Denayer, *Sep. Purif. Technol.* **299** (2022) 121660.
- [168] S.A. Anuar, W.N. Wan Isahak, M.S. Masdar, *Int. J. Energy Res.* **44** (2020) 3148–3159.
- [169] Z. Wu, X.-H. Du, Q.-F. Zhang, M. Strømme, C. Xu, *Nano Res.* (2023) 1–9.
- [170] H. Yuan, J. Chen, D. Li, H. Chen, Y. Chen, *Chem. Eng. J.* **373** (2019) 171–178.
- [171] J.J. Manyà, D. García-Morcote, B. González, *Appl. Sci.* **10** (2020) 376.
- [172] (a) P. Jin Ong, Y. Leow, X. Yun Debbie Soo, M. Hui Chua, X. Ni, A. Suwardi, C. Kiang Ivan Tan, R. Zheng, F. Wei, J. Xu, X. Jun Loh, D. Kai, Q. Zhu, *Waste Manag.* **157** (2023) 339–347; (b) P.J. Ong, Z.X.J. Heng, Z. Xing, H.Y.Y. Ko, P. Wang, H. Liu, R. Ji, X. Wang, B. H. Tan, Z. Li, *Trans. Tianjin Univ.* **29** (2023) 225–234; (c) X. Yun Debbie Soo, J. Min Regine See, W. Wu, S. Wang, H. Liu, P. Wang, D. Kai, J. Kong, E. Ye, R. Ji, *ChemistrySelect* **8** (2023) e202304794.
- [173] W. Cao, H. Xu, X. Zhang, W. Xiang, G. Qi, L. Wan, B. Gao, *Chem. Eng. J.* **471** (2023) 144523.
- [174] (a) H. Zhu, J. Mah Jian Qiang, C.G. Wang, C.Y. Chan, Q. Zhu, E. Ye, Z. Li, X. J. Loh, *Bioact. Mater.* **18** (2022) 471–491; (b) M. Liu, Y. Chen, Q. Zhu, J. Tao, C. Tang, H. Ruan, Y. Wu, X.J. Loh, *Chem. Asian J.* **17** (2022) e202200396.
- [175] A. Sayari, Y. Belmabkhout, R. Serna-Guerrero, *Chem. Eng. J.* **171** (2011) 760–774.
- [176] M.G. Plaza, C. Pevida, B. Arias, M.D. Casal, C.F. Martín, J. Fermoso, F. Rubiera, J. J. Pis, *J. Environ. Eng.* **135** (2009) 426–432.
- [177] H. Cui, J. Xu, J. Shi, N. Yan, Y. Liu, *Energy* **187** (2019) 115936.
- [178] (a) M.T. Mota-Martinez, J.P. Hallett, N. Mac Dowell, *Sustain. Energy Fuels* **1** (2017) 2078–2090; (b) Y. Ma, J. Gao, Y. Wang, J. Hu, P. Cui, *Int. J. Greenh. Gas Control* **75** (2018) 134–139; (c) D. Hospital-Benito, J. Lemus, C. Moya, R. Santiago, V.R. Ferro, J. Palomar, *Chem. Eng. J.* **407** (2021) 127196.
- [179] T. Stoffregen, S. Rigby, S. Jovanovic, K.R. Krishnamurthy, *Energy Procedia* **63** (2014) 1456–1469.
- [180] S. Saito, M. Udatu, H. Kitamura, S. Murai, Y. Kato, Y. Maezawa, H. Watando, *Energy Procedia* **51** (2014) 176–183.
- [181] D. Valencia-Marquez, A. Flores-Tlacuahuac, L. Ricardez-Sandoval, *AIChE J.* **62** (2016) 3298–3309.
- [182] M. Hasib-ur-Rahman, M. Siaj, F. Larachi, *Chem. Eng. Process. Process Intensif.* **49** (2010) 313–322.
- [183] (a) J. de Riva, J. Suarez-Reyes, D. Moreno, I. Díaz, V. Ferro, J. Palomar, *Int. J. Greenh. Gas Control* **61** (2017) 61–70; (b) M.T. Mota-Martinez, P. Brandl, J.P. Hallett, N. Mac Dowell, *Mol. Syst. Des. Eng.* **3** (2018) 560–571; (c) P. García-Gutiérrez, J. Jacquemin, C. McEllis, I. Dimitriou, S.F.R. Taylor, C. Hardae, R.W.K. Allen, *Energy Fuels* **30** (2016) 5052–5064; (d) Y. Huang, X. Zhang, X. Zhang, H. Dong, S. Zhang, *Ind. Eng. Chem. Res.* **53** (2014) 11805–11817; (e) M.B. Shiflett, D.W. Drew, R.A. Cantini, A. Yokozeki, *Energy Fuels* **24** (2010) 5781–5789; (f) H. Zhai, E.S. Rubin, *Energy Procedia* **63** (2014) 1321–1328.
- [184] N.R. Sukor, A.H. Shamsuddin, T.M.I. Mahlia, M.F. Mat Isa, *Processes* **8** (2020) 350.
- [185] M.M. Shah, J. Haley, N. Hassan, T. McNamara, A. Laugwitz, L. Ganzer, A. Stevens, A. Kumar, D. McNally, R. McLandborough, Linde Inc., 2023.
- [186] N. Singh, G. Nagpal, S. Agrawal, *Environ. Technol. Innov.* **11** (2018) 187–240.
- [187] A. Khaleel, P.N. Kapoor, K.J. Klubunde, *Nanostruct. Mater.* **11** (1999) 459–468.
- [188] J.R. de Andrade, M.F. Oliveira, M.G. da Silva, M.G. Vieira, *Ind. Eng. Chem. Res.* **57** (2018) 3103–3127.
- [189] F.O. Ochedi, J. Yu, H. Yu, Y. Liu, A. Hussain, *Environ. Chem. Lett.* **19** (2021) 77–109.
- [190] K. Elsaied, A.G. Olabi, T. Wilberforce, M.A. Abdelkareem, E.T. Sayed, *Sci. Total Environ.* **763** (2021) 144202.
- [191] D.M. D'Alessandro, B. Smit, J.R. Long, *Angew. Chem. Int. Ed.* **49** (2010) 6058–6082.
- [192] D. Matovic, *Energy* **36** (2011) 2011–2016.
- [193] X. Zhu, T. Ge, F. Yang, R. Wang, *Renew. Sustain. Energy Rev.* **137** (2021) 110651.
- [194] S. Mouhoubi, L. Dubois, P.L. Fosbøl, G. De Weireld, D. Thomas, *Chem. Eng. Res. Des.* **158** (2020) 46–63.
- [195] W. Fan, W. Gao, C. Zhang, W.W. Tjiu, J. Pan, T. Liu, J. Mater. Chem. **22** (2012) 25108–25115.
- [196] S. Seo, B. Lages, M. Kim, J. CO₂ Util. **36** (2020) 244–252.
- [197] S. Laribi, L. Dubois, G. De Weireld, D. Thomas, *Int. J. Greenh. Gas Control* **90** (2019) 102799.
- [198] L. Cao, X. Zhang, Y. Xu, W. Xiang, R. Wang, F. Ding, P. Hong, B. Gao, *Sep. Purif. Technol.* **287** (2022) 120592.